

AFTERSHOCK ANALYSIS IN THE MAINLAND SOUTHEAST ASIA



A Thesis Submitted in Partial Fulfillment of the Requirements
for the Degree of Master of Science in Geology

Department of Geology

FACULTY OF SCIENCE

Chulalongkorn University

Academic Year 2018

Copyright of Chulalongkorn University

การวิเคราะห์แผ่นดินไหวตามในพื้นที่แผ่นดินไหวภูมิภาคเอเชียตะวันออกเฉียงใต้



วิทยานิพนธ์นี้เป็นส่วนหนึ่งของการศึกษาตามหลักสูตรปริญญาวิทยาศาสตรมหาบัณฑิต

สาขาวิชาธรณีวิทยา ภาควิชาธรณีวิทยา

คณะวิทยาศาสตร์ จุฬาลงกรณ์มหาวิทยาลัย

ปีการศึกษา 2561

ลิขสิทธิ์ของจุฬาลงกรณ์มหาวิทยาลัย

AFTERSHOCK ANALYSIS IN THE MAINLAND SOUTHEAST ASIA



A Thesis Submitted in Partial Fulfillment of the Requirements
for the Degree of Master of Science in Geology

Department of Geology

FACULTY OF SCIENCE

Chulalongkorn University

Academic Year 2018

Copyright of Chulalongkorn University

Thesis Title	AFTERSHOCK ANALYSIS IN THE MAINLAND SOUTHEAST A SIA
By	Miss Premwadee Traitangwong
Field of Study	Geology
Thesis Advisor	Associate Professor Santi Pailoplee, Ph.D.

Accepted by the FACULTY OF SCIENCE, Chulalongkorn University in Partial
Fulfillment of the Requirement for the Master of Science

..... Dean of the FACULTY OF SCIENCE
(Associate Professor Polkit Sangvanich, Ph.D.)

THESIS COMMITTEE

..... Chairman
(Professor Montri Choowong, Ph.D.)

..... Advisor
(Associate Professor Santi Pailoplee, Ph.D.)

..... Examiner
(Piyaphong Chenrai, Ph.D.)

..... External Examiner
(Assistant Professor Krit Won-in, Ph.D.)

CHULALONGKORN UNIVERSITY

เปรมวดี ไตรตั้งวงศ์ : การวิเคราะห์แผ่นดินไหวตามในพื้นที่แผ่นดินใหญ่ภูมิภาคเอเชียตะวันออกเฉียงใต้. (AFTERSHOCK ANALYSIS IN THE MAINLAND SOUTHEAST ASIA) อ.ที่ปรึกษา
วิทยานิพนธ์หลัก : รศ. ดร.สันติ ภัยหลบลี้

ในการศึกษานี้มุ่งเน้นที่จะวิเคราะห์พฤติกรรมของแผ่นดินไหวตามที่จะเกิดขึ้นในพื้นที่แผ่นดินใหญ่ภูมิภาคเอเชียตะวันออกเฉียงใต้ ด้วยวิธีการทางแผ่นดินไหวเชิงสถิติซึ่งประกอบไปด้วย ความเค้นทางธรณีแปรสัณฐาน, อัตราการสลายตัวของแผ่นดินไหวตามและการแบ่งพลังงานในการปลดปล่อย, ขนาดสูงสุดของแผ่นดินไหวตามและรูปแบบการเกิดแผ่นดินไหว โดยหลังจากการจัดกลุ่มฐานข้อมูลแผ่นดินไหว กลุ่มข้อมูลแผ่นดินไหว 1,697 กลุ่มจะแสดงถึงข้อมูลแผ่นดินไหวตามอย่างแท้จริงที่จะนำมาทำการวิเคราะห์โดยแยกเป็น 13 โซน จากการวิเคราะห์ด้วยวิธีที่แตกต่างกัน พบว่าขนาดสูงสุดของแผ่นดินไหวตามในพื้นที่ศึกษาจะขึ้นอยู่กับขนาดของแผ่นดินไหวหลักโดยมีค่าความแตกต่างกันอยู่ในช่วง 0.4-2.5 ซึ่งในพื้นที่ intraplate จะมีค่าความต่างมากกว่าในพื้นที่ interplate โดยเฉพาะอย่างยิ่งในพื้นที่ทางตะวันตกและทางใต้ของประเทศไทยที่มีค่าความต่างค่อนข้างน้อย ส่วนค่าอัตราการสลายตัวและจำนวนทั้งหมดของแผ่นดินไหวตามจะมีค่ามากขึ้นเมื่อเทียบกับขนาดของแผ่นดินไหวที่ใหญ่ขึ้น และสำหรับแผ่นดินไหวตามที่จะเกิดขึ้นจะมีการกระจายตัวทั่วทั้งพื้นที่เมื่อเทียบกับแผ่นดินไหวหลัก ($D_c \sim 2$)

นอกจากนี้ การศึกษาค่า b เป็นการศึกษาเกี่ยวกับความเครียด โดยในเชิงพื้นที่ ค่า b ของแผ่นดินไหวตามจะมีค่าอยู่ในช่วง 0.8-1.8 ซึ่งแตกต่างจากค่า b ของแผ่นดินไหวหลักโดยทั่วไปที่มีค่าประมาณ 1.0-1.2 ส่วนในเชิงเวลา พบว่าในช่วงแรกเมื่อเกิดแผ่นดินไหวหลัก ความเครียดจะยังคงสูงอยู่และค่อยๆลดลงไปซึ่งถือได้ว่า มีการคายพลังงานออกไป โดยมีความแปรผกผันกับค่า b สุดท้ายนี้ สำหรับค่า b และค่า D_c พบว่า ความสัมพันธ์ระหว่างค่า D_c และ ค่า b จะแปรผันตามกันเช่นเดียวกับความสัมพันธ์ระหว่างค่า D_c และอัตราส่วนระหว่างค่า a และ b

ภาควิชา ภาควิชาธรณีวิทยา

ลายมือชื่อนิสิต

สาขาวิชา ธรณีวิทยา

ลายมือชื่อ อ.ที่ปรึกษาวิทยานิพนธ์หลัก

ปีการศึกษา 2561

5872142423 : MASTER OF SCIENCE

AFTERSHOCK / EARTHQUAKE DECLUSTERING / MAINLAND SOUTHEAST ASIA / BATH'S LAW /
GUTENBERG-RICHTER RELATIONSHIP / MODIFIED OMORI'S LAW / FRACTAL DIMENSION

Premwadee Traitangwong :
AFTERSHOCK ANALYSIS IN THE MAINLAND SOUTHEAST ASIA. ADVISOR: Assoc. Prof.
Santi Pailoplee, Ph.D.

In this study, the characteristics of the aftershock in the mainland Southeast Asia (MSEA) were investigated using the several seismological techniques, i.e., i) the Gutenberg-Richter relationship (G-R relationship) ii) the modified Omori's law iii) the Bath's law and iv) the fractal dimension. After declustering, 1,697 clusters during 1985-2017, which represent the aftershocks occurring after mainshock were investigated in 13 seismic source zones recognized in the MSEA. According to the Bath's law, the maximum magnitude of the aftershock depends on the magnitude of the mainshock, with the difference value between 0.4-2.5. In the intraplate zone, it is less than in the interplate zone, especially in Western Thailand and Southern Thailand zones (0.4-0.7). Next, the decay rate of the aftershock and the number of aftershocks based on the modified Omori's law are positive relation with the magnitude of mainshock. After that the fractal dimension (D_c) for 13 zones are approximately 2.0, which means the distribution of the aftershocks in the MSEA are distributed into two-dimensional fault plane.

In addition, for the spatial investigation, the b values of aftershock from the G-R relationship are in range of 0.8-1.8 that different from the mainshock. While for the temporal investigation, it is confirmed that the beginning of the mainshock is high stress, and then gradually release the accumulated stress. Finally, the relationship of the D_c and b values is positive correction as well as the relationship of the D_c values and a-b ratios.

Department: Department of Geology Student's Signature

Field of Study: Geology Advisor's Signature

Academic Year: 2018

ACKNOWLEDGEMENTS

I would like to sincerely thank my Advisor, Associate Professor Dr. Santi Pailoplee, Department of Geology, Faculty of Science, Chulalongkorn University for his supports, encouragements, significant advises, reviews of thesis and advice on how to be a good researcher.

I thank Mr. Santawat Sukrungsri, Thai Meteorological Department for his valuable suggestion.

I thank to Mr. Peeranat Longsombun, Thai Meteorological Department for giving advice about programing in this study.

Finally, I must express my deep respectfulness and gratitude to my family for their encouragement and support everything I do throughout my life.

Premwadee Traitangwong



TABLE OF CONTENTS

	Page
ABSTRACT (THAI).....	D
ABSTRACT (ENGLISH).....	E
ACKNOWLEDGEMENTS	F
TABLE OF CONTENTS	G
LIST OF TABLES.....	J
LIST OF FIGURES	L
CHAPTER 1 INTRODUCTION.....	1
1.1. Background.....	1
1.2. Seismotectonic Setting.....	6
1.3. Study Area and Scope of Study.....	9
1.4. Objective.....	11
CHAPTER 2 THEORY AND METHODOLOGY.....	12
2.1. Theory.....	12
2.1.1. Gutenberg-Richter relationship	12
2.1.2. Omori’s Law.....	13
2.1.3. Bath’s Law.....	13
2.1.4. Fractal Dimension	14
2.2. Literature Review.....	14
2.2.1. Gutenberg-Richter relationship	14
2.2.2. Omori’s Law.....	22
2.2.3. Bath’s Law.....	26

2.2.4. Fractal Dimension	28
2.3. Methodology	31
2.3.1. Thesis Preparation	33
2.3.2. Improvement Data.....	33
2.3.3. Earthquake Declustering.....	33
2.3.4. Analyze the Characteristics of Aftershock	33
2.3.5. Comparative Interpretation of Aftershock Characteristics.....	34
CHAPTER 3 SEISMICITY DATA AND COMPLETENESS.....	35
3.1. Earthquake Catalogue Collecting.....	35
3.2 Earthquake Magnitude Conversion.....	39
3.2.1 Body-wave Magnitude (m_b) and Moment Magnitude (M_w).....	40
3.2.2 Surface-wave Magnitude (M_s) and Moment Magnitude (M_w)	41
3.3 Earthquake Declustering	41
3.4. Seismic Source Zone.....	47
CHAPTER 4 AFTERSHOCK CLUSTER.....	52
4.1. Relationship between Magnitude of Mainshock and Its Largest Aftershock.....	53
4.2. Decay rate of aftershock activity.....	59
CHAPTER 5 SEISMIC STRESS AND PATTERN	65
5.1. Rose Diagram.....	65
5.2. Co-seismic Stress.....	70
5.3) Seismic Pattern	79
CHAPTER 6 DISCUSSION.....	83
6.1. Relationship between the Magnitude of Mainshock and Its Largest Aftershock	83

6.2. Decay rate of aftershock activity..... 88

6.3. Co-seismic Stress 90

6.4. D_c and b relationship..... 93

6.5. Rose Diagram..... 96

CHAPTER 7 CONCLUSION 109

REFERENCES 111

VITA..... 121



LIST OF TABLES

	Page
Table 1.1 Maximum aftershock that follow the largest mainshock in the world.....	5
Table 2.1 Characteristic variable of the aftershock sequence observed and estimated have many parameters such as magnitude of mainshock (m_{ms}), magnitude of completeness (M_c), b value, aftershock maximum magnitude (m_{as}), difference between magnitude of mainshock and the maximum aftershock (Δm) (Hamdache et al., 2013).....	28
Table 3.1 Examples of earthquake catalogue.....	36
Table 3.2 The format of the earthquake catalogue is sorted by Longitude, Latitude, Year, Month, Day, Mw, Depth, Hr, Min and Sec.	45
Table 3.3 The example of first output from declustering by run code through python	46
Table 3.4 The example of second output from declustering by run code through python which consists of the aftershocks of mainshock.	47
Table 3.5 Group of the earthquake cluster in each seismic source zones in the MSEA that followed by Pailoplee and Choowong (2013) and the case study that used to analyze the characteristic of the aftershock.....	50
Table 4.1 The relationship between the magnitudes of mainshock and the largest aftershock in the study area is shown in equation.	56
Table 4.2 The difference in magnitude between mainshock and its largest aftershock of seismic source zone in the MSEA.....	59
Table 4.3 Calculated values of p, c and K from the modified Omori's law in the seismic source zone in the MSEA.....	62
Table 5.1 Estimated values of a, b and M_c from the frequency-magnitude distribution in the 13 seismic source zone in the MSEA.	73

Table 5.2 Spatial characteristic (fractal dimension) and seismic pattern in the 13 seismic source zone in the MSEA..... 82

Table 6.1 The case study of the earthquake for 13 seismic source zones (A to M) in the MSEA that represents the distribution of the aftershock occurring after the mainshock and the focal mechanism that indicates the fault types, including the parameters (Remark: Lat=Latitude, Lon=Longitude)..... 97

Table 6.2 Collecting the information used to interpret the relationship of the fault type and the aftershocks distribution for 13 seismic source zones (A to M) in the MSEA. (Remark: D_1 =Normal-dip slip, D_2 =Reverse-dip slip, S_1 =Left-lateral strike slip, and S_2 =Right-lateral strike slip) 103



LIST OF FIGURES

	Page
<p>Figure 1.1 The damage after a strong earthquake (a) the Mw 9.0 earthquake on December 26th, 2004 at off the coast of Sumatra in western Indonesia (https://www.thairath.co.th/) (b) Mw 6.8 earthquake on March 24th, 2011 at Tarlay City, Myanmar (http://www.nydailynews.com)</p>	6
<p>Figure 1.2 Map of the MSEA showing (a) the 13 seismic source zones (b) The remarkable fault zones (Pailoplee and Choowong, 2013).....</p>	7
<p>Figure 1.3 Map of the MSEA and the 13 designated seismic zones (A to M). Red lines indicate the fault lines compiled by Pailoplee et al. (2009). Grey polygons represent the geometry of the individual seismic source zones proposed by Pailoplee and Choowong (2013).....</p>	10
<p>Figure 2.1 Frequency-magnitude distributions of the G-R relationship for (a) İzmit and (b) Düzce aftershocks in Turkey that shown a-value and b value (Bayrak and Öztürk, 2004).....</p>	15
<p>Figure 2.2 (a) Map of the b value for İzmit sequence using all aftershocks with M is more than or equal to 3.4 and starting time is 0.01 days which b value was estimated by the maximum likelihood method. (b) Map of the p value. Both of b and p value are color-coded and plotted at each node (Bayrak and Öztürk, 2004).....</p>	16
<p>Figure 2.3 (a) Map of the b value for Düzce sequence using all aftershocks with M is more than or equal to 3.3 and starting time is 0.01 days which b value was estimated by the maximum likelihood method. (b) Map of the p value. Both of b and p value are color-coded and plotted at each node (Bayrak and Öztürk, 2004).....</p>	17
<p>Figure 2.4 Map of earthquakes ($M \geq 4$) of two aftershock series in off NW Sumatra that related the mainshock of (a) December 26th, 2004 and (b) March 28th, 2005 (Nuannin et al., 2012).....</p>	18
<p>Figure 2.5 Spatial distribution of b values (left) and p values (right) in the 2004 earthquake. The red color is represented the high b and p values while the blue</p>	

color is represented the low b and p values. The star marks the epicenter of the 2004 mainshock (Nuannin et al., 2012)..... 18

Figure 2.6 Spatial distribution of b value (left) and p value (right) in the 2005 earthquake (Nuannin et al., 2012). The red color is represented the high b and p values while the blue color is represented the low b and p values. The star marks the epicenter of the 2005 mainshock..... 19

Figure 2.7 Plot of the frequency-magnitude relationship of Gutenberg-Richter's law for the aftershock sequences in South and Southeastern Spain: (a) for the Mula 1999, Bullas 2002, LaPaca 2005 and Lorca 2011 aftershock sequences, (b) for the Adra 1993, Gador 2002, Alboran 1997, Aboran 2008a and 2008b aftershock sequences, (c) for the aftershock sequences Coripe 2007 and 2008 (Hamdache et al., 2013). 20

Figure 2.8 Frequency-magnitude distribution of the G-R relationship is calculated by the maximum likelihood method that show b value and magnitude of completeness (M_c) (Yadav et al., 2012)..... 22

Figure 2.9 Graph shows the occurrence rate of the aftershock sequences in South and Southeastern Spain as a function of time that composed of the p, c and k parameters: (a) for the Mula 1999, Bullas 2002, LaPaca 2005 and Lorca 2011 aftershock sequences, (b) for the Adra 1993, Gador 2002, Alboran 1997, Aboran 2008a and 2008b aftershock sequences and (c) for the aftershock sequences Coripe 2007 and 2008 (Hamdache et al., 2013)..... 23

Figure 2.10 The correlation between the b and p values (Hamdache et al., 2013). The black circles represent the b and p value in each aftershock sequence. The dashed lines are indicated to 95% of confidence limits..... 25

Figure 2.11 Graph show the occurrence rate of the aftershock sequences in Pakistan as a function of time that composed of the p, c and k parameters from the modified Omori's law (Yadav et al., 2012). 26

- Figure 2.12** A relationship between the magnitude of the mainshock and the maximum magnitude of aftershock (a) for all sequence (b) for the sequence with the number of aftershock ≥ 50 events (Chan and Wu, 2013). 27
- Figure 2.13** Plot log-log scale of the correlation integral versus distance that the fractal dimension (D_c) is estimated by slope of the linear fit the data: (a) for the Mula 1999, Bullas 2002, LaPaca 2005 and Lorca 2011 aftershock sequences, (b) for the Adra 1993, Gador 2002, Alboran 1997, Aboran 2008a and 2008b aftershock sequences and (c) for the aftershock sequences Coripe 2007 and 2008 (Hamdache et al., 2013). 29
- Figure 2.14** The correlation between the fractal dimension and the b value (Hamdache et al., 2013). The plot of Chen et al. (2006) is shown in dash lines. The regression plot is shown as solid line that acquired $D_c = 1.67b$, with a coefficient of relation equal to 0.92. 30
- Figure 2.15** Graph shows the fractal dimension of the aftershocks distribution. Solid circles present the data for which best fit is performed for the computation of D_c value (Yadav et al., 2012). 31
- Figure 2.16** Simplified flow chart showing the methodology applied in this study... 32
- Figure 3.1** Map of the MSEA and the 13 seismic source zones that proposed by Pailoplee and Choowong (2013) showing the distribution of the earthquake during 1985 to 2017. Red lines indicate the fault lines proposed by Pailoplee et al. (2009). 38
- Figure 3.2** The earthquake catalogue of the NEIC database recorded since 1985 – 2017 (end of August)..... 39
- Figure 3.3** Empirical relationships between moment magnitude (M_w) and body-wave magnitude (m_b) 40
- Figure 3.4** Empirical relationships between Surface-wave Magnitude (M_s) and Moment Magnitude (M_w) 41
- Figure 3.5** Aftershock identification windows in term of (a) space and (b) time are shown as a function of the mainshock magnitude (Stiphout et al., 2012). 44

Figure 3.6 The 13 seismic source zones in the mainland Southeast Asia by Pailoplee and Choowong (2013).....	49
Figure 3.7 Map of the MSEA showing the distribution of the earthquake cluster in 13 seismic source zone a) the cluster of earthquake b) the cluster of earthquake after separated to 13 zones following Pailoplee and Choowong (2013).	51
Figure 4.1 Map showing the case study of the earthquake cluster in each earthquake source zones in the MSEA (stars). Red lines indicate the significant fault zones. The black lines indicate the boundary of 13 seismic source zone.....	53
Figure 4.2 The graph plots of the magnitude of mainshock and the largest aftershock in each other zone in the MSEA.....	57
Figure 4.3 The temporal change of the number of aftershock per day in the 13 seismic source zones and in the MSEA.....	63
Figure 5.1 The rose diagrams showing the distribution of the aftershocks in each cluster of mainshock in the MSEA.	69
Figure 5.2 The frequency-magnitude distribution in the 13 seismic source zones and in the MSEA from the G-R relationship.	72
Figure 5.3 The temporal variations of the b value in the 13 seismic source zones in the MSEA.	77
Figure 5.4 Graph illustrates the fractal dimension of the distribution of aftershock in the 13 seismic source zones and in the MSEA.....	80
Figure 6.1 Map showing distribution of the average difference value between magnitude of the mainshock and the maximum aftershock for 13 seismic source zones (A to M) proposed in the MSEA.	84
Figure 6.2 Map showing distribution of the maximum difference value between magnitude of the mainshock and the maximum aftershock for 13 seismic source zones (A to M) proposed in the MSEA.	85

- Figure 6.3** Map showing distribution of the standard deviation of difference value between magnitude of the mainshock and the maximum aftershock for 13 seismic source zones (A to M) proposed in the MSEA..... 87
- Figure 6.4** The bar chart showing the decay rate of the aftershock (days) for 13 seismic source zones (A to M) proposed in the MSEA, which varies according to the magnitude of the mainshock. 88
- Figure 6.5** The bar chart showing the total number of the aftershocks that occurred after the mainshock for 13 seismic source zones (A to M) in the MSEA as shown by the magnitude of the mainshock, which is from 4.0 to 7.0 (a to d)..... 89
- Figure 6.6** The graph showing the difference between the b values of the mainshock (Pailoplee and Choowong, 2014) and the aftershock (in this study) for 13 seismic source zones (A to M) in the MSEA. 92
- Figure 6.7** The bar chart showing the difference between the b values of the mainshock (Pailoplee and Choowong, 2014) and the aftershock (in this study) for 13 seismic source zones (A to M) in the MSEA. 93
- Figure 6.8** The empirical relationships for 13 seismic source zones (A to M) in the MSEA. (a) Between the D_c and b values and (b) between the D_c values and a/b ratios. The dash lines represent the linear regression fitted with the cluster of earthquake. 94
- Figure 6.9** The relationships between the distribution of aftershocks that divided into 4 quadrants and the fault type in the MSEA..... 107
- Figure 6.10** Coulomb seismic stress changes due to the M_W -5.3 foreshock, M_W -6.4 mainshock and M_W -6.4 mainshock doublet and the distribution of the aftershocks (yellow circles) (Yadav et al., 2012). Red stars represent the foreshock, mainshock and mainshock doublet while the focal mechanism for foreshock, mainshock and mainshock doublet are shown by beach ball..... 108

CHAPTER 1

INTRODUCTION

1.1. Background

The mainland Southeast Asia (MSEA) is considered as one of the most seismically active in the world (Pailoplee and Choowong, 2014). Tectonically, the MSEA, is covered with major structures, basins, and tectonic blocks, which according to the Indo-Australian and Eurasian plate collision (Polachan et al., 1991). The M_W -9.0 earthquake generated on December 26th, 2004 at the Sumatra–Andaman subduction zone has destroyed the infrastructures and buildings in this area and adjacent areas that surrounding its source (Martin, 2005). Based on Park et al. (2005), this earthquake was the third largest earthquake in the world since 1990. In addition, The M_W -6.8 earthquake at Tarlay City, the Thailand-Myanmar border generated on March 24th, 2011 (Wang et al., 2014). And recently, the M_W -6.3 earthquake generated on May 5th, 2014 in the Northern Thailand. According to the major earthquakes mentioned above, it is possible to identify that the MSEA region is a significant earthquake source that caused severe damage and casualties. In addition, from the instrumental earthquake records, it is known that there is still a continuous hazardous earthquakes in this area. Therefore, the MSEA should be clarified the earthquake hazard.

According to previous research work in the MSEA, seismologists have studied about several earthquake forecasting methods in the study area for help to reduce loss of life and property. The methods can be divided into two main parts, e.g., i) Paleo-seismological study and ii) Statistical seismology. This information can be explained about the characteristic of the earthquake such as seismotectonic and the earthquake in terms of time, space and magnitude. In this section shown research works about the earthquake in the MSEA region.

Up to the present, several techniques of earthquake studies are developed that are organized in a group called the statistical seismology e.g. seismicity rate

change (Z value) (Wiemer and Wyss, 1994), Region-Time-Length algorithm (RTL) (Sobolev and Tyupkin, 1997), Frequency-magnitude distribution (Gutenberg and Richter, 1944) and Fractal Dimension (Grassberger and Procaccia, 1983).

According to Region-Time-Length algorithm (RTL) (Sobolev and Tyupkin, 1997), this method use for investigate the anomalous of seismic quiescence and activate before the large earthquakes and provide the information for determining the hazardous area that might be generated by the large earthquakes in the future. Sukrungsri and Pailoplee (2015) applying Region-Time-Length algorithm (RTL) evaluate precursory seismicity changes before the major earthquakes along the Sumatra-Andaman subduction zone, the result shown the seismic quiescence state started 0.1-5.2 years before the main shock and revealed that there are four prospective areas might be generated by the upcoming large earthquakes, namely i) Aceh city, northernmost of Sumatra Island, ii) Offshore western Sumatra Island, iii) Sittwe city, western Myanmar and iv) Offshore northern Nicobar Islands, Traitangwong and Pailoplee (2017) using RTL-algorithm to evaluate precursory seismicity changes along the Sagaing fault zone, Central Myanmar, the result shown the quiescence maps that indicated the western Myitkyina and the area in the vicinity of the Naypyidaw are the risk area from the major earthquakes in the future. And Pipattanajaroenkul (2014) applying RTL-algorithm to evaluated the precursory seismicity changes along the western Thailand border, the result shown the quiescence maps that indicated the area in northern part that covers the Pan Luang fault and Moei-Tongyi fault and the area in southern part that covers the Tavoy fault, the Three pagoda fault and the Sri sawat fault are the risk area from the major earthquakes in the future.

Based on seismicity rate change (Z value) (Wiemer and Wyss, 1994), this technique using investigate the anomalous of seismic activities before major earthquake and indicated the potential risks same Region-Time-Length algorithm (RTL) (Sobolev and Tyupkin, 1997). For example, Puangjaktha and Pailoplee (2018)

study the potential risk areas of the strong to major earthquake in future in the Thailand-Laos-Myanmar border region that using the seismicity rate change (Z value) method to applied, the result shown there are two prospective areas might be generated by the upcoming major earthquakes: the eastern part of Myanmar and some areas in the northern part of Laos. Pailoplee et al. (2017) evaluated Z value along the Sagaing fault zone, Central Myanmar that shown the Sagaing fault along Myitkyina and Naypyidaw cities might be posed by the hazardous earthquake in the future as same the results of Traitangwong and Pailoplee (2017). And then, Panwoon (2014) applying Z value to evaluated seismicity rate change along the strike-slip fault system, Thailand-Myanmar border that shown the prospective areas might be generated by the upcoming major earthquakes as same. As mentioned above, Region-Time-Length algorithm (RTL) and seismicity rate change (Z value) will only be studied with the mainshock in order to identify potential risk areas in the future.

Besides, there are other techniques to study the earthquake. (Pailoplee and Choowong, 2013) estimate the probabilities of earthquake occurrences in the MSEA region using the concept of frequency-magnitude distributions (Gutenberg and Richter, 1944), which results in 100% probabilities of earthquake 6.0 occur in the next 25 years in the MSEA. One year later, Pailoplee and Choowong (2014) obtain the relationship between parameter from the frequency-magnitude distributions (Gutenberg and Richter, 1944) and the fractal dimension (Grassberger and Procaccia, 1983) that imply the level of tectonic stress and interpret as if any area have high-tectonic stress, it is prospective area that might be generated by the upcoming large earthquakes.

From all of the above, statistical seismology in the MSEA, there are only studies related to mainshock. In general, the earthquake is one of the most devastating disasters that caused damage to the economy and loss of life. Not only does the mainshock caused damage and fatalities, but the aftershock also affected

as same as because when mainshock occur, it will cause many damage or the structure cracks. And then, the aftershock followed, it causes more damage or the structure cracks that may collapse. This is reason why this study chose to study about the characteristics of the aftershock in the MSEA.

According to the earthquake sequence, one cluster of earthquake consists of 3 types, i.e., i) foreshock, ii) mainshock and iii) aftershock. This damage is mainly caused by the main shock because the mainshock will be the largest magnitude, but the aftershock can also affect and cause harm as well (Figure 1.1). Based on literature review, when the M_W -9.0 earthquake on December 26th, 2004 at off the coast of Sumatra in western Indonesia, then it caused the M_W -6.9 aftershock in same area, which compared with the M_W -6.8 mainshock earthquake at Tarlay city, Myanmar. It can be seen that not only does the mainshock caused damage and fatalities, but the aftershock also affected as same as. Moreover, when aftershocks occur several times, they may affect to buildings and structures that have been damaged by the mainshock, resulting in more subsidence and rupture. For this reason, it can be said that the aftershock is also a disaster.

Therefore, it is essential to study the characteristic of aftershock in order to be used the information for assessing aftershock in the future and used to plan for prevent and mitigate potential disasters in the future.

Table 1.1 Maximum aftershock that follow the largest mainshock in the world.

Location	Date	Mainshock	Maximum Aftershock
Off the West Coast of Northern Sumatra	26 Dec 2004	9.1	6.9
Near the East Coast of Honshu, Japan	11 Mar 2011	9.0	7.1
Offshore Maule, Chile	27 Feb 2010	8.8	7.1
Assam Tibet	15 Aug 1950	8.6	8.0
Northern Sumatra, Indonesia	28 Mar 2005	8.6	6.7
Northern coast of Chile	01 Apr 2014	8.2	7.6
Nepal	25 Apr 2015	7.9	7.3
West of Port-au-Prince, Haiti	12 Jan 2010	7.0	5.9
Tarlay, Myanmar	24 Mar 2011	6.9	5.5





Figure 1.1 The damage after a strong earthquake (a) the Mw 9.0 earthquake on December 26th, 2004 at off the coast of Sumatra in western Indonesia (<https://www.thairath.co.th/>) (b) Mw 6.8 earthquake on March 24th, 2011 at Tarlay City, Myanmar (<http://www.nydailynews.com>)

1.2. Seismotectonic Setting

Tectonic activity in the MSEA region is caused by the collision of the Indo-Australian and Eurasian tectonic plates (Polachan et al., 1991, Fenton et al., 2003) that the several major earthquake in this region occur due to Indo-Australian plate move to underneath Eurasian plate. According to Pailoplee and Choowong (2013), the seismic source zones in the MSEA region can be divided into 13 zones (Figure 1.2) which the detail can be explained as follow.

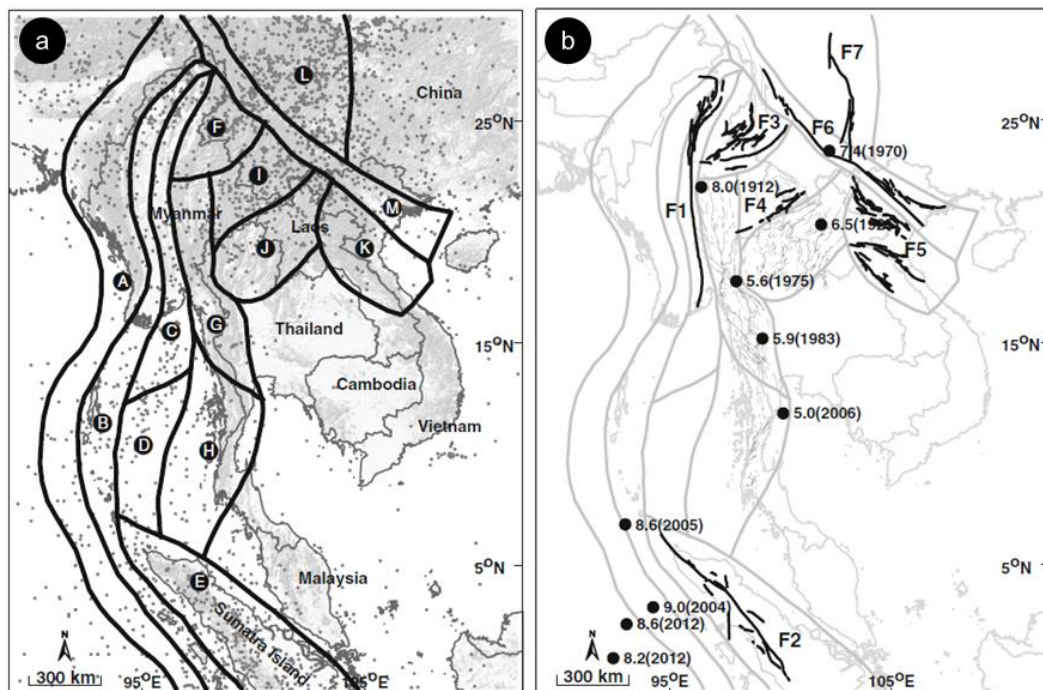


Figure 1.2 Map of the MSEA showing (a) the 13 seismic source zones (b) The remarkable fault zones (Pailoplee and Choowong, 2013).

The Sumatra-Andaman subduction zone is related to the collision zone between the Indo-Australian and Eurasian plate that divided into two seismotectonic setting as follows. The Sumatra-Andaman Interplate (zone A) is generated a shallow-focus earthquakes while the Sumatra-Andaman Intraslab (zone B) is generated an intermediate to deep-focus earthquake (>35 km.) under the western Myanmar, Sumatra and Nicobar Islands (Paul et al., 2001).

For the Sagaing fault zone (zone C), which is a right strike-slip active fault zone that striking north-south direction in the central part of Myanmar. The highest slip rate of this fault is approximately 23 mm/yr. (Bertrand and Rangin, 2003)

Beside the Sumatra-Andaman subduction zone, Zone D, the Andaman Basin is determined as the backarc region in the Sumatra-Andaman subduction zone which has the active east-west rifting process until now (Rajendran et al., 2003, Khana and Chakraborty, 2005).

While, the major inland strike-slip faults in the southern part of Sumatra-Andaman Intraslab is called the Sumatra fault zone (zone E) that trending northwest-southeast in Sumatra Island.

The strike-slip fault systems along the Thailand-Laos-Myanmar borders are divided into two systems. First, the northeast-southeast strike-slip faults are defined as zone H that including the Ranong and Klong Marui fault zones. And second, the northwest-southeast strike-slip faults are grouped into zone G that consist of i) Sri Sawat fault (Nuttee et al., 2005), ii) Moei-Tongyi fault (Pailoplee et al., 2009) and iii) Three Pagoda fault (Rhodes et al., 2015).

Some active faults are located in the northern Thailand such as the Lampang-Phrae (Udchachon et al., 2005), Theon (Charusiri et al., 2004) and Mae Tha fault zones (Rhodes et al., 2004) that are grouped into the northern Thailand-Dein Bein Phu (zone J) (Pailoplee and Choowong, 2013).

For the northern Vietnam, northern Myanmar, southern China, and northern Laos are located in the northern part of the MSEA which relate to the Indo-Australian and Eurasian plate collision that cause of the NE-SW and NW-SE complex shear zone and the strike-slip fault (Polachan et al., 1991). In this region is divided into two seismic source zones that consist of i) the Hsenwi-Nanting fault zones (zone F) and ii) Jinghong-Mengxing fault zones (zone I) (Lacassin et al., 1998).

In the eastern part of the MSEA, the Northwest-Southeast fault zones are located in the northern Vietnam such as the Song Da, Song Ma fault (Phoung, 1991), Song Ca fault (Takemoto et al., 2005) and Song Chay fault (Cuong and Zuchiewicz, 2001). In this region, all fault zones are defined as zone K, namely the Song Da-Song Ma fault zones. In addition, there is a significant fault zone in the eastern part of the MSEA which namely the Red River fault zone (zone M) that striking along the China-Vietnam border with 810 km. (Duong and Feigl, 1999).

In the southern China, there is a last seismic source zone in the MSEA region which relate to the Eurasian plate. This seismic source zone are defined as zone L, namely the Xianshuihe fault zone that lies in north-south direction (Eleftheria et al., 2004).

1.3. Study Area and Scope of Study

In this study, focuses on the analysis of characteristics of aftershock in the MSEA which is located between latitudes 4°N 33°N and longitudes 86°E 115°E (Figure 1.3). According to Pailoplee and Choowong (2013), the MSEA is separated to 13 seismic source zone that cover many countries such as Thailand, Myanmar, China, Laos, Cambodia, Vietnam and Indonesia (Sumatra-Andaman). Geographically, the MSEA is the one of the most seismically active regions that is generated a frequent and large earthquake from the past to the present. There are many largest earthquake that will generate a severe impact on both life and property and the potential hazards. This is the reason why this area is chosen. In this study, using the several method for analysis of characteristics of aftershock. First method is the Gutenberg-Richter relationship which can also be called b-value can be describe the seismic stress change (Gutenberg and Richter, 1944). Next, the modified Omori's law is a law for analyze the decay rate of aftershock activity (Utsu et al., 1995). And then, the maximum magnitude of aftershock that compare with mainshock can be described by the Bath's law (Bath, 1965). The last method for analyze the seismic pattern of earthquake is the fractal dimension (Grassberger and Procaccia, 1983).

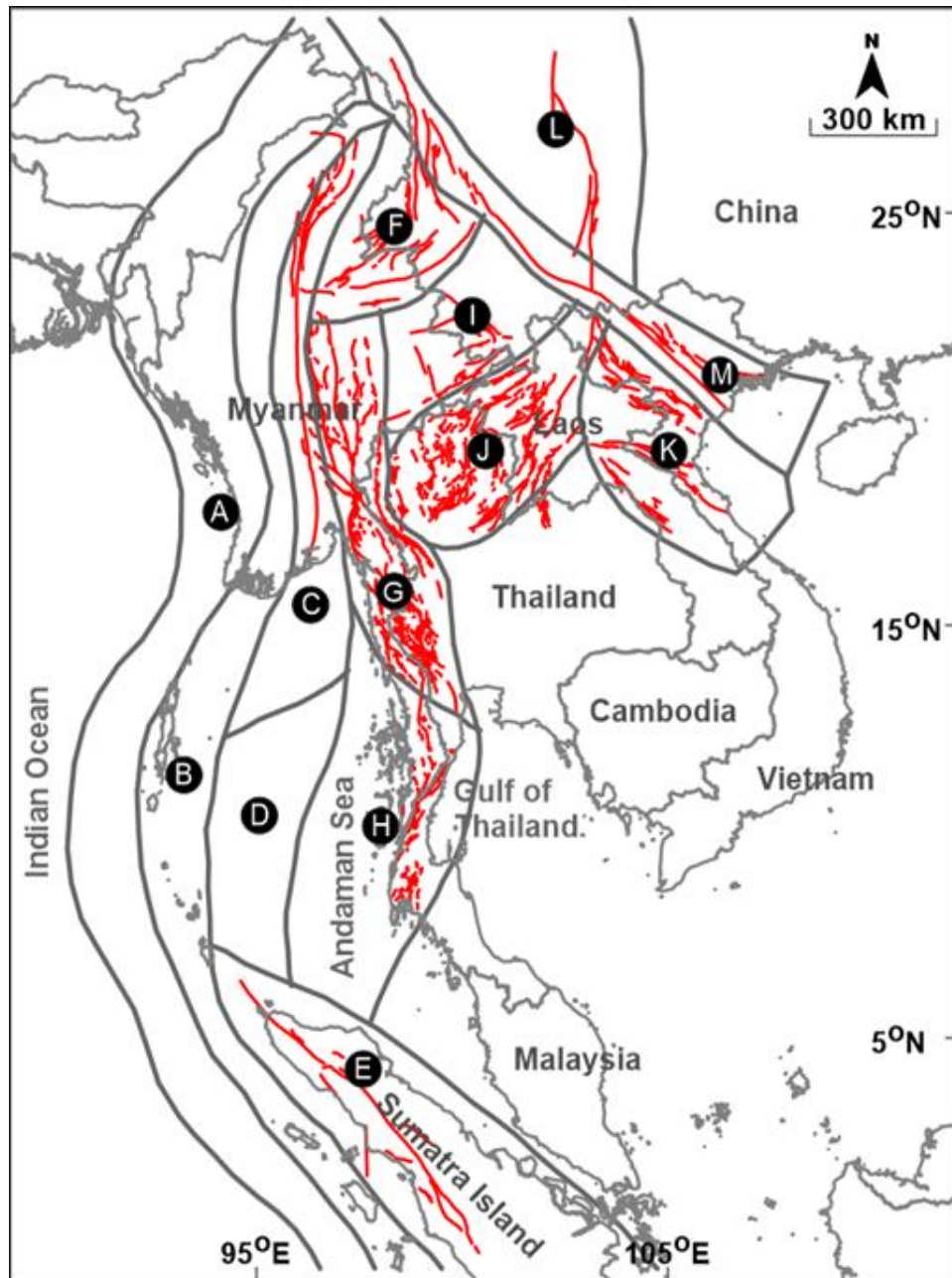


Figure 1.3 Map of the MSEA and the 13 designated seismic zones (A to M). Red lines indicate the fault lines compiled by Pailoplee et al. (2009). Grey polygons represent the geometry of the individual seismic source zones proposed by Pailoplee and Choowong (2013)

1.4. Objective

From the previous works described above, in most cases, the statistical seismology in the MSEA will focus on the mainshock. Whether it is describing the characteristics of the earthquake in terms of time, space and magnitude including the damage and impact. However, in the statistical seismology investigation that focused on the aftershock in this area is not enough. In addition, from the review of data on the damage caused by the earthquake, it is not only the mainshock but also, the aftershock can affect both life and property as well, or the impact is greater. For this reason, this study will only focus on the aftershock in the MSEA. The purposes of this study are,

- To evaluate the characteristics of the aftershock (the maximum magnitude and decay rate of aftershock activity as compared to mainshock) in the MSEA.
- To study the pattern of the earthquake (point, line and plane) of the aftershock in the MSEA.
- To analyze the seismic stress changes after the mainshock in the MSEA.

CHAPTER 2

THEORY AND METHODOLOGY

From the past until now, there are many earthquake forecasting techniques that developed by seismologists based on field investigation, basis knowledge about geotectonic and historical earthquakes (Charusiri et al., 2007). Based on literature reviews, mostly seismologists choose to use the statistical seismicity methods to analyze and evaluate behavior of the earthquake. The statistical methods are several methods that are mostly used for only study about mainshock but some technique, it is used for analyze the aftershock.

This section describes the concept of statistical seismicity and process of analysis of characteristics of the aftershock in the MSEA. According to literature reviews, the theory that will be used in this analysis about the aftershock, found that there are several concepts as follows, i.e., i) Gutenberg-Richter's law, ii) Omori's law, iii) Bath's law and iv) Fractal Dimension that explained in detail as follows.

2.1. Theory

2.1.1. Gutenberg-Richter relationship

The aftershock activity is described by the empirical relation which namely the Gutenberg-Richter magnitude-frequency relationship (G-R relationship). This relation is a power law of size distribution during the aftershock that is well described by Gutenberg and Richter (1944). The equation used in this study can be expressed as equation (2.1).

$$\log(N) = a - bM \quad (2.1)$$

Where N is the cumulative number of earthquake with magnitude equal to or greater than M , and a and b are empirical constants vary in a specific time and window. The

constant a describes the seismic activity, whereas the constant b indicates the tectonic parameter that describing tectonic stress and the relative occurrence of small to large earthquake. Higher b values related to decrease the accumulated stress (Scholz, 1968, Wyss, 1973).

2.1.2. Omori's Law

Theoretically, the temporal decay of aftershock activity from the mainshock is well described by the modified Omori's law (Utsu, 1961) which express as (2.2).

$$n(t) = \frac{K}{(t + c)^p} \quad (2.2)$$

Where $n(t)$ is the number of aftershocks per unit time (t) after the mainshock, K , p and c are parameter constants. The parameter K is determined by the total number of events in the sequence, the constant c is controlled by the rate of activity in the beginning part of the sequence. And the p value is a crucial parameter which describes the frequency of the decay of aftershocks. From Omori's law, p value is equal to 1 but in generally, p value varies from 0.9 to 1.5 (Utsu et al., 1995) or changes between 0.6-1.8 (Wiemer and Katsumata, 1999) which the variability of value depends on the condition of tectonic in the region such as the structural heterogeneity, stress and temperature of the crust. Therefore, this law is one of the way used to describe the characteristics of aftershock.

2.1.3. Bath's Law

The maximum magnitude of aftershock which follow a mainshock is the essential behavior of aftershock. Based on literature review, the largest aftershock of the mainshock can be described by the relationship called Bath's law. This law represents the difference ΔM between the magnitude of the mainshock (M_{ms}) and the largest aftershock (M_{as}^{max}) is shown in the equation 2.3.

$$\Delta M = M_{ms} - M_{as}^{max} \quad (2.3)$$

Where ΔM is about 1.2 that reference from the concept of Bath in 1965.

2.1.4. Fractal Dimension

In order to investigate the spatial clustering of aftershock, the spatial fractal dimension is the way to help in this study which used correlation integral mode (Grassberger and Procaccia, 1983) that shown in the equation 2.4.

$$C(r) = \frac{2}{N(N-1)} N(R < r) \quad (2.4)$$

Where N is the number of earthquakes investigated and $N(R > r)$ is the number of event pairs separated by R distance smaller than r . If the distribution is fractal, the relation will follow the equation 2.5 (Kagan and Knopoff, 1980).

$$C(r) \sim r^{D_c} \quad (2.5)$$

Where D_c is the spatial fractal dimension that can be estimated by the slope of the best-fitted linear of graphs $\log(C(r)) - \log(r)$. According to Khattri (1995) and Yadav et al. (2011), D_c value will be interpreted differently, as D_c approach zero, the distribution of all events is concentrated in one point. In case of D_c close to 1, the distribution of events will be approach into line. If close to 2 indicates that the events is distributed to plane pattern. When tends to 3, it can be indicated that the earthquake fractures are filling up a crustal volume.

2.2. Literature Review

2.2.1. Gutenberg-Richter relationship

Bayrak and Öztürk (2004), study the characteristics of the aftershock that shown the spatial and temporal variations in the five months after the mainshock in August 17th, 1999 at İzmit and November 12th, 1999 at Düzce in Turkey by using the b value of the G-R relationship for analyze that estimated by the maximum likelihood

method, found that the magnitude of completeness (M_c) is about 2.6 for İzmit and 2.8 for Düzce. And the b value is calculated as 1.10 ± 0.03 and 1.16 ± 0.05 , respectively (Figure 2.1). After that, the b value in terms of spatial variation for İzmit is remain varies from 0.8 to 1.5 in İzmit and from 0.8 to 1.6 in Düzce. The lower b values indicate that there has been a rise of the stress and occur the largest fault plane that are found in near the epicenter of the mainshock, followed Figure 2.2a and 2.3a. Furthermore, the p value is a statistical method for analyze the characteristics of the aftershock in this work that is described in the next section.

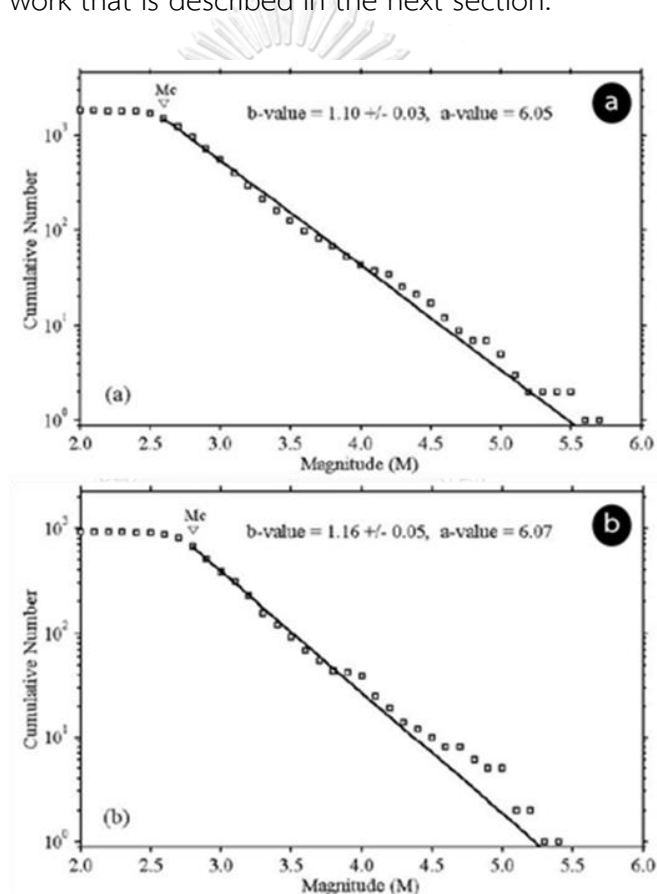


Figure 2.1 Frequency-magnitude distributions of the G-R relationship for (a) İzmit and (b) Düzce aftershocks in Turkey that shown a-value and b value (Bayrak and Öztürk, 2004).

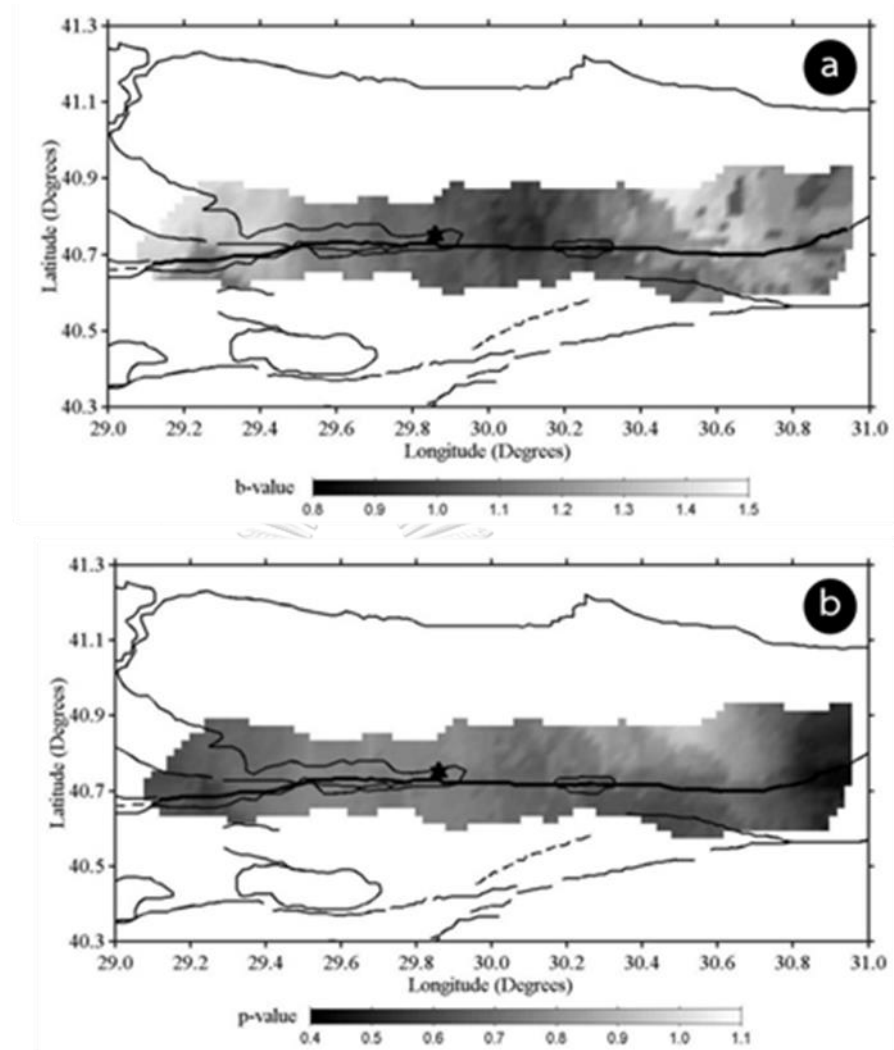


Figure 2.2 (a) Map of the b value for İzmit sequence using all aftershocks with M is more than or equal to 3.4 and starting time is 0.01 days which b value was estimated by the maximum likelihood method. (b) Map of the p value. Both of b and p value are color-coded and plotted at each node (Bayrak and Öztürk, 2004).

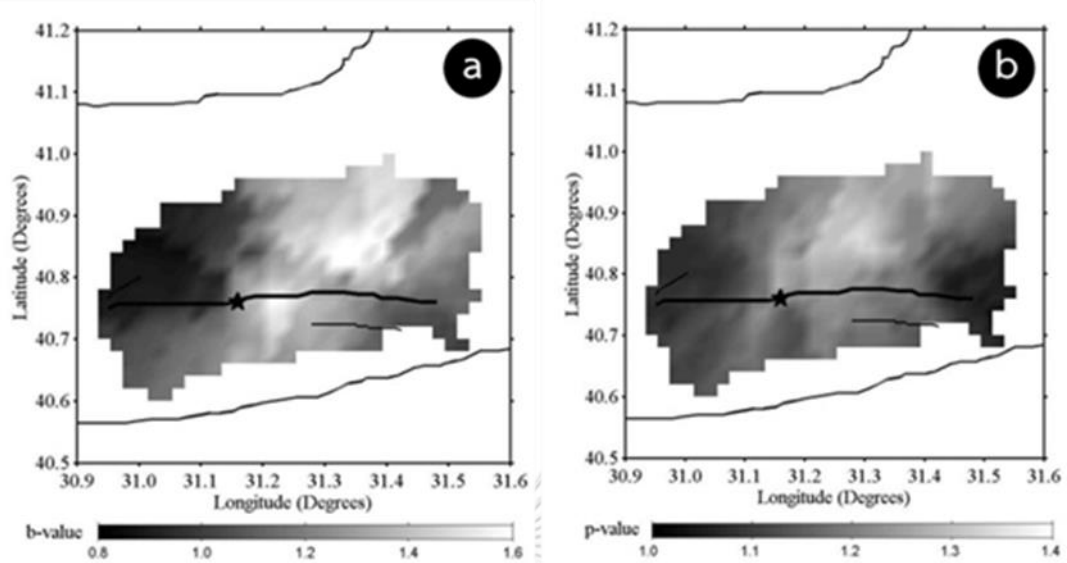


Figure 2.3 (a) Map of the b value for Düzce sequence using all aftershocks with M is more than or equal to 3.3 and starting time is 0.01 days which b value was estimated by the maximum likelihood method. (b) Map of the p value. Both of b and p value are color-coded and plotted at each node (Bayrak and Öztürk, 2004).

Nuannin et al. (2012), analyze the spatial and temporal characteristics of two aftershock series in off NW Sumatra (Figure 2.4) by using the maximum likelihood method for calculate the b value of frequency-magnitude distribution. Based on the largest earthquake of the December 26th, 2004 ($M_W = 9.0$), the b value in the spatial distribution varies from 0.74 to 1.66 while the spatial distribution of b value on March 28th, 2005 ($M_W = 8.6$) varies from 1.1 to 2.1, followed Figure 2.5a and 2.6a. The temporal variation of the b value in this study, areas of low b value will be shown as this area is increased the accumulate stress. In 2004, before the largest earthquake roughly 6 months, the b value were reduced around 1.8 to 1.4, which means preparing to release energy or earthquake will be occurred. Moreover, this work uses other methods for analyzing the characteristics of aftershock sequences that is explained in the next section.

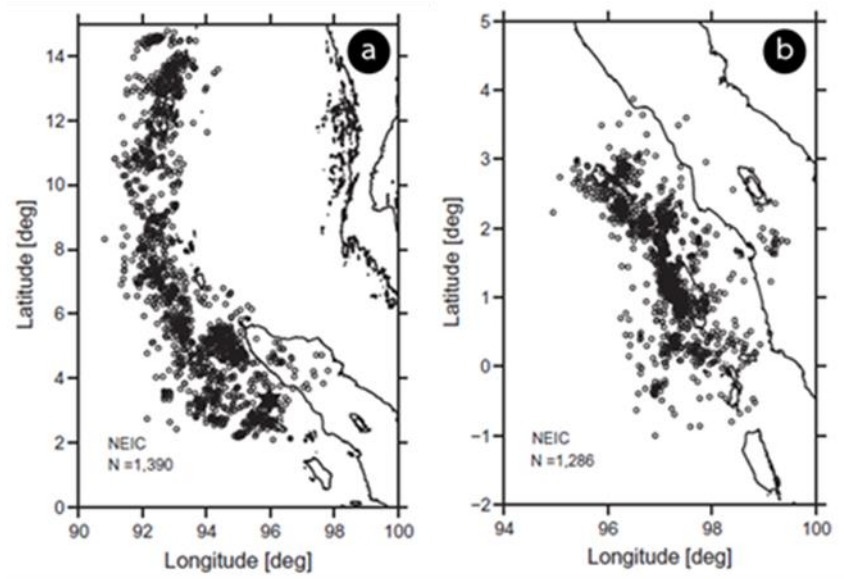


Figure 2.4 Map of earthquakes ($M \geq 4$) of two aftershock series in off NW Sumatra that related the mainshock of (a) December 26th, 2004 and (b) March 28th, 2005 (Nuannin et al., 2012).

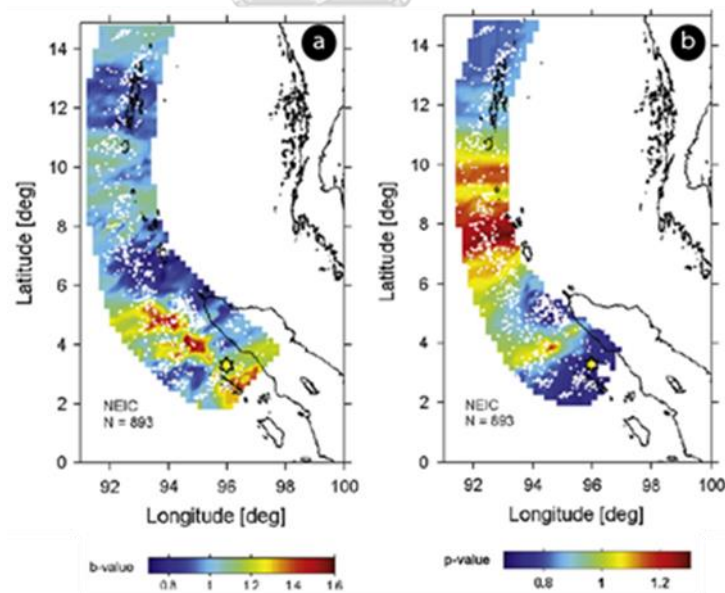


Figure 2.5 Spatial distribution of b values (left) and p values (right) in the 2004 earthquake. The red color is represented the high b and p values while the blue color is represented the low b and p values. The star marks the epicenter of the 2004 mainshock (Nuannin et al., 2012).

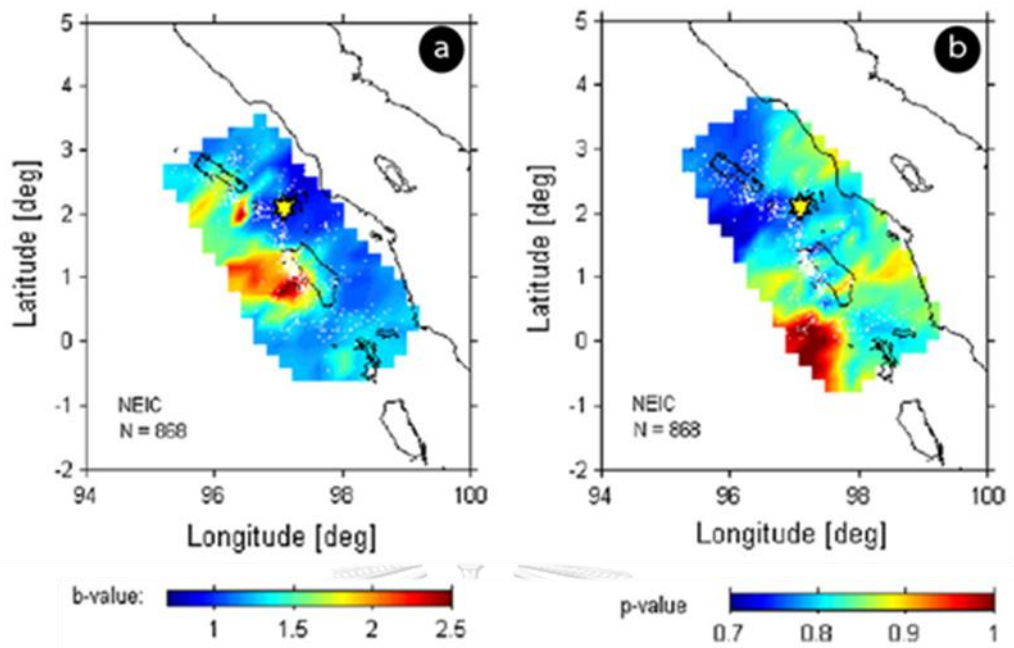


Figure 2.6 Spatial distribution of b value (left) and p value (right) in the 2005 earthquake (Nuannin et al., 2012). The red color is represented the high b and p values while the blue color is represented the low b and p values. The star marks the epicenter of the 2005 mainshock.

Hamdache et al. (2013), study the characteristics of eleven aftershock sequence, as occurred in the South and Southeast of Spain by b value parameter. The evaluated b value that was found from 0.77 ± 0.05 to 1.18 ± 0.10 (Figure 2.7), which the estimated b value close to the typical value from the frequency-magnitude relationship ($b \sim 1$). In addition, study the relationship between the fractal dimension and b value and the relation between b and p value which discussed in the next section.

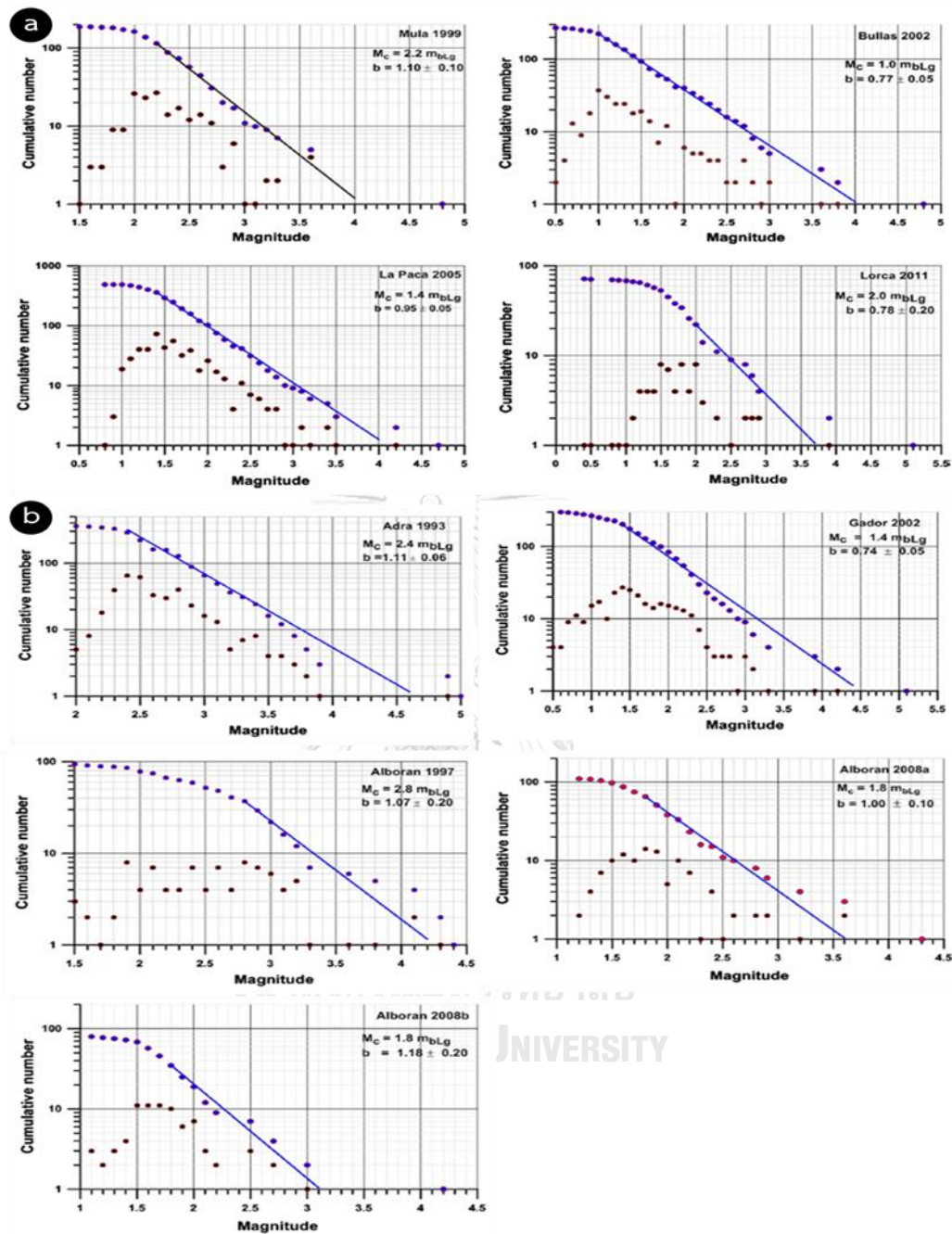


Figure 2.7 Plot of the frequency-magnitude relationship of Gutenberg-Richter's law for the aftershock sequences in South and Southeastern Spain: (a) for the Mula 1999, Bullas 2002, LaPaca 2005 and Lorca 2011 aftershock sequences, (b) for the Adra 1993, Gador 2002, Alboran 1997, Alboran 2008a and 2008b aftershock sequences, (c) for the aftershock sequences Coripe 2007 and 2008 (Hamdache et al., 2013).

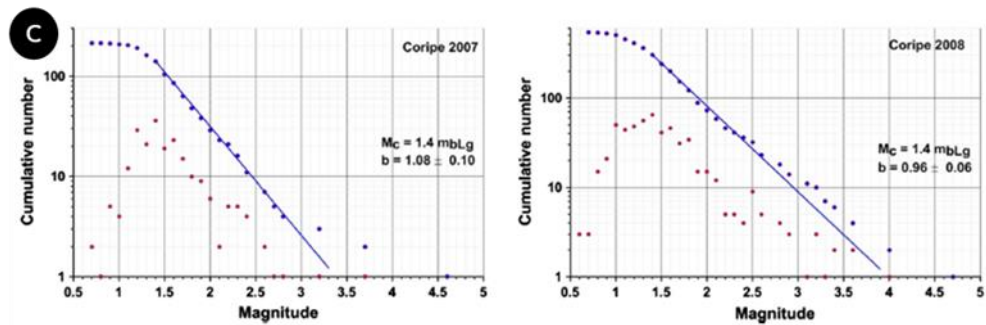


Figure 2.7 (Cont.) Plot of the frequency-magnitude relationship of Gutenberg-Richter's law for the aftershock sequences in South and Southeastern Spain: (a) for the Mula 1999, Bullas 2002, LaPaca 2005 and Lorca 2011 aftershock sequences, (b) for the Adra 1993, Gador 2002, Alboran 1997, Aboran 2008a and 2008b aftershock sequences, (c) for the aftershock sequences Coripe 2007 and 2008 (Hamdache et al., 2013).

Yadav et al. (2012), study the characteristics of the aftershock from 6.4 earthquake during the 2008 Baluchistan in southwestern Pakistan by using statistical analysis as b values, p values, fractal dimension and energy partitioning due to aftershock. In this section shows the b value that is calculated by the maximum likelihood is 1.03 ± 0.42 (Figure 2.8), which are close to the value that is specified about 1.0 (Udias, 1999). The other statistical analysis methods are described in the next section.

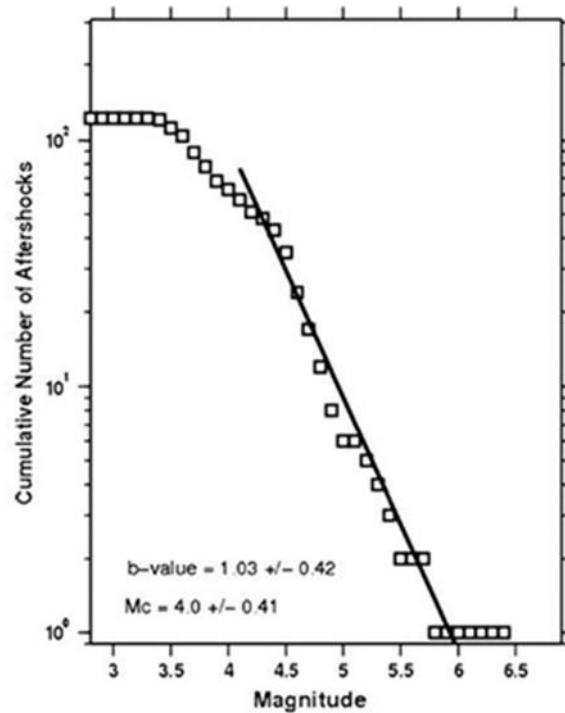


Figure 2.8 Frequency-magnitude distribution of the G-R relationship is calculated by the maximum likelihood method that show b value and magnitude of completeness (M_c) (Yadav et al., 2012).

2.2.2. Omori's Law

Bayrak and Öztürk (2004), study the spatial and temporal variations in the five months after the mainshock in the August 17th, 1999 at İzmit and in the November 12th, 1999 at Düzce in Turkey by using the b and p values for analyze, found that the p value of İzmit remain varies from 0.4 to 1.1. While in Düzce, the p value remain varies from 1.0 to 1.1. From figure 2.2 and 2.3, The lower b value is related to the higher p value, which indicate that there has been a rise of the stress and occur the largest fault plane that are found in near the epicenter of the mainshock.

Nuannin et al. (2012), analyze the spatial and temporal characteristics of two aftershock series by using the b and p value. Based on the largest earthquake of the December 26th, 2004 ($M_w = 9.0$) and the March 28th, 2005 ($M_w = 8.6$) in off NW Sumatra (Figure 2.4) found that the p value in the spatial variation remain from 0.69

to 1.25 and 0.7 to 1.0, respectively (Figure 2.5 b and 2.6 b). Areas of high p value will be shown as this area is faster decay rate activity of aftershock that located on the far from the hypocenter which relate to low b value that is negative relationship.

Hamdache et al. (2013), study the characteristics of eleven aftershock sequence, as occurred in the South and Southeast of Spain by two parameters: b value and p value. The evaluated p value that was found from 0.75 ± 0.03 to 1.43 ± 0.10 , which the estimated p value demonstrates a decay rate of aftershock (Figure 2.9). As while the relation between b and p value has negative relationship from the graph that shown in equation $p = -1.90b + 2.82$ and $r^2 = 0.92$ (Figure 2.10).

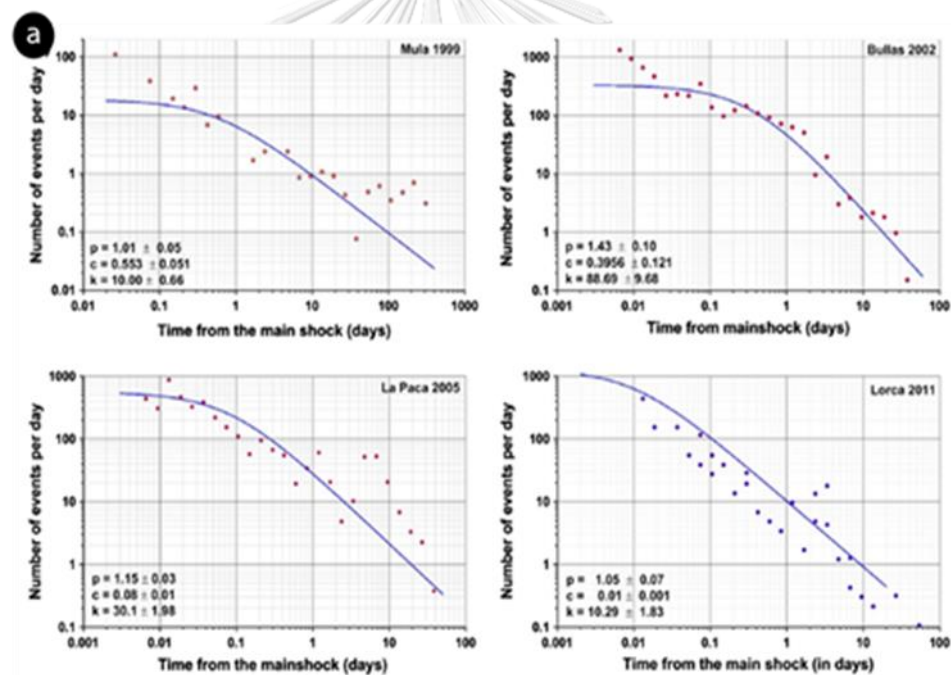


Figure 2.9 Graph shows the occurrence rate of the aftershock sequences in South and Southeastern Spain as a function of time that composed of the p, c and k parameters: (a) for the Mula 1999, Bullas 2002, LaPaca 2005 and Lorca 2011 aftershock sequences, (b) for the Adra 1993, Gador 2002, Alboran 1997, Aboran 2008a and 2008b aftershock sequences and (c) for the aftershock sequences Coripe 2007 and 2008 (Hamdache et al., 2013).

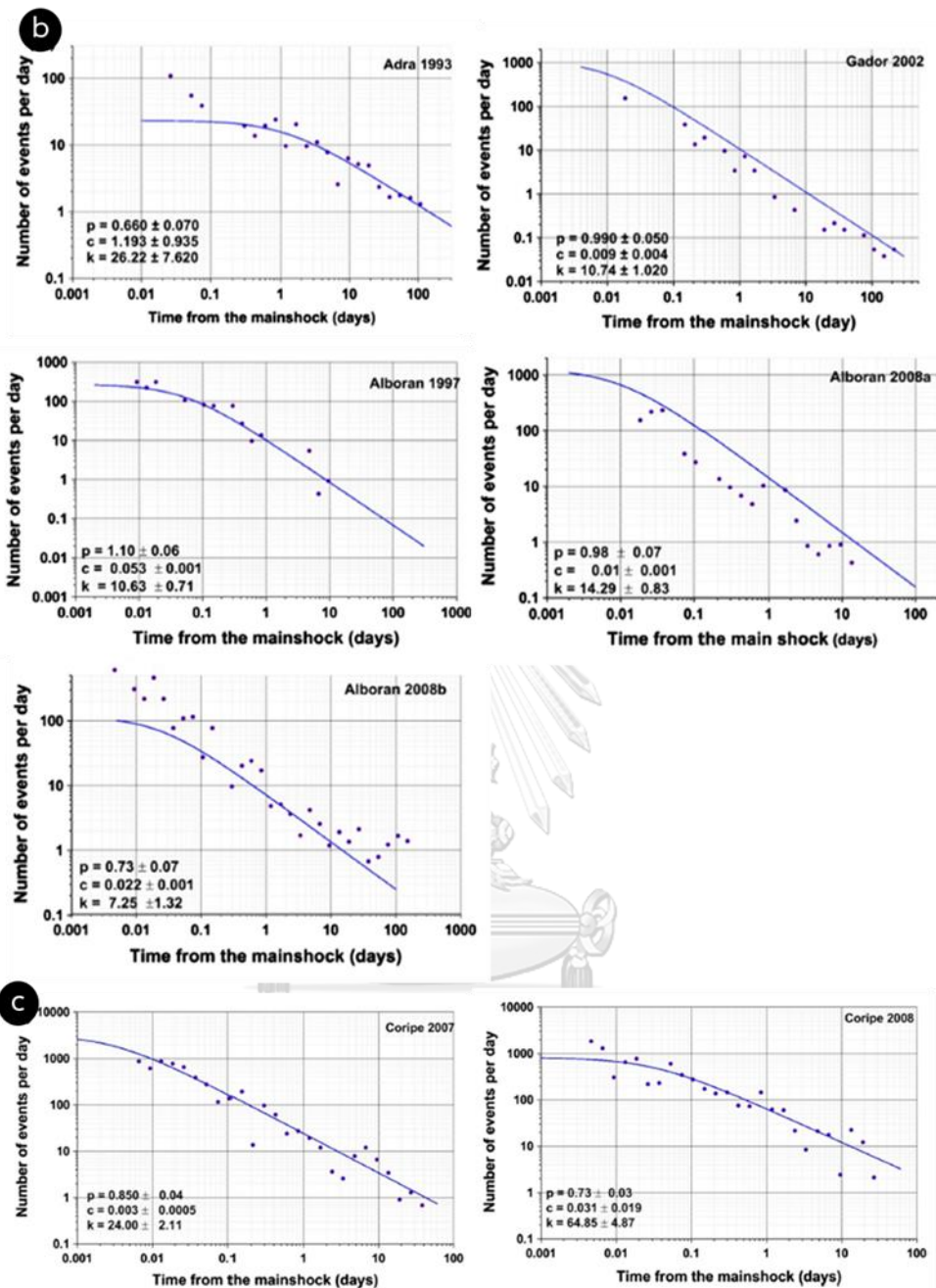


Figure 2.9 (Cont.) Graph shows the occurrence rate of the aftershock sequences in South and Southeastern Spain as a function of time that composed of the p , c and k parameters: (a) for the Mula 1999, Bullas 2002, LaPaca 2005 and Lorca 2011 aftershock sequences, (b) for the Adra 1993, Gador 2002, Alboran 1997, Aboran 2008a and 2008b aftershock sequences and (c) for the aftershock sequences Coripe 2007 and 2008 (Hamdache et al., 2013).

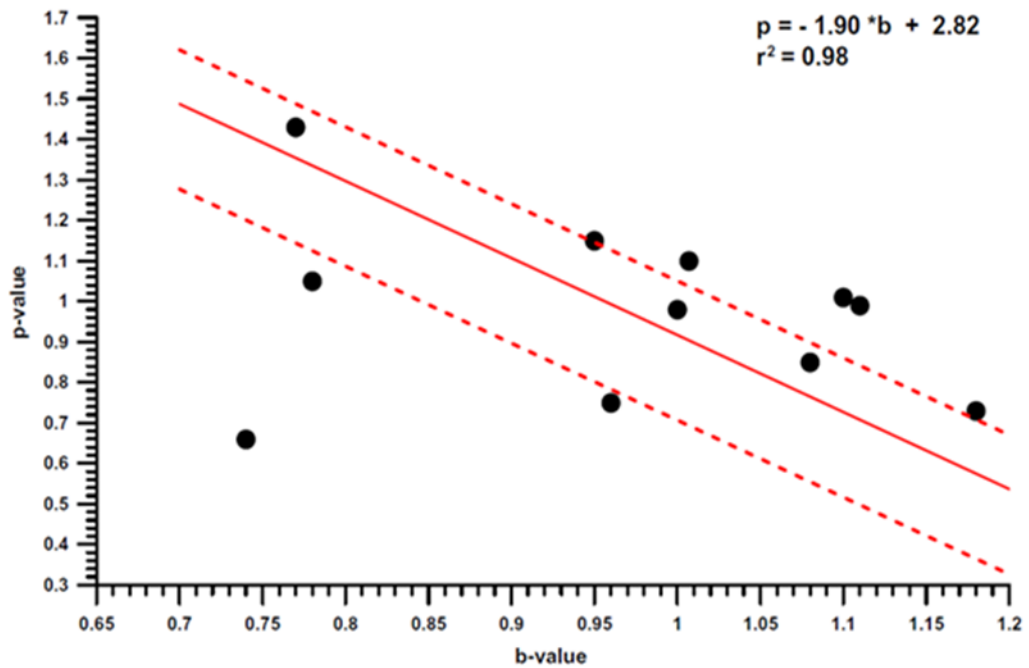


Figure 2.10 The correlation between the b and p values (Hamdache et al., 2013). The black circles represent the b and p value in each aftershock sequence. The dashed lines are indicated to 95% of confidence limits.

Yadav et al. (2012), study the characteristics of the aftershock from 6.4 earthquake during the 2008 Baluchistan in southwestern Pakistan by using statistical analysis as b value, p value, fractal dimension and energy partitioning due to aftershock. The p value is 0.89 ± 0.07 , which will be less than the standard values from the Omori, 1984 that indicated slowly the decay rate of aftershock activity in area (Figure 2.11).

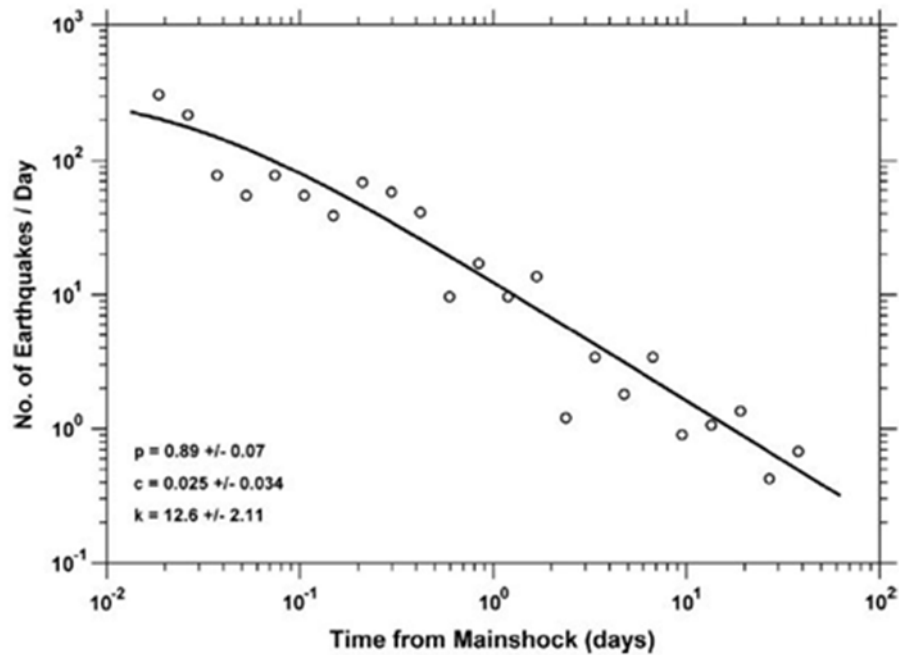


Figure 2.11 Graph show the occurrence rate of the aftershock sequences in Pakistan as a function of time that composed of the p , c and k parameters from the modified Omori's law (Yadav et al., 2012).

2.2.3. Bath's Law

Chan and Wu (2013) study the characteristics of the maximum magnitude in Taiwan by using Bath's law and the value of b from the G-R relationship. From the many cases of observation, the results suggested that G-R Law is the best value for determining the maximum aftershock magnitudes. The difference between magnitude of mainshock and its largest aftershock in Taiwan is in accordance with the Bath's law which is equal to 1.2. And the modified Omori's law used for assessing the temporal decays of the maximum aftershock magnitudes which the low deviation equivalent to 0.13 between the observations and the models (Figure 2.12).

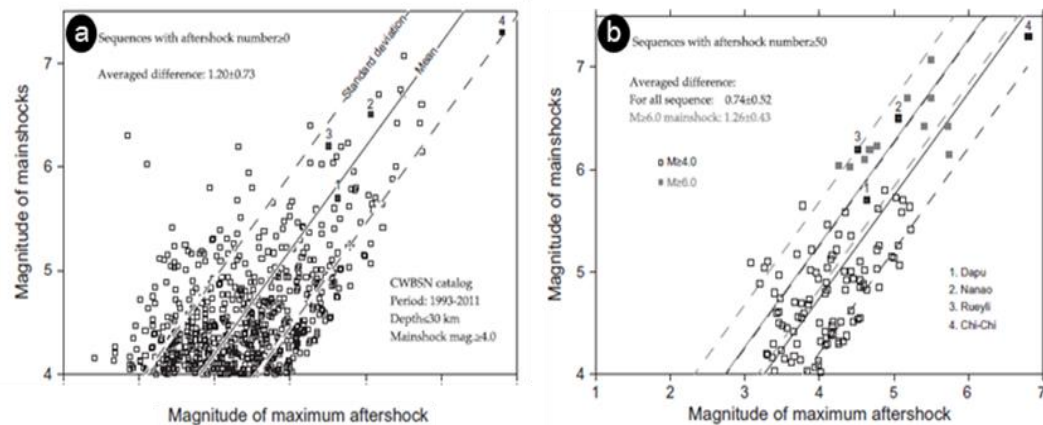


Figure 2.12 A relationship between the magnitude of the mainshock and the maximum magnitude of aftershock (a) for all sequence (b) for the sequence with the number of aftershock ≥ 50 events (Chan and Wu, 2013).

Yadav et al. (2012), study the characteristics of the aftershock from 6.4 earthquake during the 2008 Baluchistan in southwestern Pakistan by using statistical analysis as b values, p values, fractal dimension and energy partitioning due to aftershock. According to Shcherbakov and Turcotte (2004) that improve the Bath's law can be analyze the energy partitioning between mainshock and aftershock as it found that 12% is related to the aftershock while 88% is related to the mainshock. The differences between the mainshock and the maximum aftershock magnitudes not in accordance with the Bath's law, because the value is less than the standard value (1.2).

Hamdache et al. (2013), study the characteristics of eleven aftershock sequence, as occurred in the South and Southeast of Spain by several statistical theory, i.e., i) b value of G-R relationship, ii) p value of the modified Omori's law, iii) the modified Bath's law and iv) he fractal dimension. The analysis of b and p values are described in section 2.2.1 and 2.2.2, respectively. As while studying the difference of the magnitude of mainshock and its largest aftershock can be calculated by the

modified Bath's law. The result are different in each area from 0.1-1.3 that concluded that the difference is based on the area in each area which does not follow the modified Bath's law (Table 2.1). In addition, this law used to consider the energy partitioning suggests that the majority cumulative energy is released in the mainshock and the minority cumulative energy is released in aftershock which is remaining.

Table 2.1 Characteristic variable of the aftershock sequence observed and estimated have many parameters such as magnitude of mainshock (m_{ms}), magnitude of completeness (M_c), b value, aftershock maximum magnitude (m_{as}), difference between magnitude of mainshock and the maximum aftershock (Δm) (Hamdache et al., 2013).

	m_{ms}	m_{min}	m_c	b-value	m_{as}^{obs}	m_{as}^e	Δm^{obs}	Δm^e	R_{ms}
Mula 1999	4.8	1.5	2.2	1.10 ± 0.10	3.6	4.1	1.2	0.7	0.1968
Bullas 2002	4.7	0.5	1.0	0.77 ± 0.05	3.8	4.1	0.9	0.6	0.1172
La Paca 2005	4.8	0.5	1.4	0.95 ± 0.05	3.8	4.1	1.0	0.7	0.1334
Lorca 2011	5.1	0.4	2.0	0.78 ± 0.20	2.9	3.8	2.2	1.3	0.0120
Adra 1993	5.0	2.0	2.4	1.11 ± 0.06	4.9	4.6	0.1	0.4	0.4169
Gado 2002	5.1	0.5	1.4	0.74 ± 0.05	4.2	4.5	1.1	0.6	0.1092
Alboran 1997	4.4	1.5	2.8	1.07 ± 0.20	4.3	4.3	0.1	0.1	0.6379
Alboran 2008a	4.3	1.2	1.8	1.00 ± 0.10	3.5	3.6	0.8	0.7	0.1513
Alboran 2008b	4.2	1.1	1.8	1.18 ± 0.10	3.0	3.1	1.2	1.1	0.0763
Coripe 2007	4.6	0.7	1.4	1.08 ± 0.10	3.7	3.4	1.1	1.2	0.0392
Coripe 2008	4.7	0.6	1.4	0.96 ± 0.06	4.0	4.0	0.7	0.7	0.1368

2.2.4. Fractal Dimension

(Hamdache et al., 2013), study the characteristics of eleven aftershock sequence, as occurred in the South and Southeast of Spain by the several parameters: b and p value, Δm and D_c . The fractal dimension (D_c) is a method for analyze the spatial aftershock distribution that calculated from plot log-log scale of correlation integral versus distance. The results are shown in Figure 2.13, where D_c ranged 1.21-2.13. In addition, the relationship between the fractal dimension and b value has positive relationships from the graph that shown in equation is $D_c = 1.67b$ and $r^2 = 0.92$ (Figure 2.14)

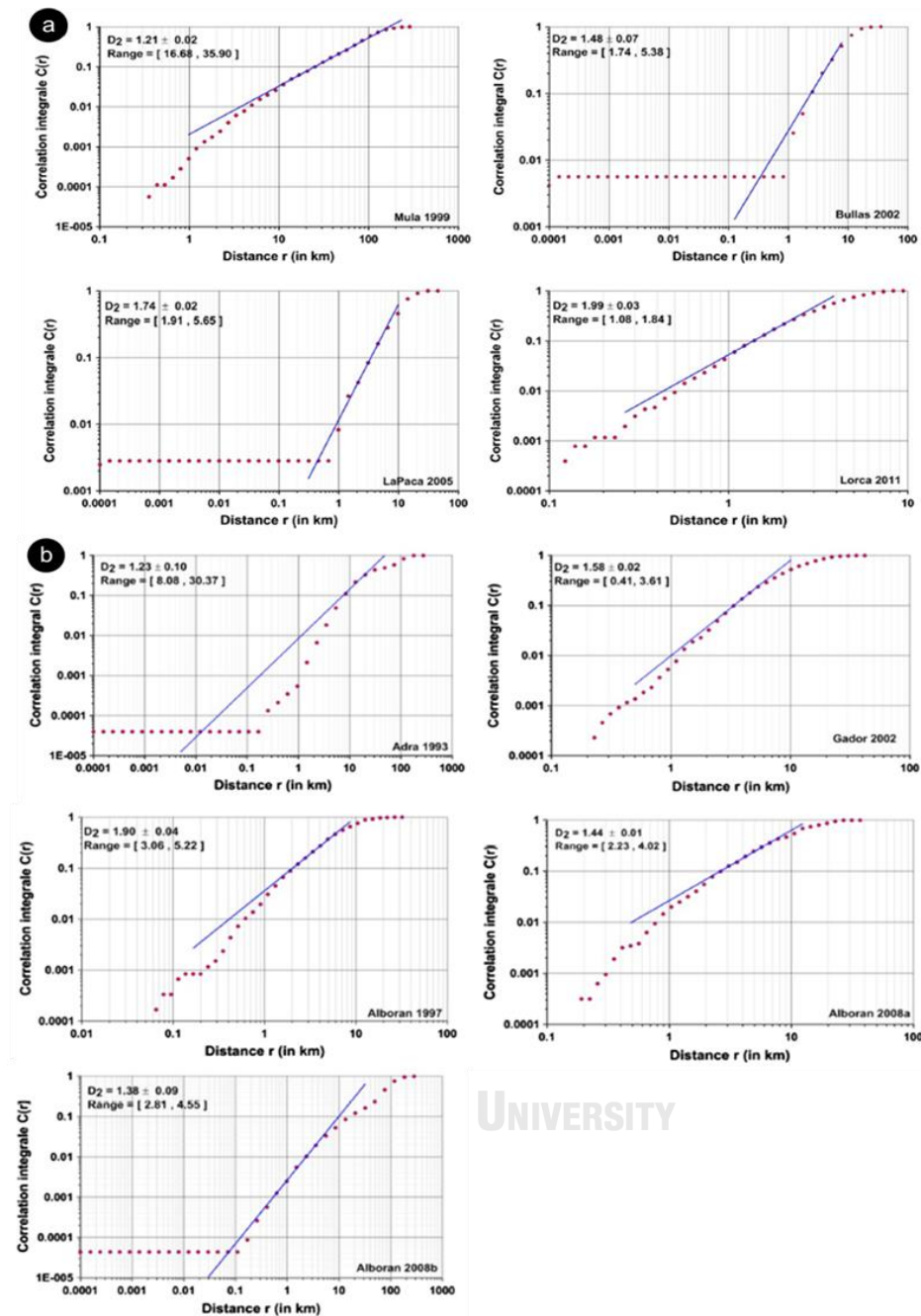


Figure 2.13 Plot log-log scale of the correlation integral versus distance that the fractal dimension (D_c) is estimated by slope of the linear fit the data: (a) for the Mula 1999, Bullas 2002, LaPaca 2005 and Lorca 2011 aftershock sequences, (b) for the Adra 1993, Gador 2002, Alboran 1997, Alboran 2008a and 2008b aftershock sequences and (c) for the aftershock sequences Coripe 2007 and 2008 (Hamdache et al., 2013).

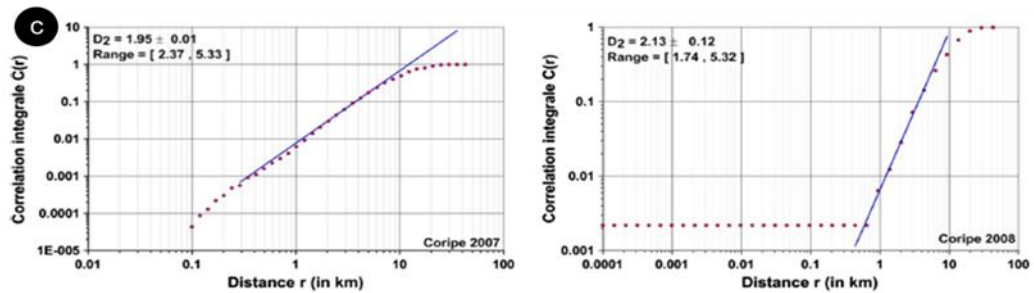


Figure 2.13 (Cont.) Plot log-log scale of the correlation integral versus distance that the fractal dimension (D_c) is estimated by slope of the linear fit the data: (a) for the Mula 1999, Bullas 2002, LaPaca 2005 and Lorca 2011 aftershock sequences, (b) for the Adra 1993, Gador 2002, Alboran 1997, Aboran 2008a and 2008b aftershock sequences and (c) for the aftershock sequences Coripe 2007 and 2008 (Hamdache et al., 2013).

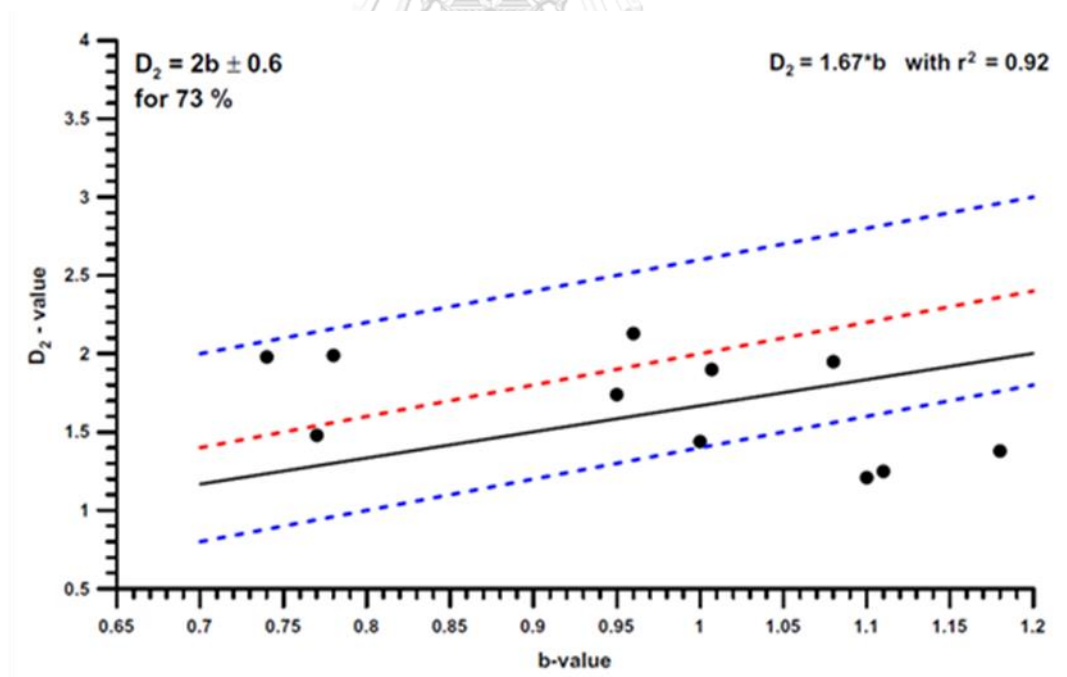


Figure 2.14 The correlation between the fractal dimension and the b value (Hamdache et al., 2013). The plot of Chen et al. (2006) is shown in dash lines. The regression plot is shown as solid line that acquired $D_c = 1.67b$, with a coefficient of relation equal to 0.92.

Yadav et al. (2012), study the characteristics of the aftershock from 6.4 earthquake during the 2008 Baluchistan in southwestern Pakistan by using fractal dimension. D_c value is 2.08 ± 0.02 , which close to 2 implied the distribution of the earthquake is in the same plane in two dimensions, shown as Figure 2.15.

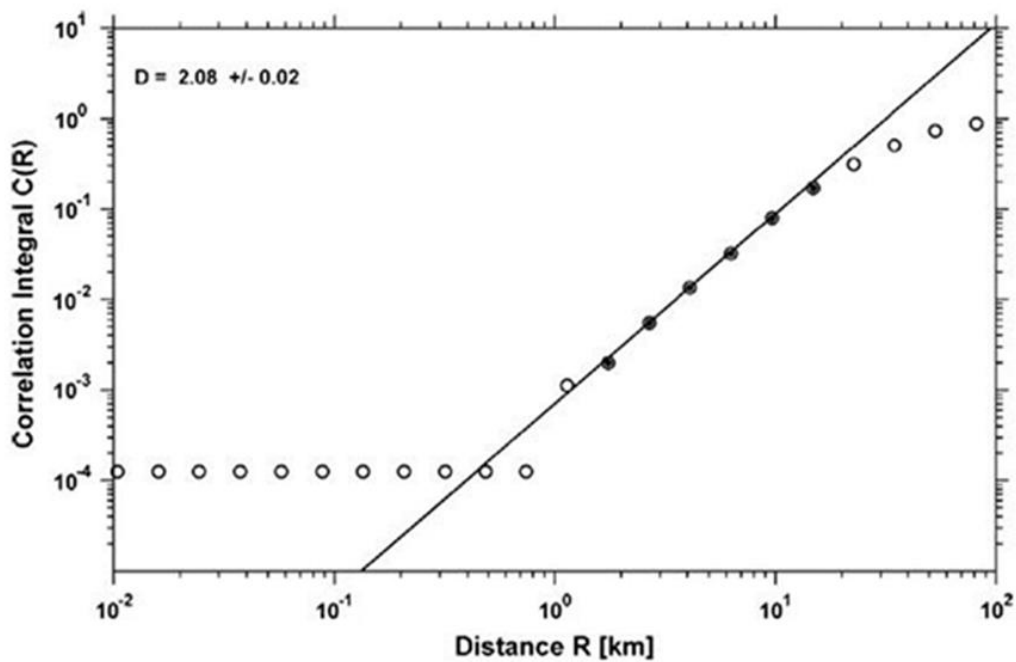


Figure 2.15 Graph shows the fractal dimension of the aftershocks distribution. Solid circles present the data for which best fit is performed for the computation of D_c value (Yadav et al., 2012).

2.3. Methodology

In this study, the methodology for analyze the characteristic of aftershock in MSEA can be divided by 5 sections that described in sequence as shown below (see also in Figure 2.16).

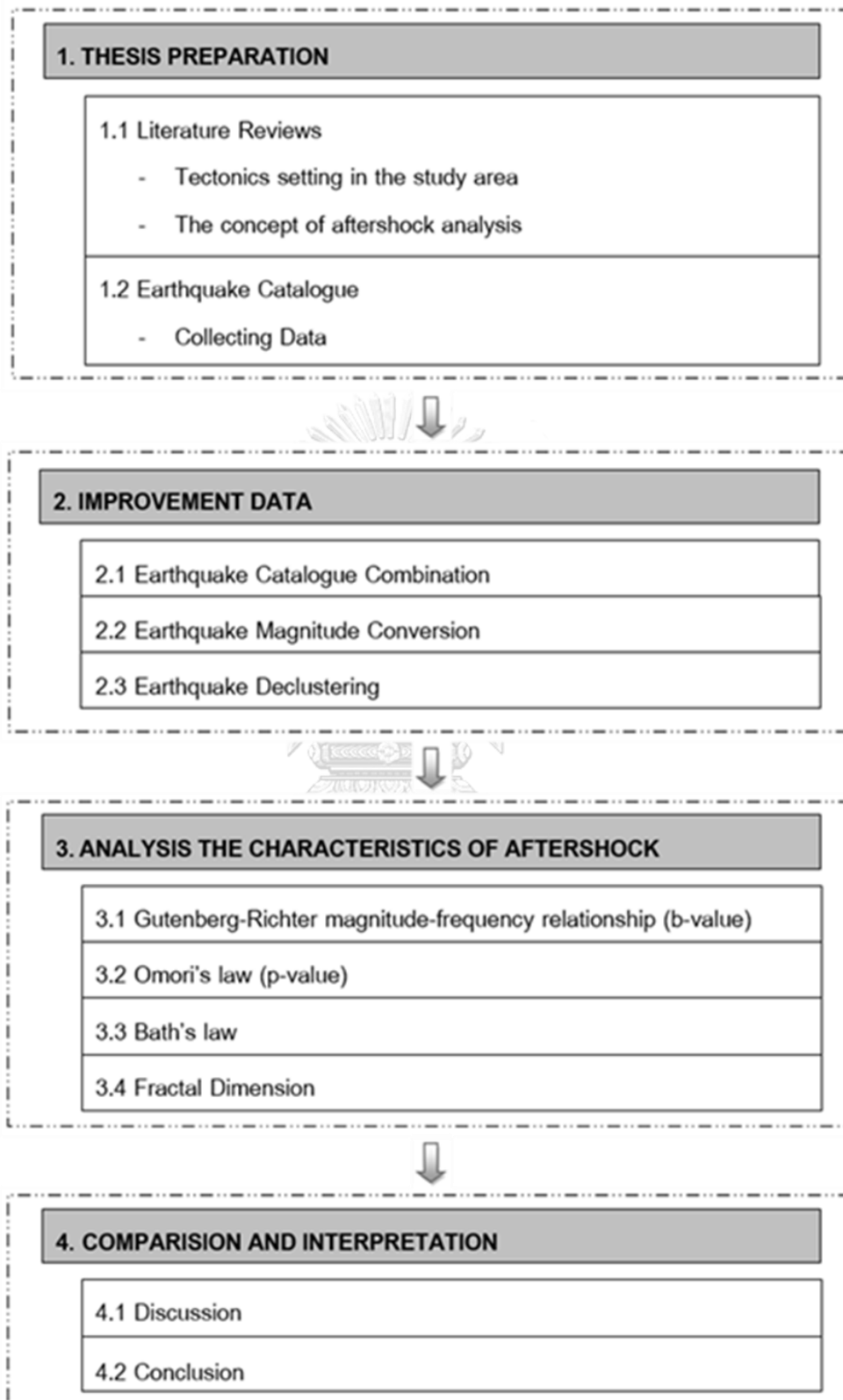


Figure 2.16 Simplified flow chart showing the methodology applied in this study.

2.3.1. Thesis Preparation

In this section consists of two main parts. First, the part of literature reviews, the previous works about study area and statistical analysis of aftershock. This procedure is intended to understand the methodology and conceptual information, including various methods that using to analyze the characteristics of aftershock, i.e., Gutenberg-Richter's law, Omori's law, Bath's law and Fractal Dimension. The second part is collected the seismicity catalogue from several earthquake data sources because earthquake data has been measured and collected by different sources that have different advantages and disadvantages.

2.3.2. Improvement Data

In the past, the earthquake catalogue has been recorded non-systematically and non-clear. Moreover, the earthquake data from various source was reported in the different magnitude scales. So, the data obtained is non-reliable and not available for statistical analysis. This is the reason that the earthquake catalogue must be updated and improved before being analyzed statistical seismology in order to obtain the most accurate earthquake catalogue. In this study, the improved section is described in more detail in chapter III and shown in Figure 2.16.

2.3.3. Earthquake Declustering

Generally the earthquakes consist of foreshock, main shock and aftershock. In this study, the aftershock was only required. It is necessary to cutoff the foreshock and mainshock in earthquake catalogue that can be cutoff by this method that shown in the next section.

2.3.4. Analyze the Characteristics of Aftershock

Based on literature review, there are several methods that used for analysis of aftershock characteristics. In this study, four methods were used: Gutenberg-Richter's law, Omori's law, Bath's law and Fractal Dimension. The outcome obtained

is the aftershock characteristics such as the maximum magnitude, the decay rate of aftershock and the seismic stress change and pattern.

2.3.5. Comparative Interpretation of Aftershock Characteristics

According to four methods (Gutenberg-Richter's law, Omori's law, Bath's law and Fractal Dimension), the aftershock characteristics are interpreted from various outputs in order to identified the unique information of aftershock in this area. Finally, the results can be used in planning for prevention and relief of disasters from aftershock in the future.



CHAPTER 3

SEISMICITY DATA AND COMPLETENESS

In seismology, the earthquake record from the past to the present can be divided into 3 parts, i.e., i) Geological record, ii) Historical record and iii) Instrumental record. Although the instrument earthquake record will not be as long as geological and historical record, this record has an advantage that reporting thoroughly and continuously. Also, the earthquake catalogue is the most important for statistical seismology whether it is seismotectonic, seismicity characteristics and seismic hazard. Worldwide, the earthquake measurement have several magnitude scales, i.e., moment magnitude (M_w) (Kanamori, 1977), body-wave magnitude (m_b) (Kanamori, 1983), surface-wave magnitude (M_s) (Gutenberg, 1945a) and local magnitude (M_L). This reason make the earthquake catalogue is incomplete that change in time and area with varying procedures.

Thereby, the earthquake data to be analyzed the statistical seismology needs to be improved before applied to study in order to obtain the most accurate and reliable results. According to the mentioned above, in this chapter, this work also revised the earthquake catalogues before analyze the characteristics of aftershock by Gutenberg-Richter's law, the modified Omori's law, Bath's law and fractal dimension in the next chapter. The methodology for improving seismicity catalogue can define as follows (see also Chapter 2 in Figure 2.16).

3.1. Earthquake Catalogue Collecting

Generally, the earthquake catalogue will be recorded until the present day by several global networks, i.e., i) the National Earthquake Information Center (NEIC), ii) the International Seismological Center (ISC), iii) the Global Centroid Moment Tensor (GCMT) and iv) Thai Methodological Department (TMD). These record earthquake are reported as details that include name of agency, location of the epicenter (longitude,

latitude and depth) occurrence time (year, month, day, hour, minute and second) and various types of magnitude that including the moment magnitude (M_W), the body-wave magnitude (m_b) and the surface-wave magnitude (M_S) (Table 3.1).

Table 3.1 Examples of earthquake catalogue.

Longitude	Latitude	Year	Month	Day	Depth	Hr	Min	Sec	M_W	m_b	M_S
94.95	32.16	2012	6	22	10	3	43	39	-	4.3	-
96.81	30.11	2012	6	22	10	4	47	50	-	4.2	-
92.49	1.27	2012	6	22	35	5	14	47	-	4.8	-
97.91	3.00	2012	6	23	102	4	34	54	6.1	6.3	-
91.27	2.76	2012	6	23	35	18	3	36	-	4.8	-
90.54	2.58	2012	6	23	18	21	27	30	5.5	5.3	5.0
90.14	1.34	2012	6	23	10	23	13	48	-	4.5	-
98.91	1.39	2012	6	24	99	4	47	24	-	4.6	-
100.75	27.73	2012	6	24	17	7	59	36	5.5	5.5	5.3
100.90	27.77	2012	6	26	10	6	21	17	-	4.4	-
97.08	1.20	2012	6	26	25	17	8	46	-	4.4	-
89.71	1.93	2012	6	26	10	18	43	14	-	4.7	-
97.17	1.13	2012	6	29	25	9	20	51	-	4.9	-
96.31	28.61	2012	6	30	25	19	43	23	-	4.7	-
94.71	25.60	2012	7	1	56	4	13	52	5.6	5.5	-
94.59	25.65	2012	7	1	63	4	54	5	-	4.3	-

However, each seismicity network has both disadvantages and advantages in the case of continuity of data, recording time and limitation of earthquake magnitude. For instance, even though the TMD has a seismicity catalogue that recorded cover range of magnitude and continuously, the seismicity data has only from 1980 to 2009. The seismicity catalogue of the GCMT is the best profit to completely analyze the seismology that consists of the all source but this catalogue is reported above 5.5 magnitude. Even if the IRIS has accurately seismicity data with

the large to medium size of earthquakes, this data is not reported in the recent time. The NEIC has the longest period of seismicity data and recorded constantly, however this data with $M < 2.9$ is not reported. In this study requires that the seismicity data used to cover the longest periods of time and not limit the range of magnitude.

The NEIC is controlled by the United State Geological Survey (USGS) which has a mission to report the earthquake immediately. The details of the report will include location, magnitude, time and other details of the measurement of seismic amplitude. The NEIC seismicity data will report promptly when the earthquake occurs due to use the automatic calculation system. The NEIC catalogue has some disadvantage, which is some error of the data that results from the automatic calculation system. However, it is also considered to be the most advanced seismicity catalogue in any time that compared to the other seismicity networks.

According to the mentioned above, in this study, it is chosen the NEIC seismicity catalogue to analyze the characteristics of aftershock in the mainland Southeast Asia.

As a result, the total earthquake catalogue contains 20,115 earthquake events, during from January 1st, 1985 to August 31st, 2017, ranging magnitude from 2.7 to 8.6 and then ranging depth of earthquake occur from 0 to 750 m. in the study area (Figure 3.2) that cover latitude between 4°N - 33°N and longitude between 86°E - 115°E (Figure 3.1).

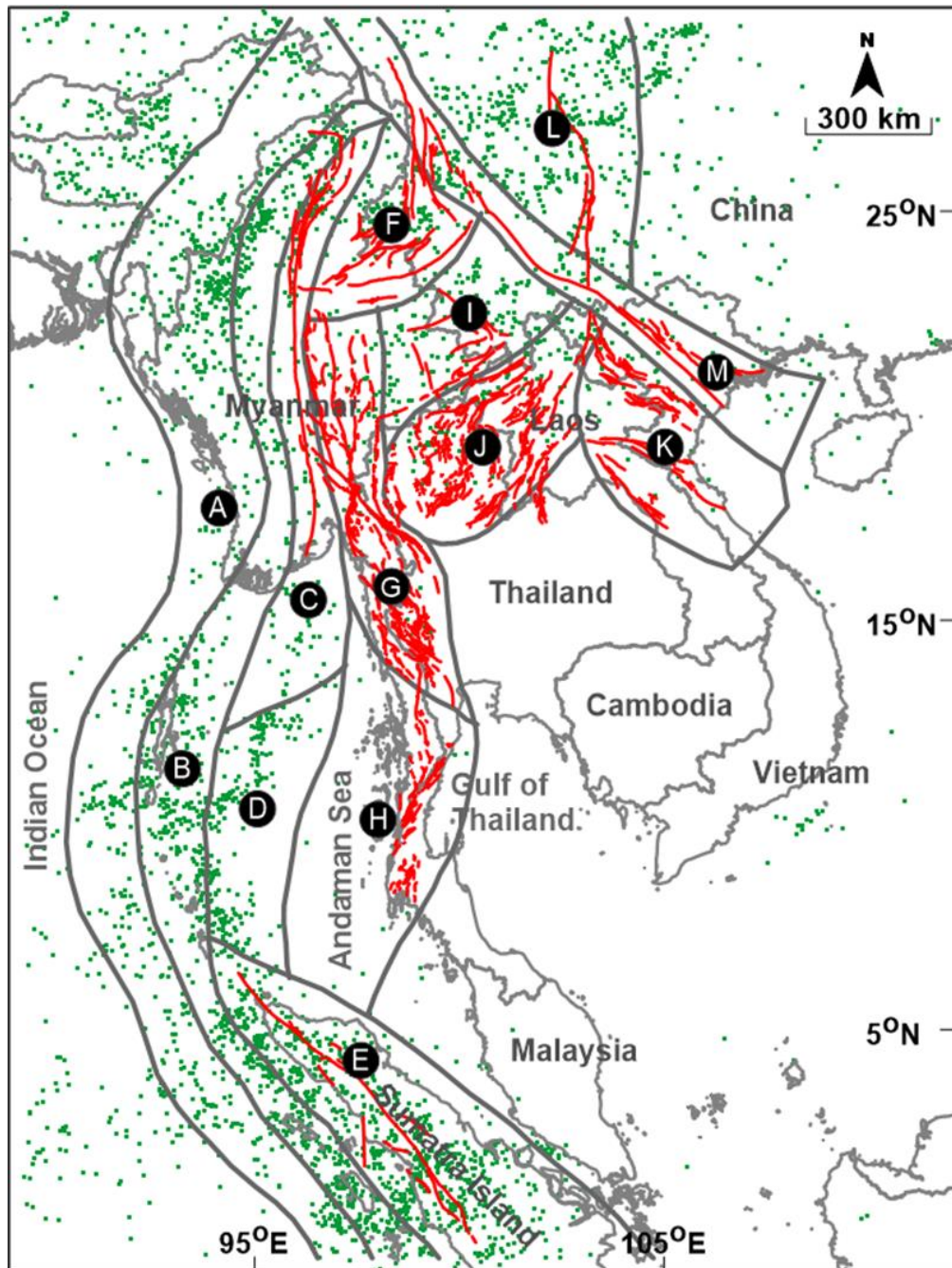


Figure 3.1 Map of the MSEA and the 13 seismic source zones that proposed by Pailoplee and Choowong (2013) showing the distribution of the earthquake during 1985 to 2017. Red lines indicate the fault lines proposed by Pailoplee et al. (2009).

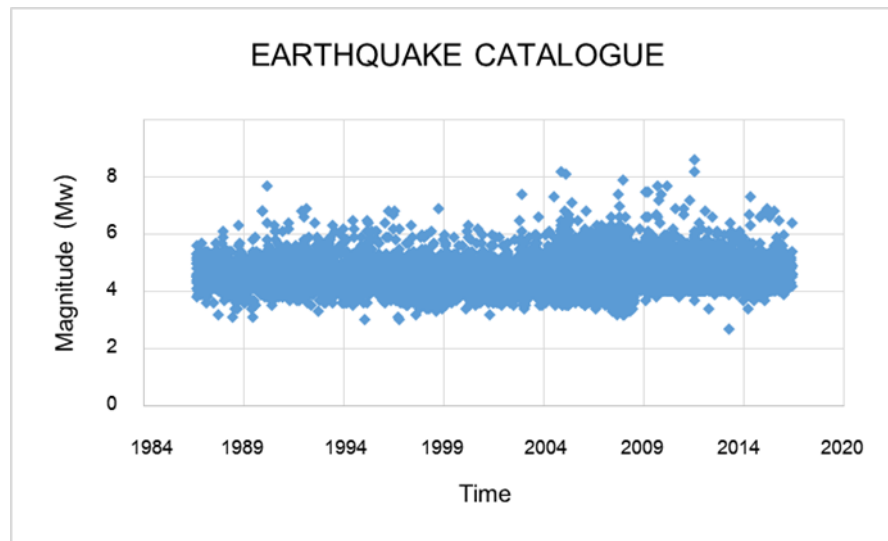


Figure 3.2 The earthquake catalogue of the NEIC database recorded since 1985 – 2017 (end of August).

3.2 Earthquake Magnitude Conversion

In the previous section, all earthquake data were combined and collected to the new catalogue which found that the earthquake catalogue consisted of the different magnitude scales, including moment magnitude (M_W), body-wave magnitude (m_b) and surface-wave magnitude (M_S). In order to use the earthquake data for analysis, it must be converted the different magnitude scales into the same standard magnitude scale. In practice, it can be explained that each magnitude scale is based on different assumptions and analysis methods which each scale has a valid but there are different values and unique meanings.

Presently, M_W is most commonly used for the statistical analysis and is most reliable since this unit can directly identify the physical characteristics of the source of earthquake and in addition, this unit is not affected by the saturation phenomenon while the large earthquakes occurred, unlike the other scales (Kanamori, 1977).

From the reasons mentioned above, this is why it is necessary to convert the other scales to the same standard. In this study, the earthquake catalogue recorded in the mainland Southeast Asia were converted to M_W scale from m_b and M_S . First step for convert is created the empirical relationship between the different magnitude scales, which is unique and different in each area that can be divided into 2 relationships, i.e., i) empirical relationship between m_b and M_W and ii) empirical relationship between M_S and M_W

The empirical relationship between the different magnitude scales based on the earthquake data in the MSEA is derived from plot graph between M_W scale in the vertical axis (y-axis) and m_b scale (the empirical relationship between m_b and M_W) or M_S scale (the empirical relationship between M_S and M_W) in the horizontal axis (x-axis). The last step is calibrated the relationship between the different scales by using the polynomial trend line, so the result is the empirical relation equation.

3.2.1 Body-wave Magnitude (m_b) and Moment Magnitude (M_W)

The earthquake catalogue recorded in the MSEA region can be created the graph of empirical relationship between m_b and M_W as Figure 3.3

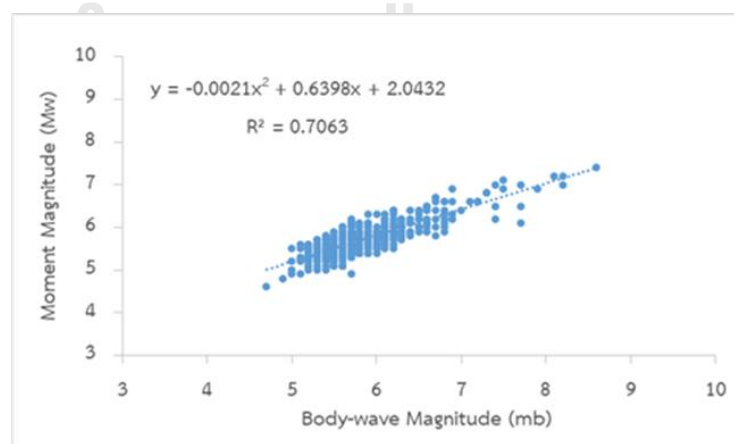


Figure 3.3 Empirical relationships between moment magnitude (M_W) and body-wave magnitude (m_b)

And the relationship equation for using to convert to M_W from m_b is given by equation (3.1)

$$M_W = -0.002m_b^2 + 0.640m_b + 2.043 \quad \text{equation (3.1)}$$

3.2.2 Surface-wave Magnitude (M_S) and Moment Magnitude (M_W)

The earthquake catalogue recorded in MSEA can be created the graph of empirical relationship between M_S and M_W as Figure 3.4

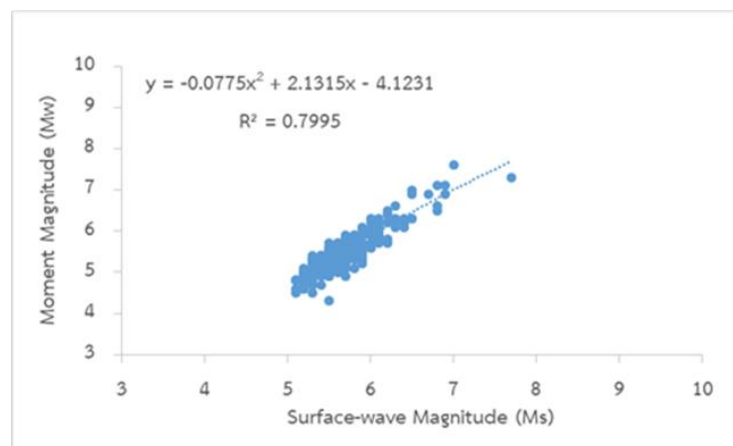


Figure 3.4 Empirical relationships between Surface-wave Magnitude (M_S) and Moment Magnitude (M_W)

And the relationship equation for using to convert to M_W from M_S is given by equation (3.1)

$$M_W = -0.078M_S^2 + 2.132M_S - 4.123 \quad \text{equation (3.2)}$$

3.3 Earthquake Declustering

Based on Stiphout et al. (2012), generally, the cluster of earthquakes can be classified into two types by the seismologists, i.e., i) Independent earthquake that called the mainshock and ii) dependent earthquake that are known as aftershock and foreshock. Independent earthquakes are caused by the stress transients that are not affected by previous and nearby earthquakes. In the dependent earthquake,

foreshock is an earthquake that generated before the largest earthquake in the nearby or same space, while aftershock is a smaller earthquake which occurs in the same location during the period following the mainshock or the larger earthquake.

In order to cluster the earthquake catalogue into foreshocks, mainshocks and aftershocks, it is necessary to use a widely known process to separate that is also called seismicity declustering. Over the years, the algorithms of seismicity declustering have been proposed. Until now, the most popular algorithm used by the researchers is the methods proposed by Gardner and Knopoff (1974) or Reasenberg (1985). Gardner and Knopoff (1974) using the inter-event distances in space and time to specified the aftershocks from seismic catalogue that known as a window method. This method can be easily explained that if an earthquake C occurs in the windows of the significant mainshocks A and B and then only the largest earthquake A or B is considered the actual mainshock of earthquake C, regardless of the possibility which earthquake C might be significantly closer in time and space to the other events. While the concept of Reasenberg (1985) is described to relate aftershock triggering inside a cluster of earthquake, it is shown that if A is the mainshock of B and B is the mainshock of C and then all of earthquakes are identified to one common cluster that the largest earthquake will be classified as the cluster of mainshock. From above mention, the aftershock identification windows can vary considerably from one idea to the other (see Figure 3.5) and usually do not result from an optimization method.

Based on the literature review, Petersen et al. (2004) chose the declustering model proposed by Gardner and Knopoff (1974) to be used to filter the earthquake catalogue before the analysis in the Sumatra-Andaman subduction zone region which is part of the MSEA. Next, Pailoplee and Choowong (2014) study on the characteristic of earthquake in the MSEA by using the frequency-magnitude distribution and fractal dimension method that the earthquake catalogue was also declustered by concept

of Gardner and Knopoff (1974). Then Puangjaktha and Pailoplee (2018) prepared the earthquake catalogue to be used to analyze the seismicity rate change that implied the prospective hazardous earthquake along Thailand-Laos-Myanmar borders based on the process of declustering of Gardner and Knopoff (1974) as well as. In addition, Traitangwong and Pailoplee (2017) use the declustering process of Gardner and Knopoff (1974) as well as the above, in order to find the precursory seismic quiescence along the Sagaing fault zone, Central Myanmar. For this reason, this study used this method to filter the earthquake catalogue before analyzing the characteristics of the aftershock in the MSEA. This method is known as a window technique that is the simple way to identify aftershocks. For each earthquake with magnitude M within the earthquake catalogue, the following earthquakes will be classified as aftershocks that if they happen inside a specified time interim $T(M)$, and within a distance interim $L(M)$. Therefore, the time-space windows are determined based on the magnitude of the largest earthquake in each sequence. The window techniques will consider both the space and time windows that is shown in the equation 3.3 and 3.4.

$$d = 10^{0.1238*M+0.983} [km] \quad \text{equation (3.3)}$$

$$t = \begin{cases} 10^{0.032*M+2.7389}, & \text{if } M \geq 6.5 \\ 10^{0.5409*M-0.547}, & \text{else} \end{cases} [days] \quad \text{equation (3.4)}$$

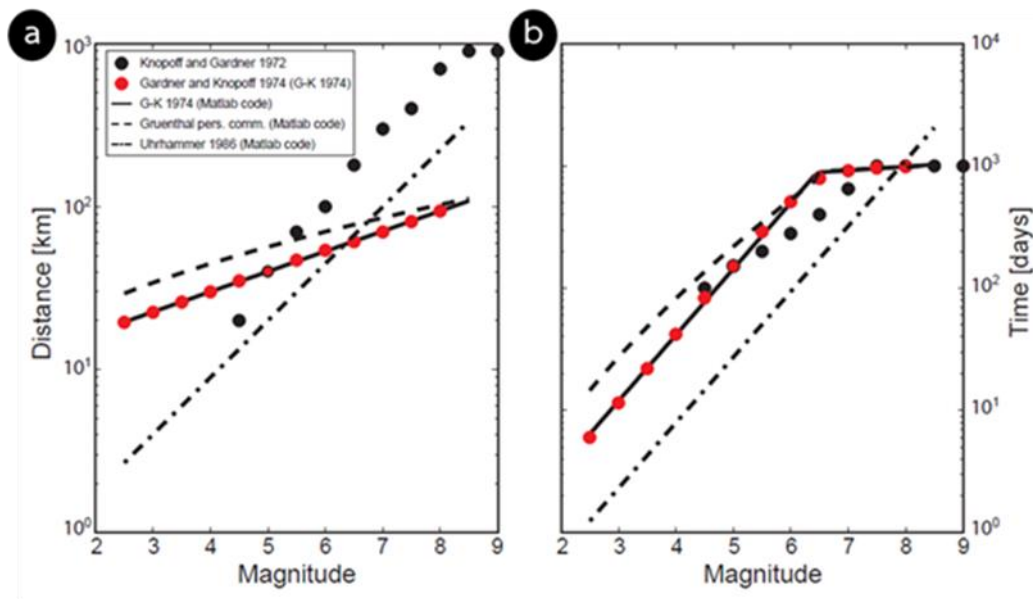


Figure 3.5 Aftershock identification windows in term of (a) space and (b) time are shown as a function of the mainshock magnitude (Stiphout et al., 2012).

In this work, the process of seismic declustering begin with the creation of the program for the sequencing of the aftershocks as a result of the mainshock, which is based on the above equation. This program is created by generate code in python program. The result of this process is the cluster aftershocks of each mainshock which will be used to analyze the characteristics of the aftershock in the next step.

The first step for declustering by this program is organized the earthquake catalogue into the .txt file format, as shown in Table 3.2. And then execute the code through python program, which results in two parts. The first part is all mainshock data in the earthquake catalogue, the maximum aftershock compared to the mainshock and the number of aftershocks in each mainshock, which is in the .csv file format as shown in Table 3.3. And the second part is the cluster of mainshock, which including all aftershocks caused by each mainshock. The number of files received is based on the number of the mainshocks as illustrated of the example file in Table 3.4.

Table 3.2 The format of the earthquake catalogue is sorted by Longitude, Latitude, Year, Month, Day, Mw, Depth, Hr, Min and Sec.

Longitude	Latitude	Year	Month	Day	M _w	Depth	Hr	Min	Sec
94.95	32.16	2012	6	22	4.3	10	3	43	39
96.81	30.11	2012	6	22	4.2	10	4	47	50
92.49	1.27	2012	6	22	4.8	35	5	14	47
97.91	3.00	2012	6	23	6.1	102	4	34	54
91.27	2.76	2012	6	23	4.8	35	18	3	36
90.54	2.58	2012	6	23	5.5	18	21	27	30
90.14	1.34	2012	6	23	4.5	10	23	13	48
98.91	1.39	2012	6	24	4.6	99	4	47	24
100.75	27.73	2012	6	24	5.5	17	7	59	36
100.90	27.77	2012	6	26	4.4	10	6	21	17
97.08	1.20	2012	6	26	4.4	25	17	8	46
89.71	1.93	2012	6	26	4.7	10	18	43	14



Table 3.3 The example of first output from declustering by run code through python

No.	longitude	latitude	year	month	day	Hour	min	sec	MW	Depth	af_index	max_mg	af_lon	af_lat	max_distance	max_dt	af_count
66	93.61	8.35	1985	4	25	14	28	53	4.9	71.7	67	4.8	93.7	8.54	24.34	0	1
69	93.61	8.55	1985	4	25	15	30	26	5.4	42.3	146	5.1	93.7217	8.57	29.89	170	3
95	98.34	-0.37	1985	7	8	13	47	42	3.9	39.3	96	3.8	98.35	-0.43	6.32	0	1
98	94.80	30.36	1985	7	18	17	40	9	4.9	6.7	99	4.7	94.91	30.38	13.01	2	3
112	95.668	32.27	1985	8	4	19	54	17	4.7	33	139	4.5	95.48	32.12	26.01	58	1
128	93.44	8.07	1985	9	8	9	23	49	4.9	80.6	133	4.7	93.30	8.04	16.019	5	1
4964	9590	3.41	2004	12	26	0	58	52	8.2	26.1	7283	6.8	95.60	2.90	99.18	1000	286
4965	94.51	4.92	2004	12	26	1	17	9	5.5	30	7280	4.4	94.62	4.59	38.480	62	1
4966	93.40	6.33	2004	12	26	1	21	19	6.1	30	5615	6	92.93	6.18	53.93	490	22
4967	93.99	7.37	2004	12	26	1	22	24	6	30	5613	5.6	93.89	7.55	50.22	224	31
4968	94.28	5.46	2004	12	26	1	25	47	6.1	30	5241	6	94.44	5.48	51.27	490	28
4969	97.67	20.89	2004	12	26	1	29	51	5.8	33	5595	5.1	97.74	20.91	25.23	17	3

Table 3.4 The example of second output from declustering by run code through python which consists of the aftershocks of mainshock.

status	longitude	latitude	year	month	day	Hour	min	sec	MW	Depth	Azimuth
Mainshock	92.77	3.36	2012	4	11	16	4	24	5.1	14.1	0
Aftershock	92.94	3.20	2012	4	11	16	31	22	4.6	35	132.69
Aftershock	92.99	3.10	2012	4	11	23	18	54	4.6	35	139.16
Aftershock	92.81	3.47	2012	4	11	23	54	6	4.2	10	341.33
Aftershock	92.59	3.68	2012	4	12	1	13	39	4.7	24	331.73
Aftershock	92.71	3.51	2012	4	12	2	42	43	4.8	24	340.68
Aftershock	92.76	3.47	2012	4	12	5	29	19	4.1	10	354.21
Aftershock	92.65	3.08	2012	4	12	7	43	46	4.7	10	203.45
Aftershock	93.11	3.43	2012	4	12	13	29	25	4.5	10	281.81
Aftershock	92.58	3.41	2012	4	12	15	7	35	4.8	24	286.06
Aftershock	92.88	3.32	2012	4	12	17	30	19	4.7	35	107.80
Aftershock	92.84	3.41	2012	4	12	19	25	56	4.8	19.7	307.26
Aftershock	92.95	3.47	2012	4	12	19	42	37	4.6	35	302.78
Aftershock	92.92	3.23	2012	4	14	9	34	7	4.1	35	128.76
Aftershock	92.72	3.02	2012	4	15	22	27	23	4.6	35	188.47
Aftershock	92.89	3.03	2012	4	17	20	40	43	4.2	35	159.99
Aftershock	92.81	3.22	2012	4	20	20	24	33	4.2	35	162.94

After the declustering process, it was found that 1,697 clusters from 20,115 earthquake events, during January 2nd, 1985 and August 21st, 2017 in the mainland Southeast Asia which each cluster consisting of the major earthquake or mainshock and the several aftershocks that occur after mainshock. Similarly, using the ZMAP program (Wiemer, 2001) that based on the concept of Gardner and Knopoff (1974) to declustering earthquake data, it was possible to distinguish 1,697 clusters from 20,115 events. As mentioned, it is supported that the program was created accurately, reliably and applicable to the other research as well.

3.4. Seismic Source Zone

In this section discusses the grouping of earthquake catalogue that will be used to analyze the characteristics of the aftershock in the mainland Southeast Asia. These data have been improved and declustered. The study area is considered to be

a large area, so it needs to be grouped into sub-areas or zones in order to make the analysis of the characteristics of the aftershock in this area more specific and accurate.

Based on literature review, there are several concepts that used in the study about the seismic source zones in the MSEA region. First work, Nutalaya et al. (1985) is divided into 12 earthquake source zones in Thailand and neighboring countries, but did not cover some of the important areas such as the Sumatra Island and the southern peninsular Thailand. After that, Charusiri et al. (2005) organized the seismic source zones by adding to 21 zones which defined the seismic source zones according to the present-day tectonic environments, the distribution of epicenter of earthquakes in the last two decades, regional geomorphology and active faults in this areas. Seismic source zone no.21 covers the southern peninsular Thailand and northern Sumatra, which is not classified as any seismic source zone of Nutalaya et al. (1985). Thereafter, Pailoplee and Choowong (2013) revised the seismic source zones in the mainland Southeast Asia that change the group and location. It is divided into 13 seismic source zones.

From the mentioned above, this study will divide the earthquake source zones in the mainland Southeast Asia based on Pailoplee and Choowong (2013) which can be separated to 13 zones (A to M) as shown in Figure 3.6 and namely; The Sumatra-Andaman interplate and intraslab (zones A and B, respectively), Sagaing fault zone (zone C), Andaman basin (zone D), Sumatra fault zone (zone E), Hsenwi-Nanting fault zone (zone F), Western and Southern Thailand (zones G and H), Jinghong-Mengxing fault zone (zone I), Northern Thailand-Dein Bein Phu (zone J), Song Da-Song Ma fault zone and Red River fault zone (zones K and M) and Xianshuihe fault zone (zone L) (Table 3.3).

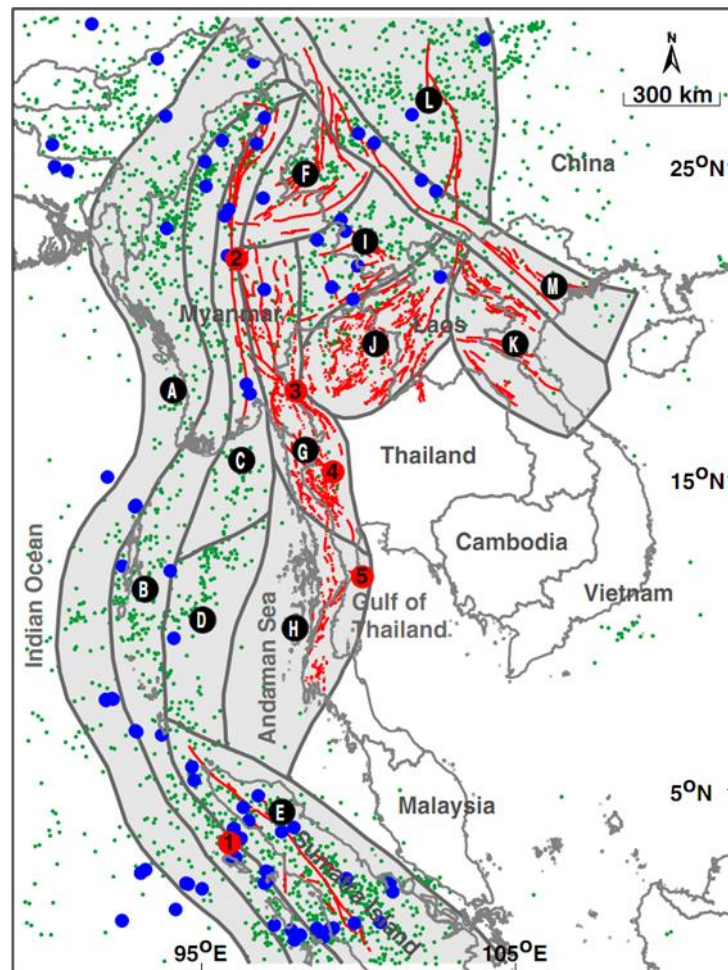


Figure 3.6 The 13 seismic source zones in the mainland Southeast Asia by Pailoplee and Choowong (2013).

After declustering, all of the earthquake cluster will be grouped into 13 groups based on the seismic source zones of Pailoplee and Choowong (2013). It is found that the total of 1,697 clusters can be divided into each zones as shown in Figure 3.7 and Table 3.5.

In order to analyze the characteristic of the aftershock in the MSEA, it is necessary to select the clusters of earthquake that will be represented in the each zone. The number of cluster of earthquake is shown in Table 3.5. This is explained in detail in the next chapter.

Table 3.5 Group of the earthquake cluster in each seismic source zones in the MSEA that followed by Pailoplee and Choowong (2013) and the case study that used to analyze the characteristic of the aftershock.

Zone code	Zone name	Number of cluster	Case Study
Zone A	Sumatra-Andaman Interplate	304	10
Zone B	Sumatra-Andaman Intraslab	429	10
Zone C	Sagaing Fault Zone	26	10
Zone D	Andaman Basin	114	10
Zone E	Sumatra Fault Zone	265	10
Zone F	Hsenwi-Nanting Fault Zone	18	10
Zone G	Western Thailand	2	2
Zone H	Southern Thailand	2	2
Zone I	Jinghong-Mengxing Fault Zones	15	10
Zone J	Northern Thailand-Dein Bein Phu	6	6
Zone K	Song Da-Song Ma Fault Zone	N/A	N/A
Zone L	Xianshuihe Fault Zone	63	10
Zone M	Red River Fault Zone	10	10

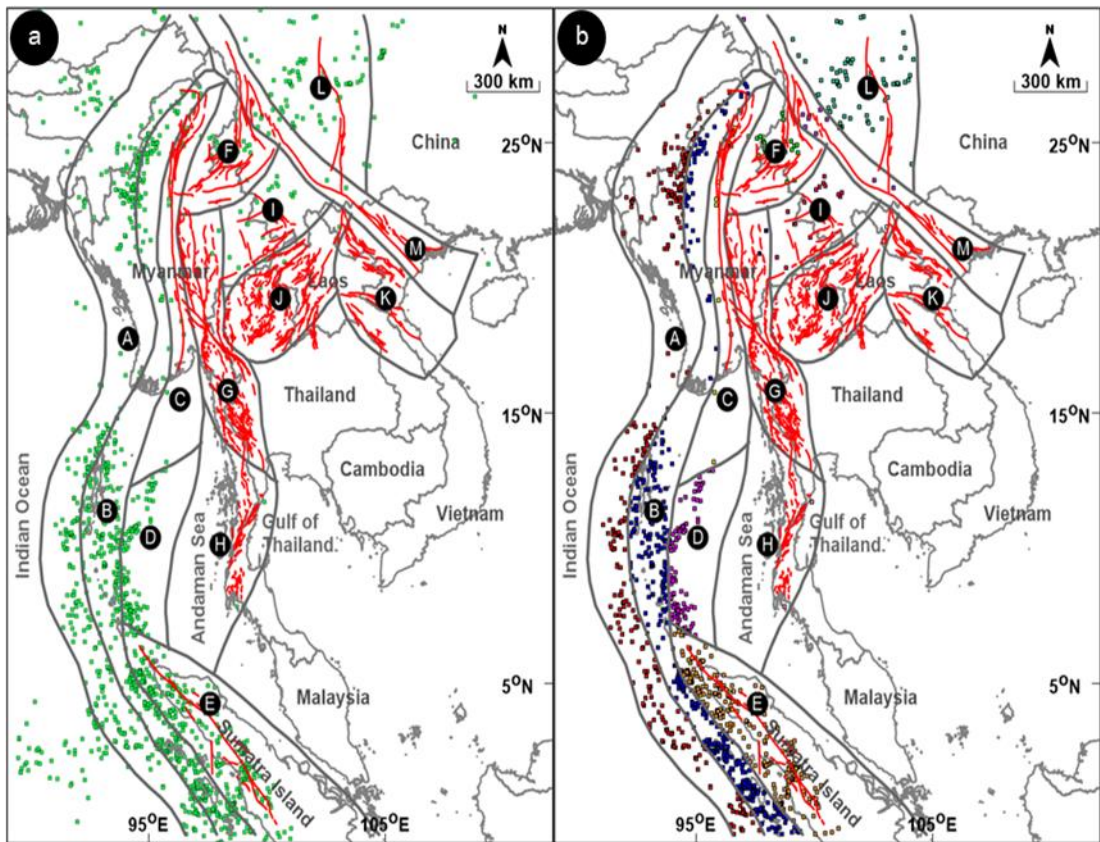


Figure 3.7 Map of the MSEA showing the distribution of the earthquake cluster in 13 seismic source zone a) the cluster of earthquake b) the cluster of earthquake after separated to 13 zones following Pailoplee and Choowong (2013).

CHAPTER 4

AFTERSHOCK CLUSTER

The characteristics of the seismic cluster have many properties which can be explained in the several statistical methods. In this study, the characteristics of the aftershock will be analyzed both the relationship between the mainshock and the largest aftershock described by Bath's law (1965) and the decay rate of aftershock following the modified Omori's law.

In the analysis of the characteristics of seismic sequence, the earthquake data must be synthesized for completeness that this method can define as follows (see also Chapter II in Figure 2.16) and then, grouping the earthquake database into small group or cluster that showing all the aftershock data follow the mainshock. Next, this earthquake data is organized into sub-areas in the MSEA. It is divided into 13 zones according to Pailoplee and Choowong (2013) that called the seismic source zone (see also Table 3.3).

For the study of the characteristics of the aftershock, this will begin with the selection of cluster of earthquakes to be represented in each zone. In this study, all 10 clusters are used in each zone. There will be different selection criteria. Zone A and B are subduction zones, where the earthquake that is disaster or impact must be greater than 6.0 magnitude. While the other zones are classified as the mainland zone, where the earthquake that is catastrophic or impact must be greater than 4.0 magnitude. In statistical terms, the number of aftershock data to be analyzed will be at least 30, so it is considered to be significant. After selecting the cluster of earthquakes according to the conditions set, only 10 cases per zone are considered as representative of each zone. The results show that the cluster of earthquakes in zone G, H and J have only 2, 2 and 6, respectively. Other zones also have 10 cluster of earthquake in all zones but lack of data in zone K that shown in Table 3.5 and

Figure 3.7 in chapter III. All these data will be analyzed for difference between magnitude of mainshock and its largest earthquake and the decay rate of aftershock.

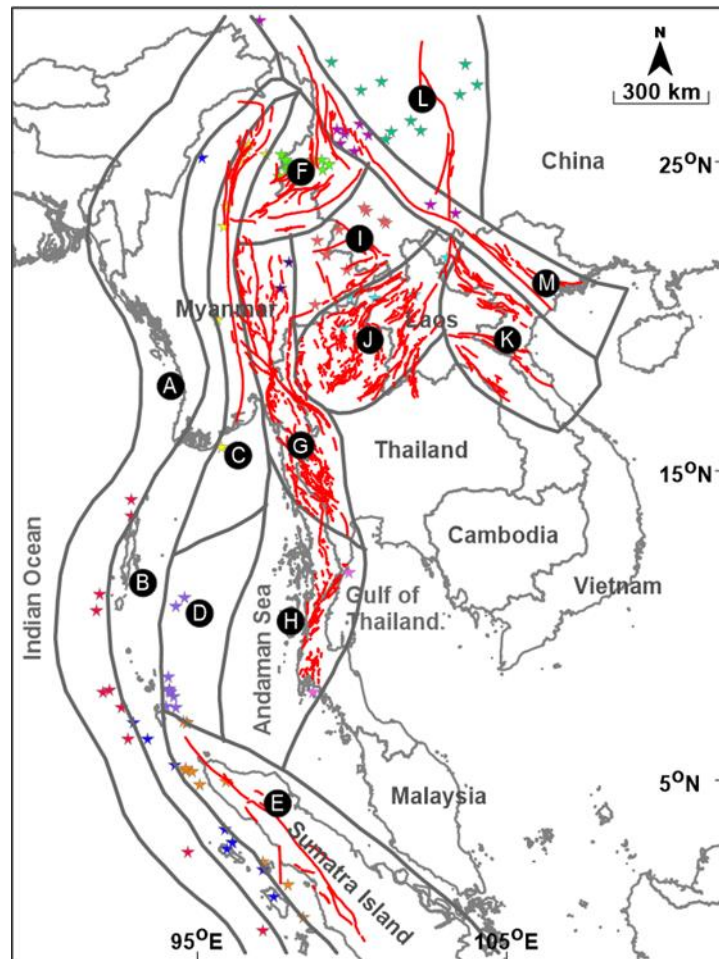


Figure 4.1 Map showing the case study of the earthquake cluster in each earthquake source zones in the MSEA (stars). Red lines indicate the significant fault zones. The black lines indicate the boundary of 13 seismic source zone.

4.1. Relationship between Magnitude of Mainshock and Its Largest Aftershock

The relationship between the magnitude of mainshock and the largest magnitude of aftershock which has been named Bath's law is one of the most characteristic of aftershock sequence. The magnitude of aftershocks is mainly related with the magnitude of mainshock in a seismic sequence (Utsu, 2002a).

From the bath's law, the difference between the mainshock magnitude and the magnitude of the largest earthquake is approximately around 1.2 but in this study, this relationship does not follow bath's law and the acceptance of all research studies. After the modified Bath's law calculation, the results of the magnitude of the largest aftershock in the MSEA does not follow the original Bath's law that can be describe as follows

According the Figure 4.2 and Table 4.1, the equations show the relationship between mainshock and maximum aftershock that display in a quadratic equation which are the MSEA and including the area is divided into 13 zones, but in the Da-Song Ma fault zones cannot find the relationship because of insufficient data in this area.

According the Table 4.2, it can be seen that the difference values between the magnitude of mainshock and maximum aftershock in the MSEA is range 0.1-3.5 and average value is 0.48.

Based on the Table 4.2, both in the Sumatra-Andaman interplate and the Sumatra-Andaman intraslab, the average value relation between mainshock and maximum aftershock is approximately 0.4. In zone A, the value is 0.47 which is in the range of 0.1-2.5, while in zone B is 0.48, with values in the range 0.1-2.3.

Refer to the Table 4.2, the average value of the difference between mainshock and maximum aftershock of Sagaing fault zone is 0.65, with values ranging from 0.1 to 1.7, while in Jinghong-Mengxing fault zones, the difference is 0.68, with values ranging from 0.1 to 1.4. It can be seen that two areas are relatively similar, that is about 0.6.

From the Table 4.2, the difference value between mainshock and maximum aftershock of the Southern Thailand and Red River fault zone has the same average at 0.3. While in Andaman basin, the average of difference is 0.37, which is close to

the Southern Thailand and Red River fault zone. The difference value in each area is in range of 0.2-0.4 in Southern Thailand, 0.1-1.2 in Red River fault zone, and 0.1-1.8 in Andaman basin.

Regarding to the Table 4.2, in the Sumatra fault zone, Hsenwi-Nanting fault zone, Western Thailand and Xianshuihe fault zone, the average value of difference between mainshock and maximum aftershock is approximately 0.5, which is explained in detail in each area. In Sumatra fault zone, the value is in the range of 0.1-2.0 and the average value is equal to 4.9. In Hsenwi-Nanting fault zone, the difference value is in the range of 0.1-1.2, and the average value is equal to 5.1. For Western Thailand, the difference value between mainshock and its largest aftershock is ranging in 0.4 to 0.7, and the average value is equal to 5.5. And finally, the average value of the difference between mainshock and maximum aftershock of Xianshuihe fault zone is 0.53, with values ranging from 0.1 to 1.4,

Finally, it can be concluded that mostly, the average difference between mainshock and its largest aftershock in each zone are in the range of 0.3-0.6, but only in the Northern Thailand-Dein Bein Fhu which is approximately 0.8 that varies from 0.2 to 1.5.

Table 4.1 The relationship between the magnitudes of mainshock and the largest aftershock in the study area is shown in equation.

Zone	Equation	R ²
ALL	$m_m = -0.06m_{af}^2 + 1.24m_{af} - 0.19$	0.59
Zone A	$m_m = -0.03m_{af}^2 + 1.05m_{af} + 0.19$	0.67
Zone B	$m_m = -0.11m_{af}^2 + 1.60m_{af} - 0.75$	0.38
Zone C	$m_m = 0.24m_{af}^2 - 2.07m_{af} + 8.67$	0.72
Zone D	$m_m = -0.14m_{af}^2 + 2.11m_{af} - 2.31$	0.61
Zone E	$m_m = -0.02m_{af}^2 + 0.89m_{af} + 0.59$	0.60
Zone F	$m_m = -0.33m_{af}^2 + 3.82m_{af} - 6.20$	0.63
Zone G	$m_m = 0.50m_{af} + 2.20$	1.00
Zone H	$m_m = 1.67m_{af} - 3.20$	1.00
Zone I	$m_m = 0.027m_{af}^2 + 0.28m_{af} + 2.59$	0.65
Zone J	$m_m = 0.04m_{af}^2 + 0.03m_{af} + 3.41$	0.87
Zone K	N/A	N/A
Zone L	$m_m = -0.04m_{af}^2 + 1.07m_{af} + 0.24$	0.59
Zone M	$m_m = -1.42m_{af}^2 + 14.22m_{af} - 30.79$	0.58

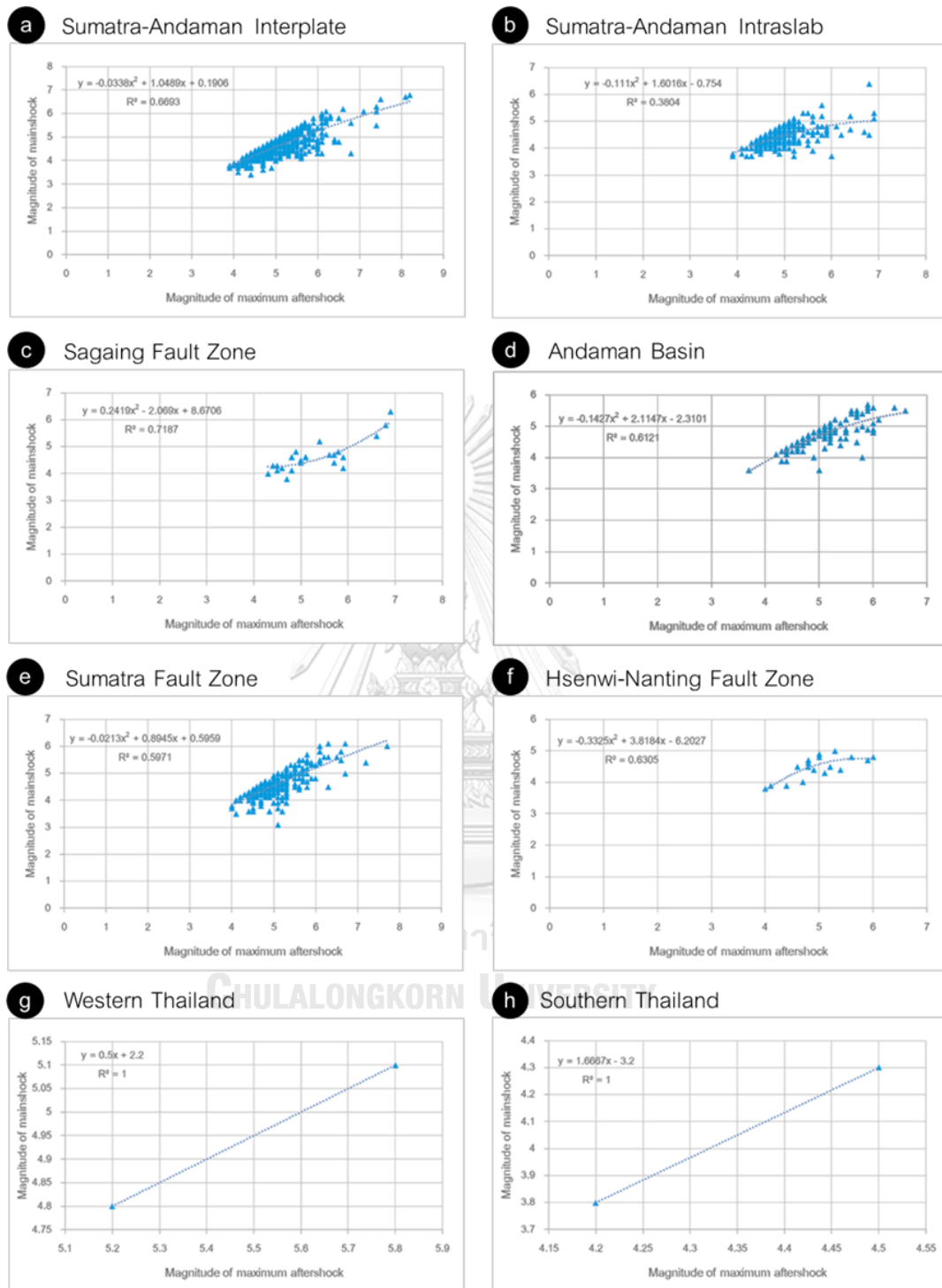


Figure 4.2 The graph plots of the magnitude of mainshock and the largest aftershock in each other zone in the MSEA.

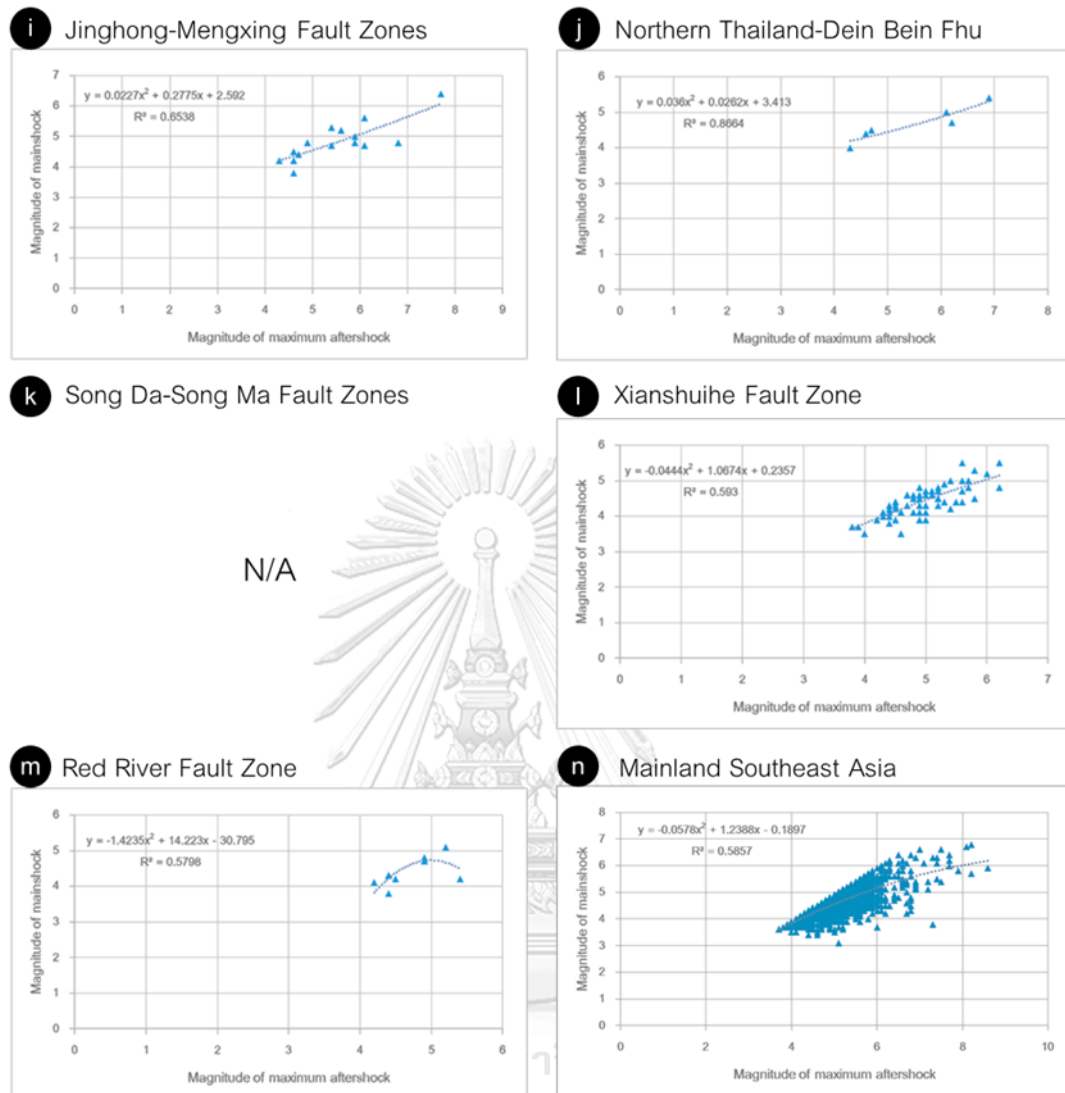


Figure 4.2 (Cont.) The graph plots of the magnitude of mainshock and the largest aftershock in each other zone in the MSEA.

Table 4.2 The difference in magnitude between mainshock and its largest aftershock of seismic source zone in the MSEA.

Zone	Range of Difference between mainshock and maximum aftershock	Average	SD
ALL	0.1-3.5	0.48	0.4
Zone A	0.1-2.5	0.47	0.39
Zone B	0.1-2.3	0.46	0.38
Zone C	0.1-1.7	0.65	0.42
Zone D	0.1-1.8	0.37	0.33
Zone E	0.1-2.0	0.49	0.36
Zone F	0.1-1.2	0.51	0.38
Zone G	0.4-0.7	0.55	0.21
Zone H	0.2-0.4	0.3	0.14
Zone I	0.1-1.4	0.68	0.57
Zone J	0.2-1.5	0.8	0.64
Zone K	N/A	N/A	N/A
Zone L	0.1-1.4	0.53	0.34
Zone M	0.1-1.2	0.3	0.35

4.2. Decay rate of aftershock activity

The temporal decay rates of aftershocks can be described by the modified of Omori's law (Utsu, 1961). The values of constant p , c and K of the equation can be estimated by using the maximum likelihood method. Typically, p value varies in the range of 0.7-1.5 which is used to describe the variation of the decay rate of aftershock. After the modified Omori's law calculation, the results of the decay rate of aftershock in the MSEA can be described by the parameters p , c and K in the equation as follows.

According to Table 4.3, showing the values calculated by the modified Omori's law, consisting of p , c and K . Overall, in the other zones, calculated p values ranged from 0.28 to 3.92 while c values ranged from 0 to 0.86 and K values ranged from 0.10 to 50.95.

From the Figure 4.3n, to show the estimate parameter for the MSEA as $p = 0.47$, $c = 0$ and $K = 34.02$ and forecasted of aftershock activity for next 100 days. The p value is less than the universal value which is 1.0.

Based on the Figure 4.3a-b, in the Sumatra-Andaman interplate and Sumatra-Andaman intraslab, the calculated p values are very similar that is approximately 0.8. The c values are 0.06 and 0.1, respectively. The K values are 7.48 and 11.06, respectively. While the decay rates of aftershock are 94 and 115 days, respectively.

According to the Figure 4.3c-d, in the Sagaing fault zone and the Andaman basin, the calculated p values are very similar, which is approximately 1.2. The parameter c and K of Sagaing fault zone are approximately 0 and 1.22, respectively while the parameter c and K of Andaman basin are approximately 0.38 and 15.97, respectively as well. Besides, the decay rate of aftershock can be estimated to 154 days for the Sagaing fault zone and 72 days for the Andaman basin.

Regarding to the Figure 4.3e, all calculated parameters in the Sumatra fault zone are $p = 0.77$, $c = 0.08$ and $K = 4.96$ while the decay rate of aftershock is approximately to 110 days.

Refer to the Figure 4.3f and 4.3i, in Hsenwi-Nanting fault zone has the calculated parameters as $p = 0.88$, $c = 0.68$ and $K = 2.00$ whilst, in Jinghong-Mengxing fault zones has the parameters as $p = 0.98$, $c = 0.00$ and $K = 1.03$. The p values are similar in both area. For the estimation of the decay rate of aftershock in each area, it is possible that the Hsenwi-Nanting fault zone will be aftershock up to 58 days

after mainshock and the Jinghong-Mengxing fault zones will be aftershock up to 132 days after mainshock.

According to the Figure 4.3g, the estimated parameters in the Western Thailand are $p = 0.48$ $c = 0.00$ and $K = 0.42$. As the decay rate of aftershock is approximately 16 days.

Refer to the Figure 4.3j, in the Northern Thailand-Dein Bein Fhu, the parameters of the decay rate of aftershock is estimated as $p = 1.18$ $c = 0.10$ and $K = 2.49$ and forecasted of aftershock activity for next 248 days.

Regarding to the Figure 4.3l and m, both of the Xianshuihe fault zone and Red River fault zone, the estimated parameter p and c are similar to at 1.0 for p value and 0 for c value, and then K values are 1.86 and 0.42 in accordingly area. Meanwhile, the decay rate of aftershock is approximately 59 days for the Xianshuihe fault zone and 11 days for the Red River fault zone.

Table 4.3 Calculated values of p , c and K from the modified Omori's law in the seismic source zone in the MSEA.

Zone	p	p_{av}	c	c_{av}	K	K_{av}
ALL	0.47	0.47	0.02	0.02	34.02	34.02
Zone A	0.62 - 1.08	0.84	0 - 0.28	0.06	1.75 - 24.56	7.48
Zone B	0.31 - 1.23	0.82	0 - 0.51	0.1	0.10 - 50.95	11.06
Zone C	0.67 - 3.92	1.2	0	0	0.29 - 2.33	1.22
Zone D	0.52 - 2.04	1.22	0 - 0.86	0.38	4.97 - 45.70	15.97
Zone E	0.63 - 1.22	0.77	0 - 0.37	0.08	0.95 - 9.98	4.96
Zone F	0.40 - 1.05	0.90	0	0	0.36 - 1.19	0.80
Zone G	0.48	0.48	0	0	0.42	0.42
Zone H	N/A	N/A	N/A	N/A	N/A	N/A
Zone I	0.86 - 1.07	0.96	0	0	0.45 - 3.61	1.09
Zone J	1.02 - 1.67	1.34	0 - 0.33	0.13	1.31 - 6.62	3.17
Zone K	N/A	N/A	N/A	N/A	N/A	N/A
Zone L	0.28 - 1.11	0.89	0 - 0.04	0.01	0.25 - 4.95	1.85
Zone M	1	1	0	0	0.28 - 0.55	0.42

Remark: av = average

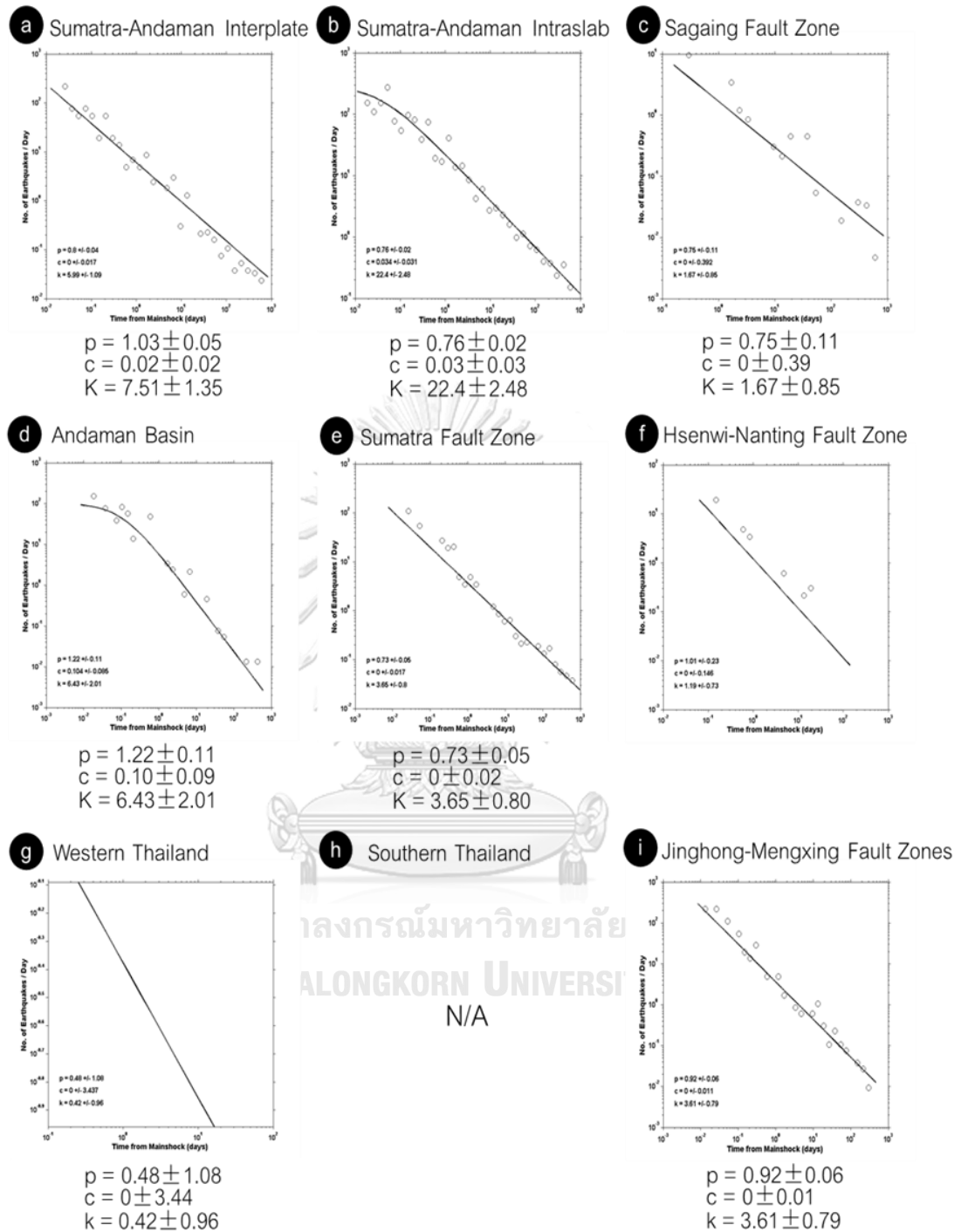


Figure 4.3 The temporal change of the number of aftershock per day in the 13 seismic source zones and in the MSEA.

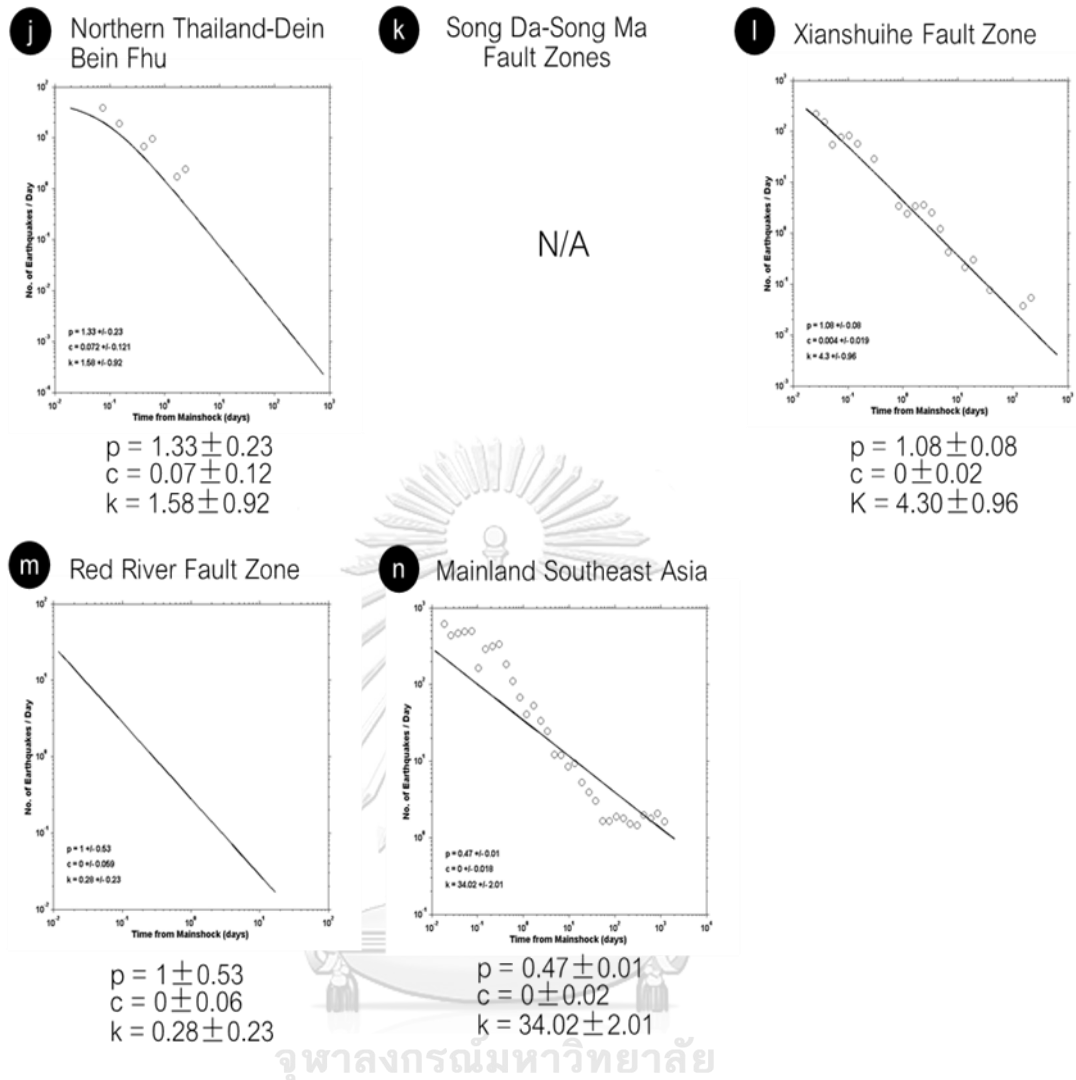


Figure 4.3 (Cont.) The temporal change of the number of aftershock per day in the 13 seismic source zones and in the MSEA.

CHAPTER 5

SEISMIC STRESS AND PATTERN

In order to investigate in detail the characteristics of the aftershock in the MSEA, it is necessary to use several statistical methods. Not only did the study in the part of maximum magnitude of aftershock and the temporal decay of aftershock that obtained in the previous chapters, but it also assessed the seismic stress and pattern in order to fully understand the characteristics of the aftershock sequence. In this chapter, the statistical seismology used in the assessment is divided into 3 parts, i.e., i) the rose diagram, ii) the magnitude-frequency relationship and iii) the spatial fractal dimension.

The statistical seismicity investigation also implements the same completeness seismicity catalogue used in the previous investigation. The earthquake data is grouped into 13 zones according to Pailoplee and Choowong (2013) and selected the major earthquake in each zone as well as the previous investigation (see also in Chapter 3). The aim of this chapter is finding the seismic stress and pattern which is one of the major characteristics of the aftershock.

5.1. Rose Diagram

In this work using the rose diagram to describe the distribution of aftershocks in same cluster relative to the mainshock in the MSEA. After recruiting representatives in each zone, which had 90 total data in 13 zones of the study area, then the plot of rose diagram was started from calculating the distance and direction between aftershocks and mainshock in the cluster. Then plotted the location of all aftershocks and mainshock using these data and the main earthquake by assigning an earthquake to the center, which determined that the mainshock was centered.

After plotting the rose diagram, the results of each cluster in each zone also have a unique distribution of aftershock. For the results of all zone in MSEA, there are up to 90 diagrams, so choose one of the diagrams to represent each zone (see also Figure 5.1). View be describe as follows.

According to the Figure 5.1a, the M_W -7.5 earthquake generated on August 10th, 2009 in the Andaman Islands which located on Sumatra-Andaman interplate (zone A), is triggering to a total of 110 aftershocks. The distribution of these aftershocks relative to the mainshock was found that distributed in two main directions. It ranges from 270 to 330 degrees and 190 to 200 degrees.

Based on the Figure 5.1b, the M_W -9.0 earthquake at off west coast of the northern Sumatra which located on Sumatra-Andaman intraslab (zone B) generated on December 26th, 2004, is triggering to a total of 286 aftershocks. The distribution of these aftershocks relative to the mainshock was found that distributed in two main directions. It ranges from 135 to 225 degrees and 300 to 360 degrees.

Refer to the Figure 5.1c the M_W -6.9 earthquake generated on January 5th, 1991 along the Sagaing fault zone (zone C) at Myanmar, is triggering to a total of 13 aftershocks. The distribution of 13 aftershocks relative to the mainshock was found that distributed in two main directions. It ranges from 245 to 270 degrees and 315 to 360 degrees.

From the Figure 5.1d, the M_W -6.4 earthquake at Nicobar Islands which located on Andaman basin (zone D) generated on March 21st, 2014, is triggering for 120 aftershocks. The distribution of 120 aftershocks relative to the mainshock was found that distributed in ranges from 90 to 180 degrees.

Based on the Figure 5.1e, 131 aftershocks occur due to the M_W -6.1 earthquake generated on January 6th, 2009 in the Northern Sumatra which located

on Sumatra fault zone (zone E). These aftershocks that related with mainshock are distributed in one direction, ranging from 225 to 325 degrees.

Regarding to the Figure 5.1f, the aftershocks occur due to the M_W -5.6 earthquake generated on April 12th, 2001 in the Yunnan province, China which located on Hsenwi-Nanting fault zone (zone F). These aftershocks that related with mainshock are distributed in ranging from 270 to 315 degrees.

Refer to the Figure 5.1g, the M_W -5.7 earthquake generated on March 1st, 1989 in Myanmar that located on Western Thailand (zone G), is triggering for aftershocks. These aftershocks that related with mainshock are distributed in two main directions. It ranges from 220 to 235 degrees and 315 to 360 degrees.

According to the Figure 5.1h, the M_W -4.5 earthquake generated on September 27th, 2006 in the Gulf of Thailand which located on zone H or Southern Thailand, is the trigger that cause the aftershocks. The distribution of these aftershocks relative to the mainshock was found in two main directions, ranging from 290 to 310 degrees and 350 to 360 degrees.

From the Figure 5.1i, the M_W -7.0 earthquake along Jinghong-Mengxing fault zones (zone I) which located on Myanmar-China border region generated on November 6th, 1988, is triggering to 43 aftershocks. The distribution of these aftershocks relative to the mainshock was found that distributed in ranges from 315 to 360 degrees.

Based on the Figure 5.1j, The M_W -6.2 earthquake in Thailand which located on Northern Thailand-Dein Bein Fhu (zone J) generated on May 5th, 2014, is the trigger that cause the 20 aftershocks. The distribution of these aftershocks relative to the mainshock was found that distributed in two main directions. It ranges from 260 to 315 degrees and 345 to 360 degrees.

Regarding to the Figure 5.1l, the aftershocks occur due to the M_w -5.6 earthquake generated on September 7th, 2012 along Xianshuihe fault zone (zone L) in the Yunnan province, China. These aftershocks that related with mainshock are distributed in ranging from 310 to 360 degrees.



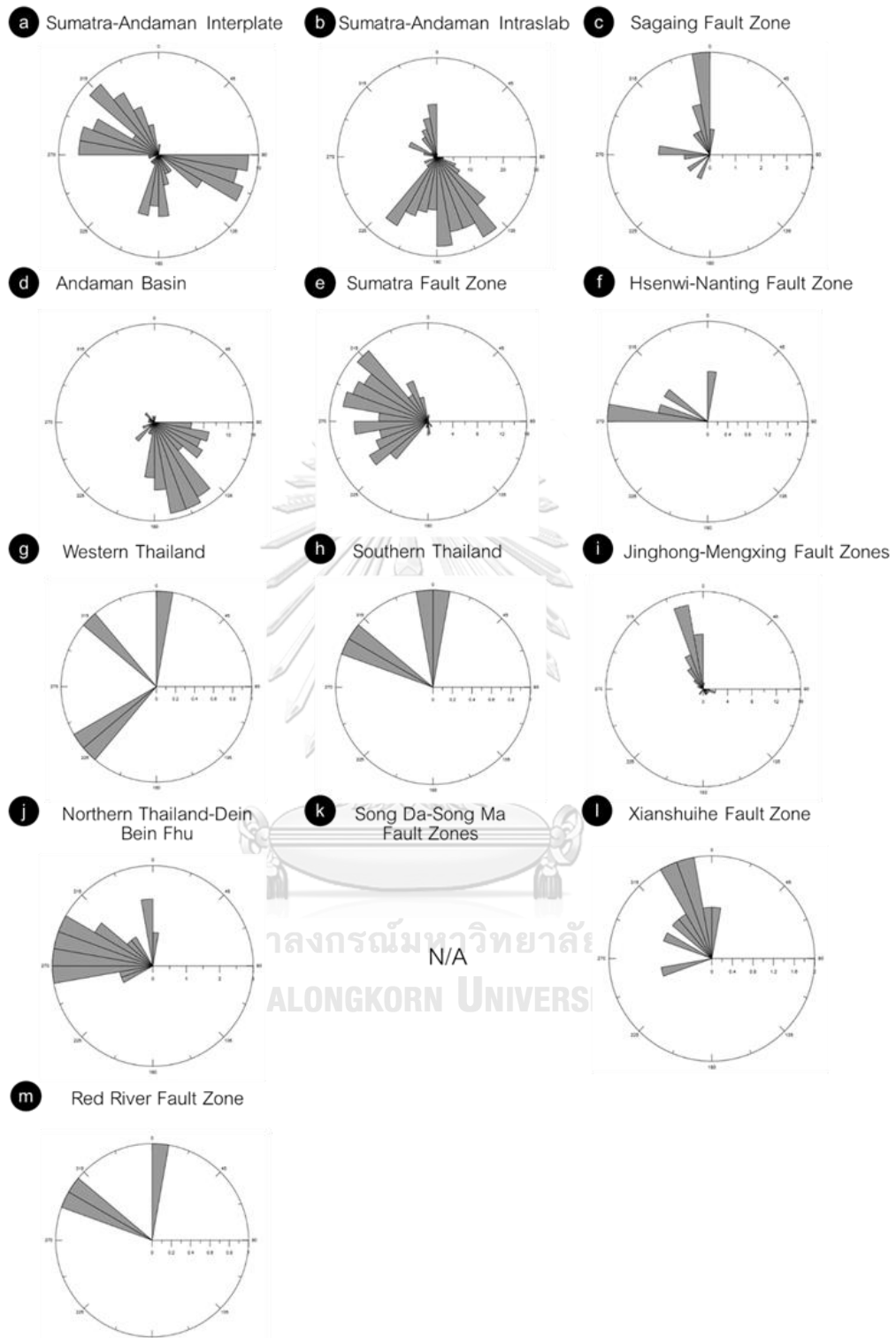


Figure 5.1 The rose diagrams showing the distribution of the aftershocks in each cluster of mainshock in the MSEA.

In the final of Figure 5.1 m, the M_W -5.0 earthquake generated on May 17th, 2016 along the Red River fault zone (zone M) which located on Yunnan province, China, is the trigger that cause the aftershocks. The distribution of these aftershocks relative to the mainshock was found in two main directions, ranging from 0 to 10 degrees and 290 to 310 degrees.

5.2. Co-seismic Stress

The frequency-magnitude distribution of earthquakes is well approximated by the G-R relationship. The a and b values of G-R relationship are estimated from ZMAP software (Wiemer, 2001) which vary in space window and specific time. The b value is the one of the significant parameter in seismology where b value describe the tectonic stress.

The first step for analyze the G-R relationship is estimated the magnitude of completeness from the G-R relationship curve by using the maximum curvature method (Woessner and Wiemer, 2005) and then, calculated the b and a values from maximum likelihood method (Utsu, 1978) for 13 zones in the MSEA.

After the G-R relationship calculation, zone G, H, K and M cannot estimate the G-R relationship plots because the earthquake data is insufficient for analysis. Overall, in the other zones, calculated b values ranged from 0.72 to 1.31. The highest b value was observed in zone D while the lowest b value was detected in zone B. Then, the estimated magnitude of completeness for the other zones varied between 4.1 and 4.9 (Table 5.2 and Figure 5.2). For detail explanation, the G-R relationship can be described as follows.

According to the Figure 5.2n, the frequency-magnitude distribution curve of the overall of the MSEA illustrates the b and a values, which are 1.14 and 9.15 respectively, and the magnitude of completeness (M_c) is calculated to 4.5.

Based on the Figure 5.2a, in Sumatra-Andaman interplate, the parameters from the estimated FMD plots are as follows: b value is 1.12, a value is 6.84 and magnitude of completeness is 4.5, whereas in the other zones that consists of the Northern Thailand-Dein Bein Fhu (Figure 5.2k) and the Jinghong-Mengxing fault zones (Figure 5.2i), the calculated b value is similar to in the Sumatra-Andaman interplate which is approximated to 1.1. The other parameters of G-R relationship include a value that is equal to 5.92 in the Northern Thailand-Dein Bein Fhu and is equal to 6.81 in the Jinghong-Mengxing fault zones and the magnitude of completeness (M_c) is calculated to 4.3 and 4.9, respectively.

Refer to the Figure 5.2b, the frequency-magnitude distribution curve of the Sumatra-Andaman intraslab shows the b and a values, which are 1.02 and 6.85 respectively, and the magnitude of completeness (M_c) is calculated to 4.5.

Regarding to the Figure 5.2c-e, the calculated b value of G-R relationship is about 1.2 in the Sagaing fault zone, the Andaman basin and the Sumatra fault zone. The other parameter described as values. The calculated a values are 7.18, 6.62 and 7.23, respectively. And then, the magnitude of completeness (M_c) is calculated to 4.9, 4.4 and 4.5, respectively.

In the final of Figure 5.2f, in the Hsenwi-Nanting fault zone, the estimated b value is equal to 1.03 with a value = 5.24 and the magnitude of completeness is calculated to 4.1. While in the Xianshuihe fault zone (Figure 5.2l), the estimated b value is equal to 0.91 with a value = 5.39 and the magnitude of completeness is calculated to 4.3. It is indicated that the b value of the both area are similar.

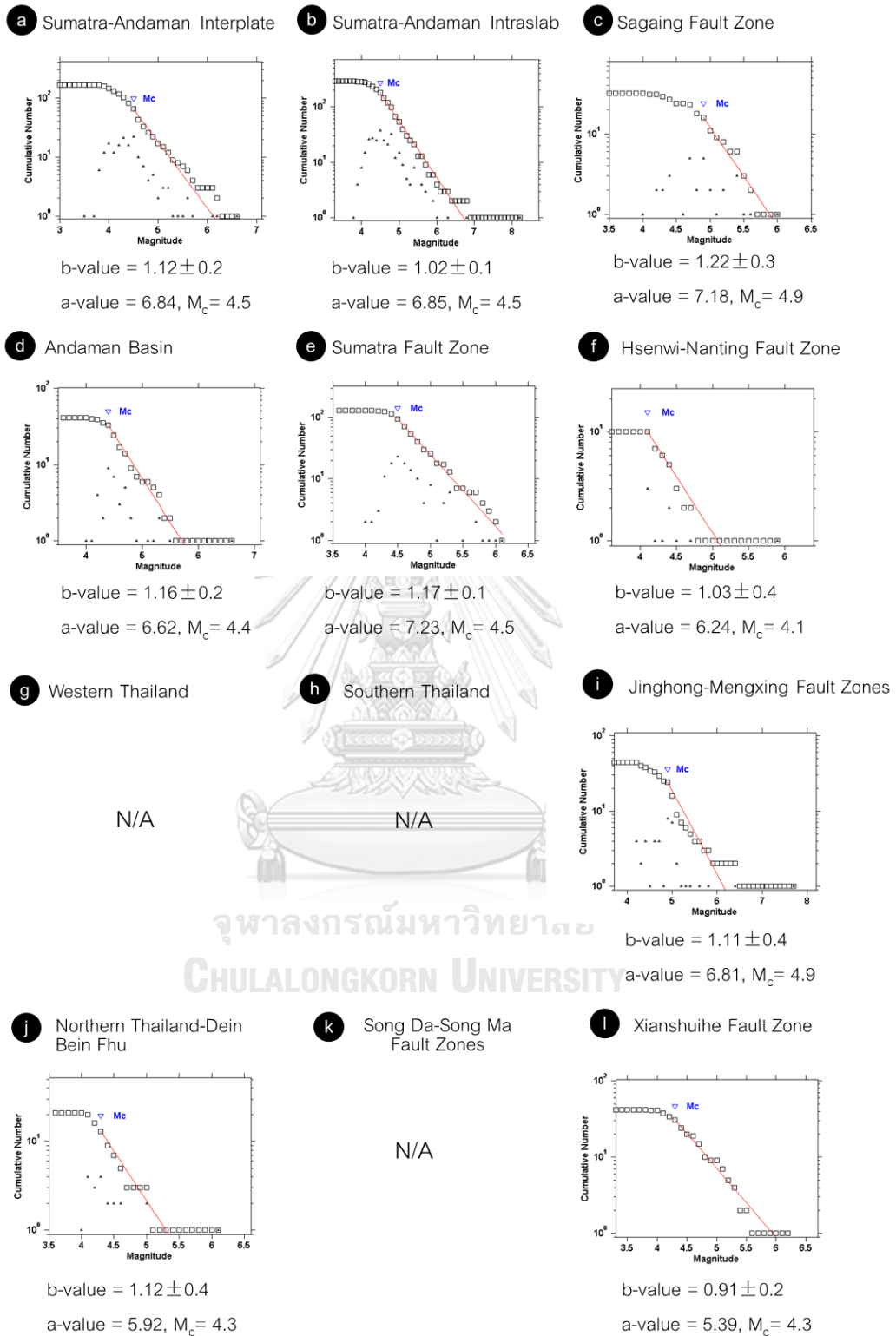


Figure 5.2 The frequency-magnitude distribution in the 13 seismic source zones and in the MSEA from the G-R relationship.

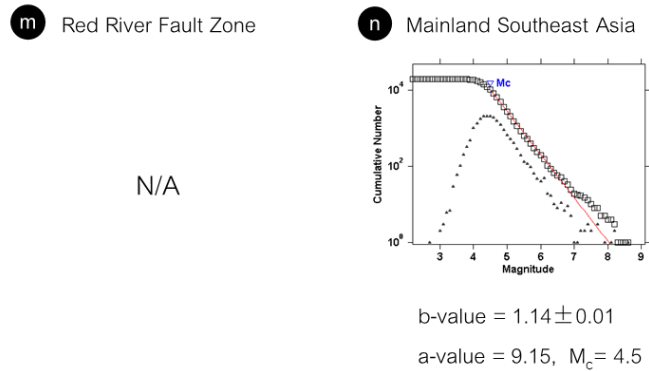


Figure 5.2 (Cont.) The frequency-magnitude distribution in the 13 seismic source zones and in the MSEA from the G-R relationship.

Table 5.1 Estimated values of a, b and M_c from the frequency-magnitude distribution in the 13 seismic source zone in the MSEA.

Zone	a	a av	b	b av	M_c
ALL	9.15	9.15	1.14	1.14	4.5
Zone A	5.48-7.58	6.32	0.84-1.31	1.06	4.4
Zone B	4.4-10.5	6.59	0.72-1.76	1.06	4.7
Zone C	3.44-6.93	5.51	0.57-1.24	0.98	4.6
Zone D	6.62-14.9	8.56	1.16-2.90	1.53	4.5
Zone E	5.45-12.4	7.39	0.86-2.37	1.29	4.6
Zone F	5.24	5.24	1.03	1.03	4.1
Zone G	N/A	N/A	N/A	N/A	N/A
Zone H	N/A	N/A	N/A	N/A	N/A
Zone I	4.73-11.70	7.75	0.88-2.00	1.33	4.9
Zone J	4.22-5.92	4.9	0.79-1.12	0.9	4.4
Zone K	N/A	N/A	N/A	N/A	N/A
Zone L	5.39-7.97	6.12	0.91-1.54	1.13	4.4
Zone M	N/A	N/A	N/A	N/A	N/A

Remark: av = average

In addition, the temporal variations of the b value were analyzed in this study which explain the change in b value as compared to time after mainshock. This work using the method of sliding and overlapping time windows which determines the minimum of the number of events in each window to be 30 events and are change in time steps of 5 events (Nuannin et al., 2005). The results of the temporal variations of the b value are shown in Figure 5.3, all of the zones have the same trend of the b value as a term of time. There is a dramatically change during the first month after mainshock. Then, after the earthquake over a period of time (~6 months), the b value is a significant increase and finally, remain steady until the last of aftershock which can be described the example as follow.

From the Figure 5.3a, in the Sumatra-Andaman interplate zone, after the M_w -6.3 earthquake generated on December 26th, 2014, there is a steep increase in the b value at the beginning of the period (~1 months) until the b value is about 0.6, after that is decreased in 2005.05 which reached its minimum (minimum b value = 0.48) before continuing to rise again that reached its maximum in 2005.2 (maximum b value = 0.75). And the last, the b value is remained steady until the last of the aftershock.

According to the Figure 5.3b, the trend of b value with time in the Sumatra-Andaman intraslab are similar to the Sumatra-Andaman interplate zone. It is explained that the b value have increased dramatically after the M_w -7.4 earthquake generated on February 20th, 2008 around 1 months until the b value is equal to 0.5. Next, there is a significant decline in the b value at 2008.3 which decreases until the minimum value (minimum b value = 0.35). And then, the b value is increased again to 0.45 and does not change until 2008.6 that is slightly increased to the maximum value (maximum b value = 0.50), after that it is remained steady until the last of the aftershock.

Based on the Figure 5.3e, the trends of b value with time in the Sumatra fault zone and the Sumatra-Andaman intraslab are likely to vary as well. But the last step of the earthquake in the Sumatra fault zone, the b value is a significant increased until the end of the aftershock. This will change as follows, the b value have increased dramatically after the M_W -6.1 earthquake generated in December 27th, 2014 until the b value is about 0.65. Next, there is a significant fall in the b value until the minimum value (minimum b value = 0.45). And then, the b value is increased again to 0.6 and is slightly decreased again until the b value is equal to 0.5, after that, it is a significant increased until the end of the aftershock.

Refer to the Figure 5.3i, the trend of b value with time in the Jinghong-Mengxing fault zones are similar to the Sumatra fault zone. But the last step of the earthquake in the Jinghong-Mengxing fault zones, it is a slight decline until the end of the aftershock. It is explained that after the M_W -7.7 earthquake generated on November 6th, 1988, there is a steep increase in the b value at the beginning of the period until the b value is about 1.2, after that it is decreased which reached its minimum (minimum b value = 1.1) before continuing to rise until the b value is approximate to 1.2 and then the b value is decreased until the minimum value again before continuing to rise that reached its maximum in 1988.95 (maximum b value = 1.8). And the last, the b value is a slightly until the last of the aftershock.

Regarding to Figure 5.3d, in the Andaman basin, after the M_W -6.4 earthquake generated on March 21st, 2014, there is a sharp rise in the b value which reached its maximum (maximum b value = 1.70) and is decreased in 2014.3 which reached its minimum (minimum b value = 1.45) before continuing to rise again and then remain steady.

According to Figure 5.3c, in the Sagaing fault zone, after the M_W -6.6 earthquake generated on September 21st, 2003, there is a steep decreased in the b value at the beginning of the period from the b value is about 1.8 to 0.8 that its

minimum value before continuing to increase again until the b value is about 1.2. Next, it is slightly decreased before continuing to gradually rise in 2004 until the b value is approximate to 1.2. And the last, the b value is remained steady until the last of the aftershock.

Based on the Figure 5.3l, In the Xianshuihe fault zone and the Sagaing fault zone have the same tendency of the temporal variations of the b value. It can be seen that the b value is decreased dramatically after the M_W -6.2 earthquake generated on February 3rd, 1996 from 2.0 to 1.0, after that is sharply increased until 1996.15. And the last, the b value is remained steady until the last of the aftershock.

In the final of the Figure 5.3n, it shows the temporal variations of the b value in the MSEA, which are not separated into the seismic source zone. It is evident that in the beginning period, it will be slightly increased to the maximum b value (maximum b value = 1.50), after which it is rapidly decreased in 1988 that the b value is approximately 1.1. Subsequently, there will be a slight increase and gradually decrease in the period from 1990-1995 that the b value is in the range of 1.0-1.1. And there is rise again before continuing to fall again in 2005. And in the final phase, it was increased again before falling sharply to the minimum value in 2009, after which b value has fluctuated.

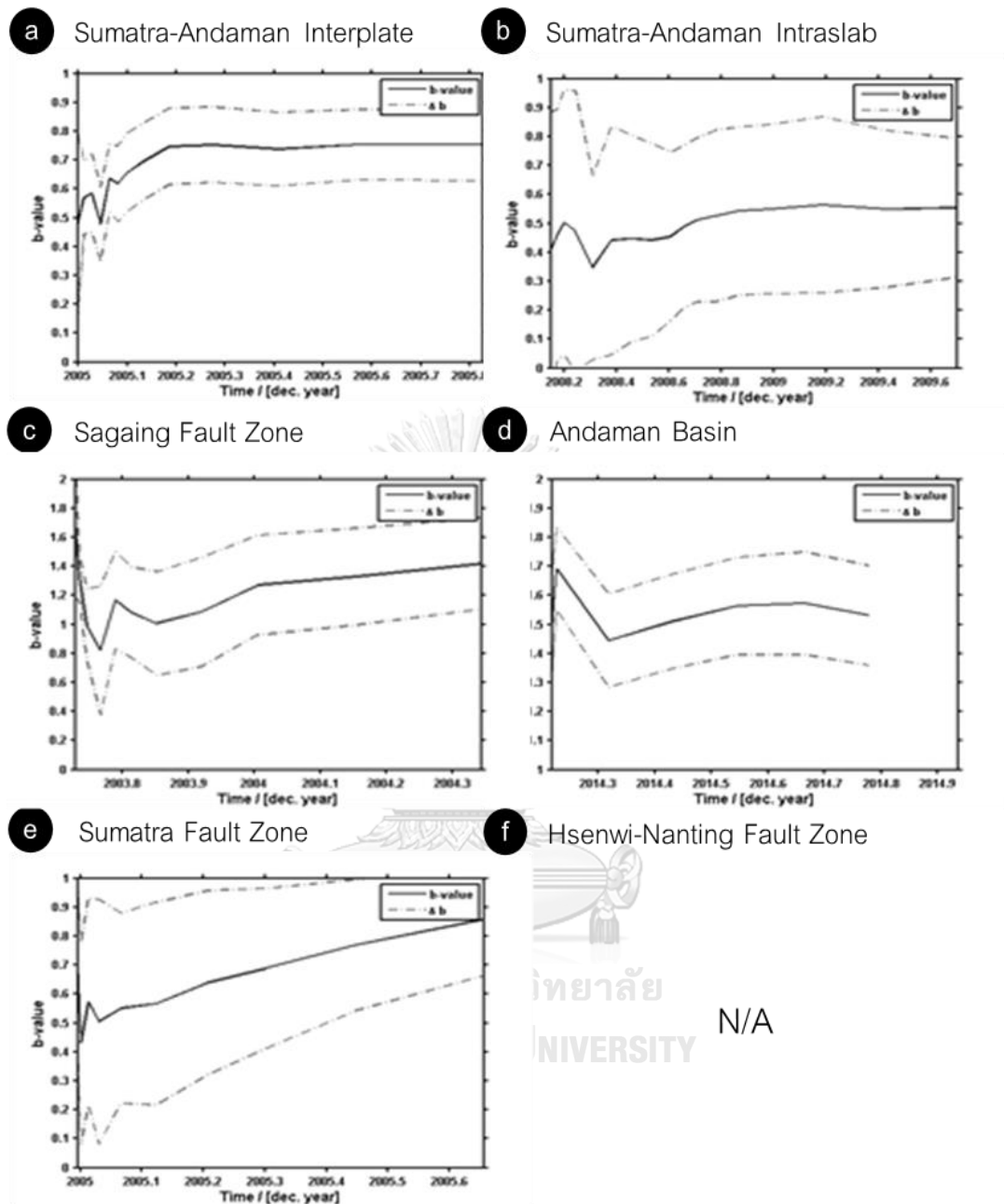


Figure 5.3 The temporal variations of the b value in the 13 seismic source zones in the MSEA.

g Western Thailand

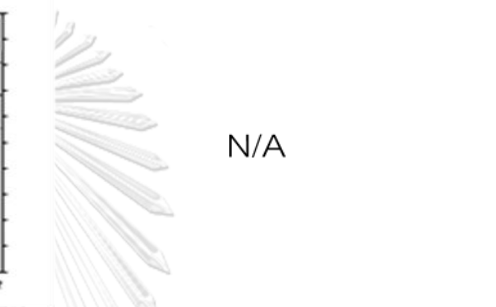
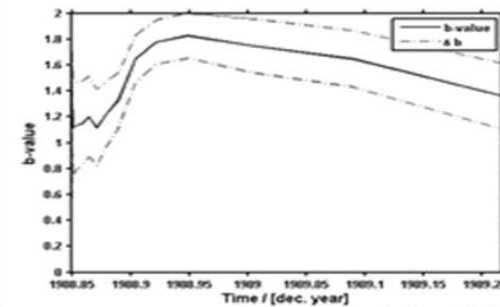
h Southern Thailand

N/A

N/A

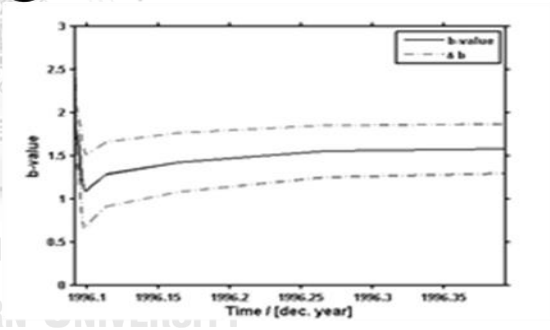
i Jinghong-Mengxing Fault Zones

j Northern Thailand-Dein Bein Fhu



k Song Da-Song Ma Fault Zones

l Xianshuihe Fault Zone



m Red River Fault Zone

n Mainland Southeast Asia

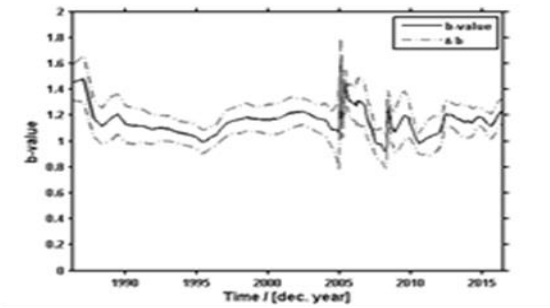


Figure 5.3 (Cont.) The temporal variations of the b value in the 13 seismic source zones in the MSEA.

5.3) Seismic Pattern

The spatial distribution of seismicity is examined through the natural way that called fractal dimension (D_c value). It describes the seismic pattern of the aftershock clusters in the earthquake. In this study, the correlation integral technique for fractal analysis (Grassberger and Procaccia, 1983) is used to investigate the spatial distribution of aftershock sequence of the MSEA. The fractal dimension can be evaluated by fitting the data with the slope in straight line from the log-log plot of $C(r)$ versus r .

After estimating the fractal dimension, D_c value cannot be estimated in zone f, g, h, j, k and m due to lack of available earthquake catalogue (<30 event). All other zones, the calculated D_c values were within the range of 1.96 to 2.58 which is considered that the D_c value approaches 2 in all zone. For the results of all zone in the MSEA can be seen in the Table 5.2 View be describe as follow examples.

From the Figure 5.3, the calculated D_c value in several zones within the study area is approximately equal to 2.2, which consists of the Sumatra-Andaman interplate (Figure 5.3a), the Andaman basin (Figure 5.3d), the Sumatra fault zone (Figure 5.3e) and the Xianshuihe fault zone (Figure 5.3l).

Refer to the Figure 5.3a and d, in the Sumatra-Andaman interplate, the calculated D_c value is approximated to 2.2 with the range 1 and 2 as 1.78 and 28.15, respectively while in the Andaman basin, the calculated D_c value is approximated to 2.2 as same as with the range 1 and 2 as 3.14 and 27.11.

Based on the Figure 5.3e and l, the calculated D_c value in 2 zones are approximately equal to 2.2, where in the Sumatra fault zone is the D_c value in the range of 1 and 2, which is 3.51 and 30.37. While in the Xianshuihe fault zone, there are D_c value in the range of 1 and 2, which are 6.94 and 27.11.

Regarding to the Figure 5.3b, the calculated D_c value is equal to 2.57 with the range 1 and 2 as 0.87 and 20.80, respectively in the Sumatra-Andaman intraslab which indicates the highest D_c value.

According to the Figure 5.3i, the calculated D_c value in the Jinghong-Mengxing fault zones is approximately 2 that is equal to 2.09 and range between 7.49 and 39.57.

According to the Figure 5.3c, the calculated D_c value in the Sagaing fault zone is indicated the lowest value that is equal to 1.96 and range between 4.09 and 39.57.

In final, the Figure 5.3n, in the overall of the MSEA, the calculated D_c value is approximated to 2.2 with the range 1 and 2 as 3.51 and 46.04, respectively.

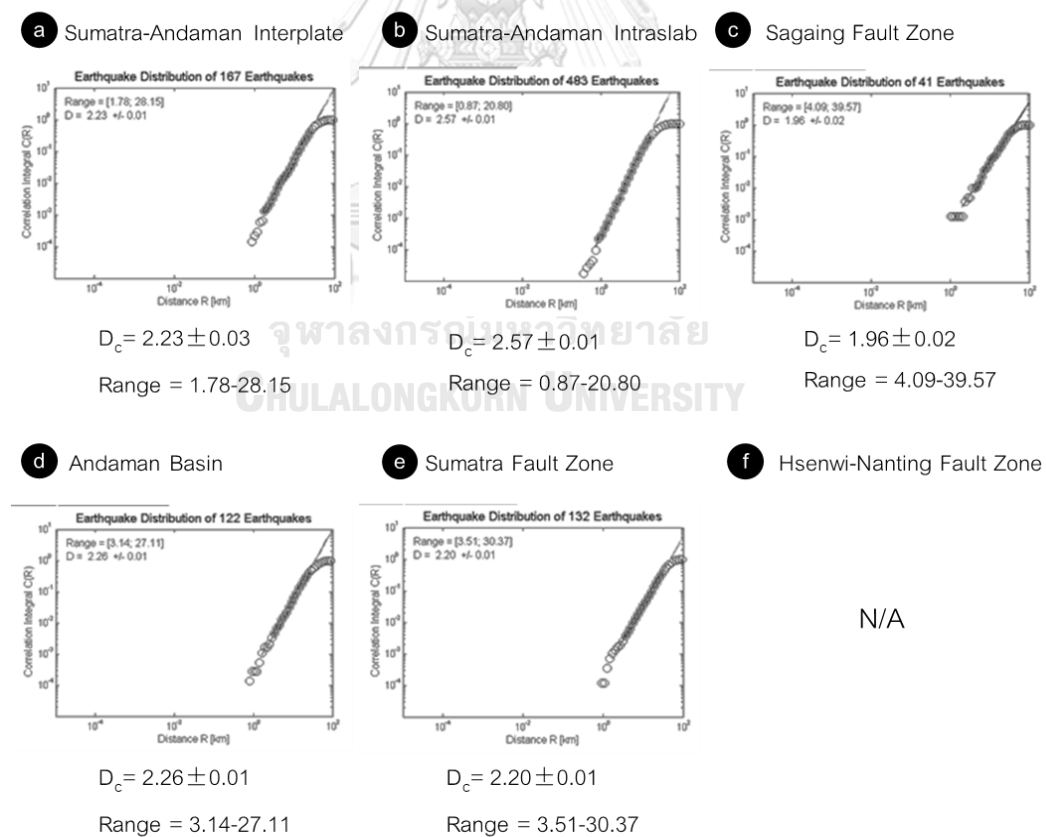


Figure 5.4 Graph illustrates the fractal dimension of the distribution of aftershock in the 13 seismic source zones and in the MSEA.

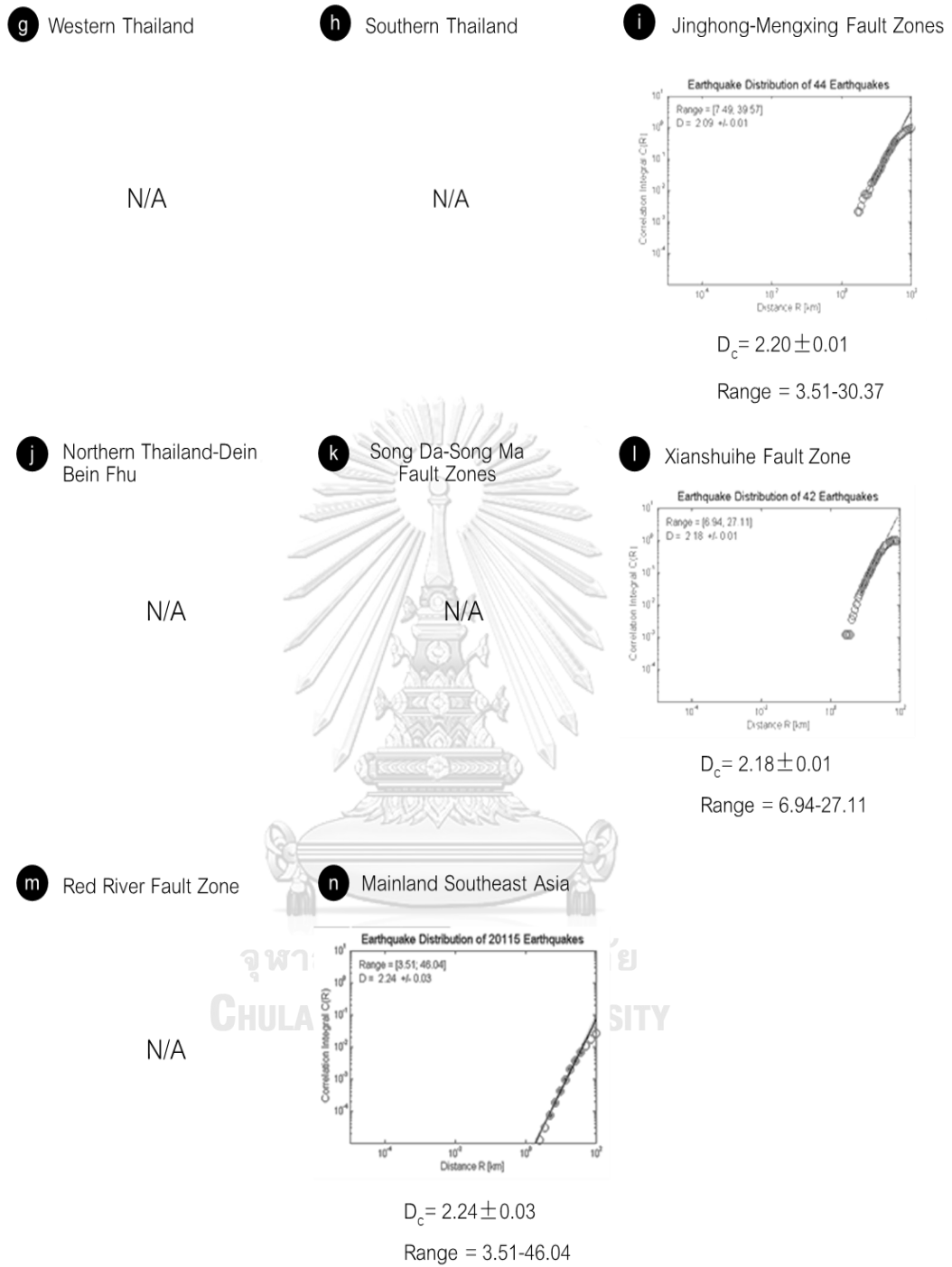


Figure 5.4 (Cont.) Graph illustrates the fractal dimension of the distribution of aftershock in the 13 seismic source zones and in the MSEA.

Table 5.2 Spatial characteristic (fractal dimension) and seismic pattern in the 13 seismic source zone in the MSEA.

Zone	D_c	R_1	R_2	Seismic pattern
ALL	2.24±0.03	3.51	46.04	Area
Zone A	2.23±0.01	1.78	28.15	Area
Zone B	2.57±0.01	0.87	20.8	Area
Zone C	1.96±0.02	4.09	39.57	Area
Zone D	2.26±0.01	3.14	27.11	Area
Zone E	2.20±0.01	3.51	30.37	Area
Zone F	N/A	N/A	N/A	N/A
Zone G	N/A	N/A	N/A	N/A
Zone H	N/A	N/A	N/A	N/A
Zone I	2.09±0.01	7.49	39.57	Area
Zone J	N/A	N/A	N/A	N/A
Zone K	N/A	N/A	N/A	N/A
Zone L	2.18±0.01	6.94	27.11	Area
Zone M	N/A	N/A	N/A	N/A

CHAPTER 6

DISCUSSION

This chapter will support the results of the previous chapter, which illustrate the characteristic of the aftershock for 13 seismic source zones in the MSEA. By comparing the results in previous chapters in each other with the previous researches which corresponded to this study. The comparison of the results was described as follows.

6.1. Relationship between the Magnitude of Mainshock and Its Largest Aftershock

According to the Bath's law (Bath, 1965), the relationship between magnitude of the mainshock and the largest aftershock in the each seismic source zone is different, which is a unique characteristic. This relationship is very useful when the earthquake occurs, the largest aftershock will be determined by the magnitude of mainshock.

The first result, Figure 6.1 illustrates the average difference value between the magnitude of the mainshock and its largest aftershock in each zone. If there is a high difference value, the aftershock will be much lower than the mainshock, which is shown in light red color. Whereas, if the difference value is low, the aftershock is not much lower than the mainshock, which is indicated by a dark red color. Overall, the difference value in the MSEA is approximately 0.5. It can be described that in Northern Thailand-Dein Bein Fhu (zone J), the average difference value is the highest (0.8). While in the Red River fault zone (zone M), the average difference value is the lowest (0.3). Mostly, in the intraplate of the MSEA, the average difference is range between 0.5 and 0.8. The average difference in Thailand is 0.6 and 0.5, which is in the Western Thailand (zone G) and the Southern Thailand (zone H), respectively. In the Red River fault zone, although it is far from Thailand, but when the earthquake

occur, it also affects Thailand as well. In addition, when the same magnitude mainshock in each other zone occurs, the aftershock in this zone will be larger than in other zones. It can be said that the larger aftershock will cause more damage.

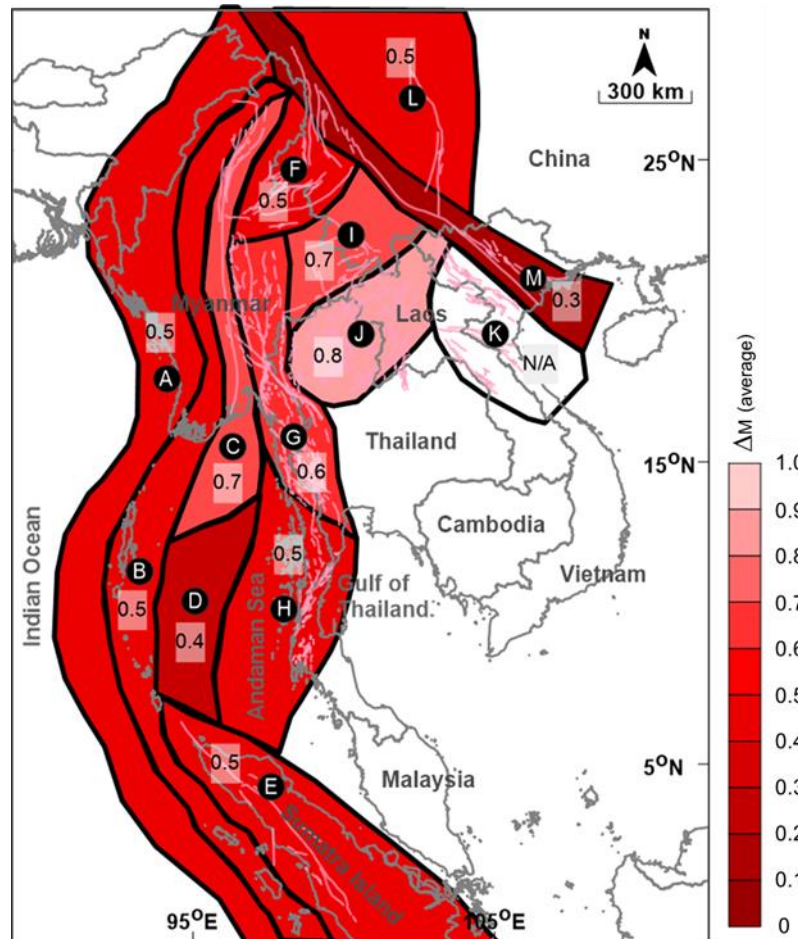


Figure 6.1 Map showing distribution of the average difference value between magnitude of the mainshock and the maximum aftershock for 13 seismic source zones (A to M) proposed in the MSEA.

In addition to the average difference, the maximum of difference value between the magnitude of the mainshock and the maximum aftershock is also significant for the interpretation of the relationship between magnitude of the mainshock and the maximum aftershock, as shown in Figure 6.2. The maximum

difference value is displayed in blue color, which if the maximum of difference value is low, the aftershock is not much lower than the mainshock, which is indicated by a dark blue color. Whereas, if the maximum difference value is high, the aftershock is much lower than the mainshock, which is shown in light blue color. Figure 6.2 shows that in the interplate zone, the difference value is in the range of 2.0-2.5 while in the intraplate zone, the difference value is in the range of 1.0-1.8, except in the Western Thailand and Southern Thailand, the difference values are lower than the other zones, which are 0.4 and 0.7, respectively.

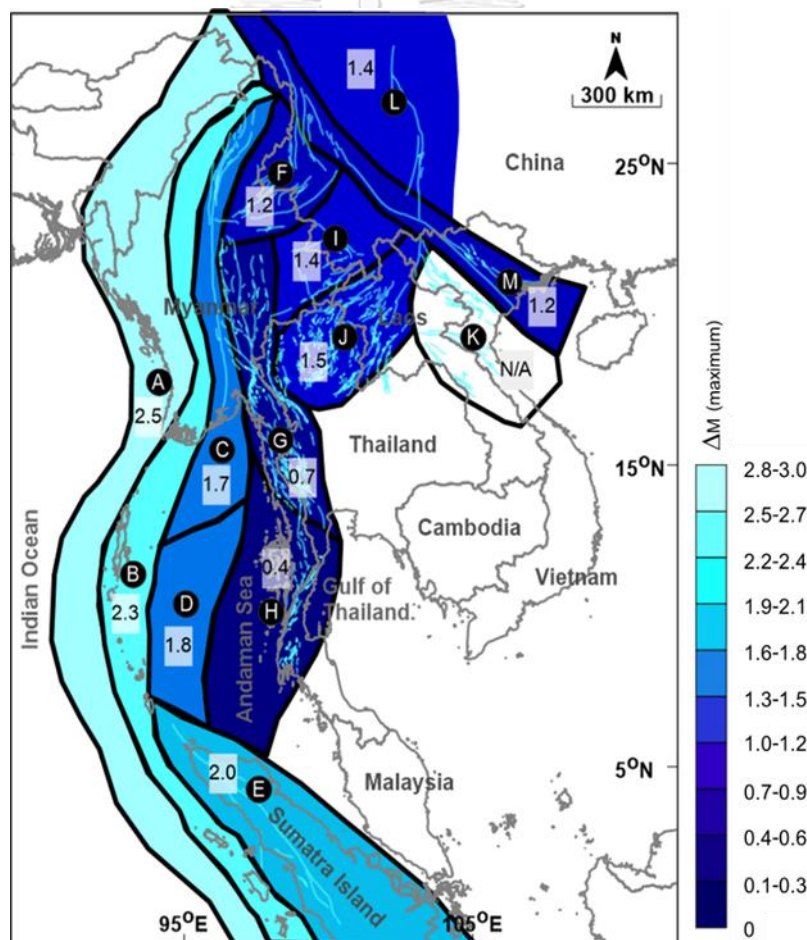


Figure 6.2 Map showing distribution of the maximum difference value between magnitude of the mainshock and the maximum aftershock for 13 seismic source zones (A to M) proposed in the MSEA.

Based on the instrumentally recorded earthquake, the mainshock that occurs in the interplate zone of the MSEA is the largest earthquake, for example, the M_W -9.0 earthquake generated on December 26th, 2004 at the Sumatra–Andaman subduction zone (Martin, 2005). However, from the results found that the aftershock with the mainshock is quite different, which means that the aftershock in this zone will be moderate magnitude, but it was also disaster. While the mainshock that occurs in the intraplate zone of the MSEA is not as large as the interplate zone, but the results show that the aftershock with the mainshock is not quite different, which means that the aftershock that occurs after the mainshock will be moderate, which is equivalent to the aftershock in the interplate zone. It is considered a disaster. Moreover, especially in the Western Thailand (zone G) and Southern Thailand (zone H), the maximum difference values are very small, although from the instrumentally recorded earthquake, the mainshocks that occur in these zones are moderate magnitude, but when the aftershock occurs, the magnitude of aftershock will be hardly any differences with the mainshock. As a result, these zones are considered to be very recognizable zones.

The final result in this section is the standard deviation of the difference between the magnitude of the mainshock and the largest aftershock in 13 seismic source zone of the MSEA. From figure 6.3, it is evident that the standard deviation in all seismic source zone of the MSEA is in the range 0.1-0.6, which means that all results in this section are intermediate reliable.

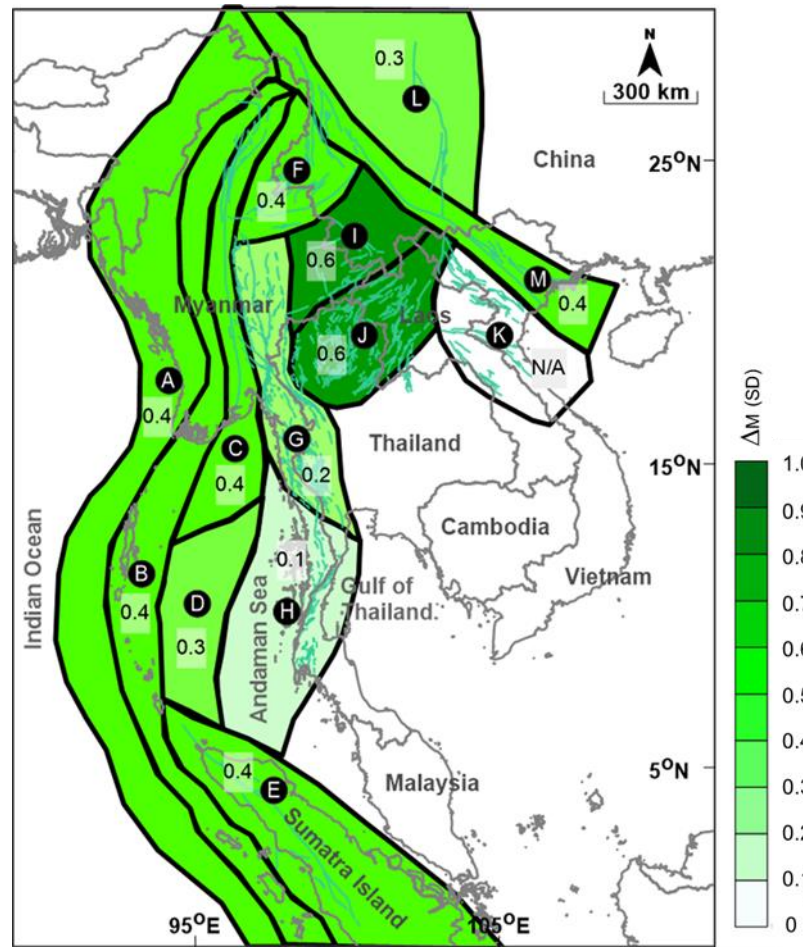


Figure 6.3 Map showing distribution of the standard deviation of difference value between magnitude of the mainshock and the maximum aftershock for 13 seismic source zones (A to M) proposed in the MSEA.

6.2. Decay rate of aftershock activity

According to the modified Omori's law (Utsu, 1961), the parameters can be described the characteristic of the aftershock that composed of the decay rate and the number of aftershock when the mainshock occurs. In this study, to select the magnitude of mainshock that is greater than 4.0 magnitude due to the earthquake is catastrophic or impact must be greater than 4.0 magnitude. First, calculate the decay rate based on Gardner and Knopoff (1974). It is said that the different magnitudes of mainshock have different the decay rates (see also in Figure 6.4).

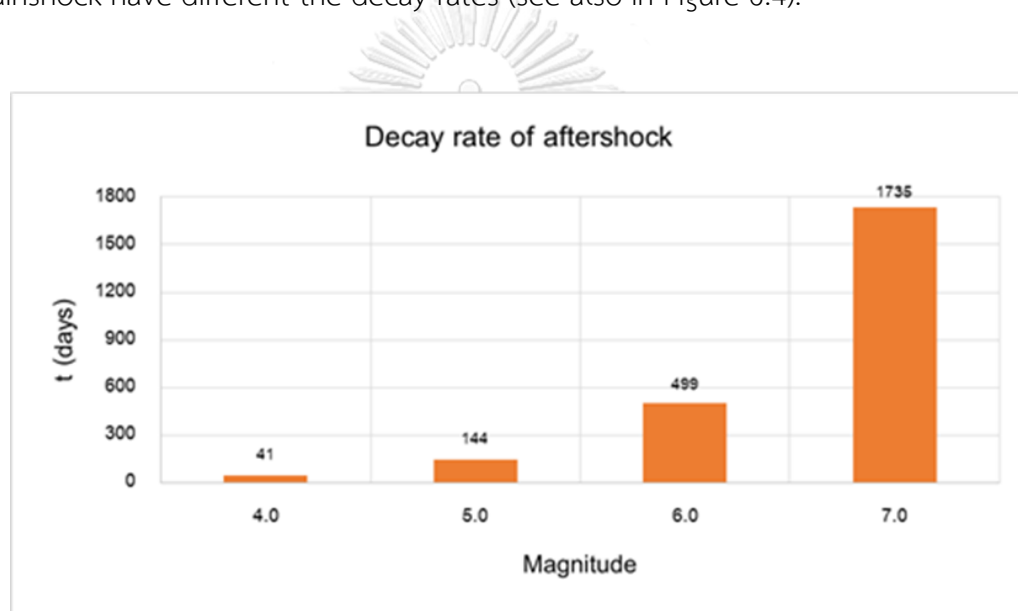


Figure 6.4 The bar chart showing the decay rate of the aftershock (days) for 13 seismic source zones (A to M) proposed in the MSEA, which varies according to the magnitude of the mainshock.

According to the Figure 6.4, the decay rate of the aftershock that occurs after magnitude 4.0 of the mainshock can be estimated to 41 days, while the decay rate of the aftershock that occurs after magnitude 5.0 of the mainshock is approximately 144 days. For magnitude 6.0 of the mainshock and magnitude 7.0 of the mainshock, the aftershocks caused by the mainshock will decay within 499 and 1,735 days, respectively.

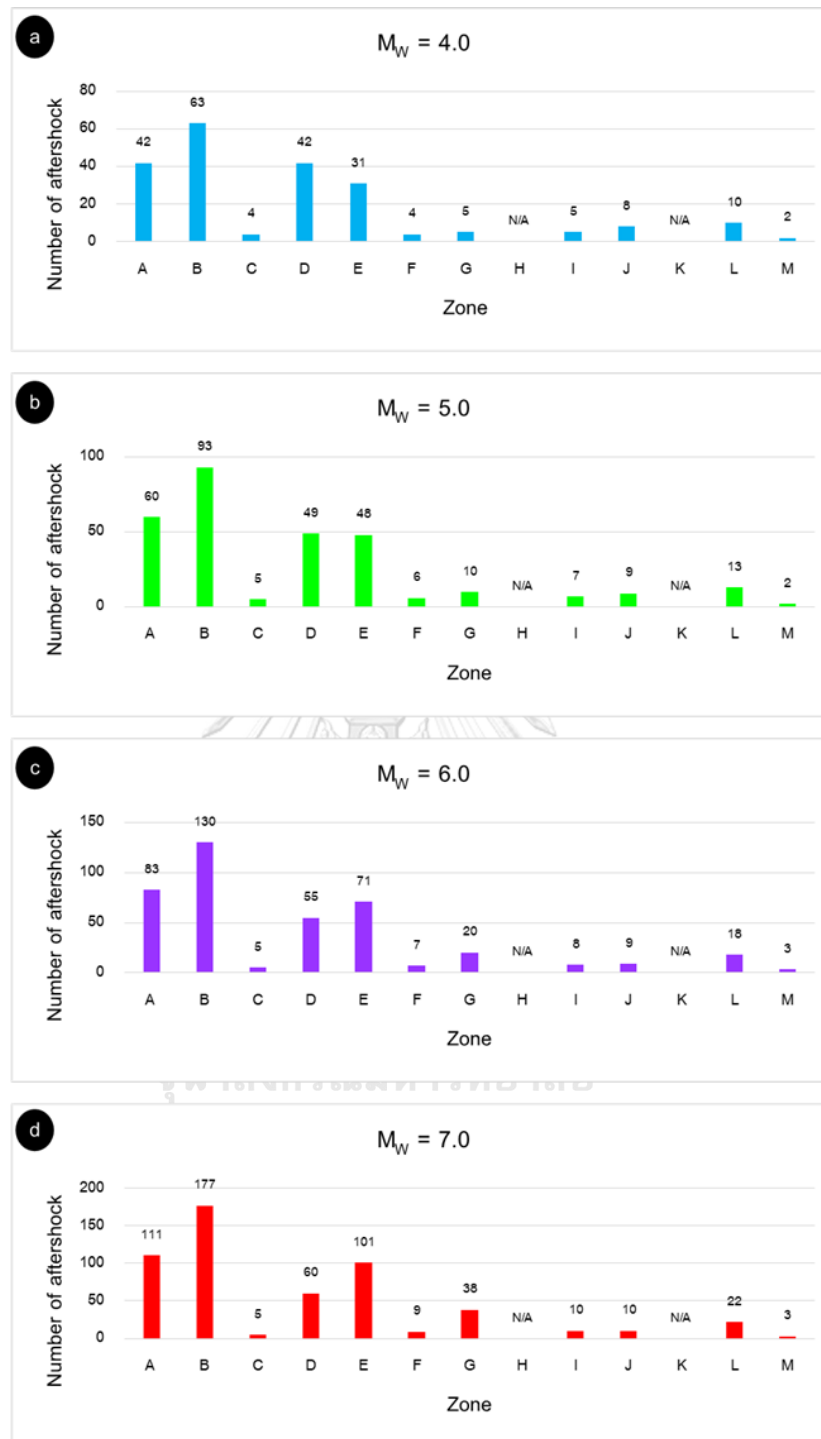


Figure 6.5 The bar chart showing the total number of the aftershocks that occurred after the mainshock for 13 seismic source zones (A to M) in the MSEA as shown by the magnitude of the mainshock, which is from 4.0 to 7.0 (a to d).

Next, evaluate the total number of aftershocks that occurred after the mainshock. The results are shown in Figures 6.5a-d, which is in order of magnitude from 4.0 to 7.0, respectively. Overall, from all of the size of magnitude, it can be divided into three groups, including the number of the aftershock that occurs after the mainshock is a lot, moderate and little. The first group consists of the Sumatra-Andaman interplate (zone A) and the Sumatra-Andaman intraslab (zone B), which are considered in the interplate.

It is found that the number of the aftershocks caused by the mainshock is more than the other zones, about 45-60 events for the M_W -4.0, and gradually increasing as the magnitude of the mainshock increases as well. The next group consists of the Andaman basin (zone D) and the Sumatra fault zone (zone E), which are considered in the intraplate. It found that there will be the number of the aftershocks caused by the mainshock in the middle compared to the other zones, about 30-40 events for the M_W -4.0, and the same gradually increasing with in the interplate zone. And the one is the other zones. The number of the aftershocks that occur after the mainshock is a little, with about 2-10 events. It will same increase in the two groups. From the above mention, it can be concluded that in the interplate zone, there will be more the number of the aftershocks than in the intraplate zone.

As mentioned above, it is found that the decay rate of aftershock will increase with the magnitude of mainshock. If the magnitude is much greater, the decay rate will increase.

6.3. Co-seismic Stress

In this work, the b value calculated from the G-R relationship (Gutenberg and Richter, 1944) is the b value of the aftershock, which is different from the typical b value calculated that is the b value of mainshock, which represents the seismotectonic stress. After calculating b value, compare the obtain b value of

aftershock with the b value of mainshock obtained from Pailoplee and Choowong (2014) in the same area in 13 seismic source zone. Figure 6.6 shows a comparison of the b values in each seismic source zone in the study area. The orange dots represent the b value of mainshock obtained from Pailoplee and Choowong (2014), while the blue dots represent the b value of aftershock in each cluster. It can be seen that most of the b value calculated from aftershock are higher than b value calculated from mainshock in all zones of the MSEA. Seismotectonically, the mainshock refers directly to the released tectonic stress. Whereas, the aftershock is a co-seismic stress change of the mainshock (Felzer et al., 2004). This means that the b value of the mainshock refers directly to the seismotectonic stress, while the b value of the aftershock refers to the co-seismic stress. It can be concluded that co-seismic stress in the MSEA is always lower than the seismotectonic stress because the b value of the aftershock (co-seismic stress) is higher than the b value of the mainshock (seismotectonic stress).

Seismotectonically, the lower b value of G-R relationship relates empirically to higher stress accumulated. Meanwhile, the higher b value of G-R relationship relates empirically to lower stress accumulated. After analyze the temporal variation of b value, the results show the trend of variation b value from the mainshock until the aftershock, which is described in Chapter V. Overall, the difference between the initial b value and the final b value is clearly different, so that the initial b value and the final b value are compared in each zone of the MSEA (Figure 6.7). By comparison, the initial b value shown in blue color is less than the final b value shown in orange color in all seismic source zone of the MSEA. In addition to this result, the rise of b value is interpreted as the stress decline following the occurrence of earthquake (Scholz, 1968, Wyss, 1973). Which means that the higher b values can be found in the areas where the stress accumulation is noticeable reduced after mainshocks.

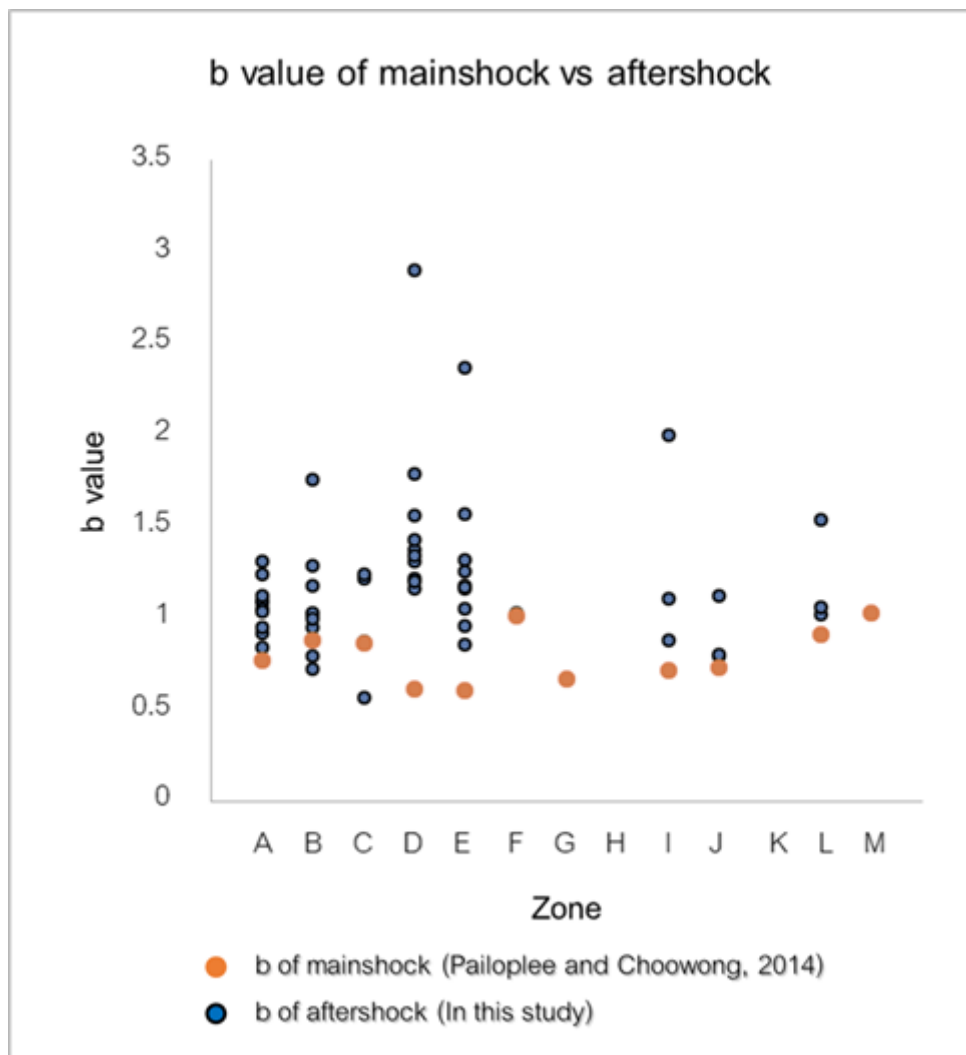


Figure 6.6 The graph showing the difference between the b values of the mainshock (Pailoplee and Choowong, 2014) and the aftershock (in this study) for 13 seismic source zones (A to M) in the MSEA.

For this reasons, it can be interpreted that at the beginning of the mainshock, there is high stress (low b), and then gradually release the accumulated stress, resulting in a gradual decline that means the occurrence of the aftershock later. It is consistent with the change of the b value that at the beginning stage, the b value is low value, and then the b value will increase that higher than the first stage.

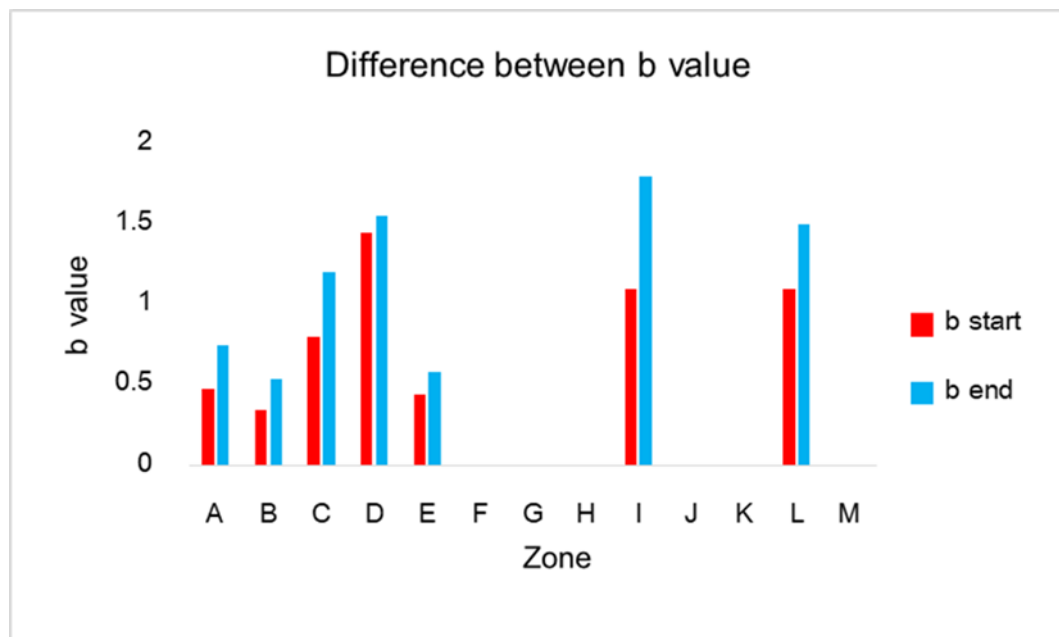


Figure 6.7 The bar chart showing the difference between the b values of the mainshock (Pailoplee and Choowong, 2014) and the aftershock (in this study) for 13 seismic source zones (A to M) in the MSEA.

6.4. D_c and b relationship

Based on the literature review, the relationship between D_c and b was a significant determinant of seismic hazards (Bayrak and Bayrak, 2011, 2012). In the previous works, Pailoplee and Choowong (2014) were calibrated the correlation between D_c and b values in the MSEA, but this correlation applies to the mainshock. This is the reason why this study chose to calibrate the empirical relationship between D_c and b that using the aftershock data. After calculating the G-R relationship or the b value, to calculate the fractal dimension or the D_c value, which can explain the spatial distribution of the aftershock in the MSEA. Based on the obtained b and D_c values (see Table 5.1 and 5.2 in Chapter V), the empirical relationship between D_c and b can be expressed as

$$D_c = 0.13b + 2.07 \quad \text{equation (6.1)}$$

The relationship of D_c and b of the aftershock in the MSEA showed a positive linear regression that shown in Figure 6.8a.

Moreover, the empirical relationship between D_c values and a/b ratios were calibrated as shown in Figure 6.8b and can be expressed as

$$D_c = 0.21(a/b) + 0.98 \quad \text{equation (6.2)}$$

The relationship between D_c values and a/b ratios of the aftershock was found to be a positive correlation as well as the relationship of mainshock from Pailoplee and Choowong (2014).

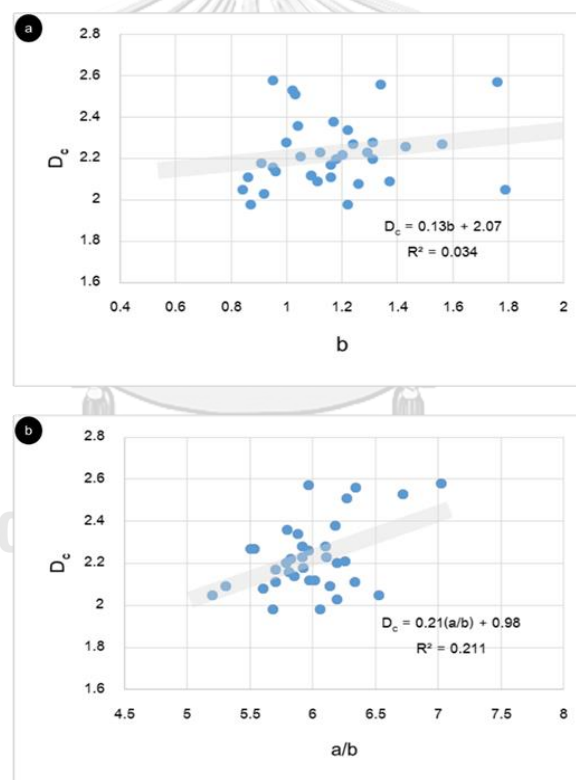


Figure 6.8 The empirical relationships for 13 seismic source zones (A to M) in the MSEA. (a) Between the D_c and b values and (b) between the D_c values and a/b ratios. The dash lines represent the linear regression fitted with the cluster of earthquake.

In addition, the correlation coefficient, the correlations of mainshock (0.65–0.68) are greater than of the correlations of aftershock (0.03-0.21). Therefore, the both relationships of mainshock are more reliable and effective than the both relationships of aftershock in the MSEA.

Besides, Figure 6.8 also shows the b and D_c values in the MSEA. In general, the b value varies from 0.6 to 1.4 (Wiemer and Katsumata, 1999), with a global average of about 1.0 (Udias, 1999) which is the b value of mainshock. While the b value in volcanic areas is high value, up to 2.0 (Warren and Latham, 1970). However, the results of this study that the b values are in the range of 0.8-1.8 which is the b value of aftershock.

As mention in Chapter II, the D_c value is used to investigate the spatial distribution of aftershock sequence. Based on Khattri (1995) and Yadav et al. (2011), D_c value will be interpreted differently, as D_c approach zero means that the distribution of the aftershock is concentrated in one point. In case of D_c close to 1 means that the distribution of the aftershock will be approach into line. If close to 2 indicates that the aftershock is distributed to plane pattern. When tends to 3, it can be indicated that the earthquake fractures are filling up a crustal volume. For the MSEA, the D_c values are in the range of 2.0-2.5 (see also in Figure 6.8). It is concluded that in the MSEA, the aftershocks are distributed into two-dimensional fault plane. In addition, based on the literature review, Most of the previous work, the D_c value is approximately to 2.0. For example, the D_c value of aftershock sequences of the major Nepal earthquake is about 1.84-1.91 (Chingtham et al., 2016). The D_c values of aftershock sequences in South and Southeastern Spain quite varies, but overall the D_c value is about 2 as well (Hamdache et al., 2013). It can be concluded that most of the D_c value of the aftershock are around 2.0.

6.5. Rose Diagram

As mention in Chapter V, in order to find the trend of the aftershock distribution in 13 seismic source zone in the MSEA, choose rose diagram to explain. The results show that in each seismic source zone, the aftershocks occurring after the mainshock are fairly widespread. For example, from Table 6.1 in zone A, the aftershocks caused by the M_W -7.5 earthquake generated on August 10th, 2009 in the Andaman Islands was found that distributed in two main directions. While the aftershocks caused by the M_W -7.5 earthquake generated on June 12th, 2010 in the Nibobar Islands was found that distributed in one directions. In zone b, it is evident that from the M_W -9.0 earthquake generated on December 26th, 2004 at off west coast of the northern Sumatra and the M_W -8.6 earthquake generated on March 28th, 2005 in the northern Sumatra, the distribution of the aftershocks is quite different, with the same distribution in two trends, but different in the direction. It can be seen that even the aftershocks occur in the same zone, the distribution of the aftershock in each mainshock is not the same. And the other case of the cluster of earthquake are detailed in Table 6.1. For this reason, it is decided to divide the distribution of the aftershocks into 4 quadrants in order to find the relationship of the distribution in each seismic source zone. After that, to consider the focal mechanism of the cluster of earthquake in order to determine the relationship between the distributions of aftershocks generated after the mainshock and the fault types.

According to the Table 6.1, it is shown that the focal mechanism of each earthquake in 13 seismic source zones that downloaded from the Global Centroid-Moment-Tensor (CMT) (www.globalcmt.org/), and then compare it with the rose diagram. Moreover, there are also several parameters, including the number of aftershocks in each cluster, the average direction of aftershock distribution, the standard deviation and the strike, dip and rake will be used to determine the fault types in the next step.

Table 6.1 The case study of the earthquake for 13 seismic source zones (A to M) in the MSEA that represents the distribution of the aftershock occurring after the mainshock and the focal mechanism that indicates the fault types, including the parameters (Remark: Lat=Latitude, Lon=Longitude)

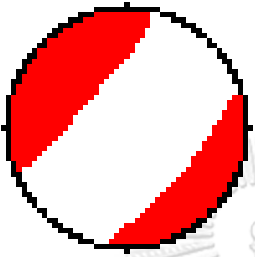
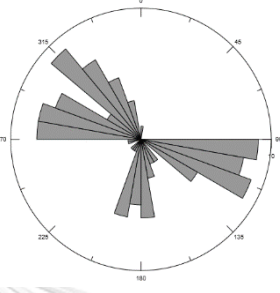
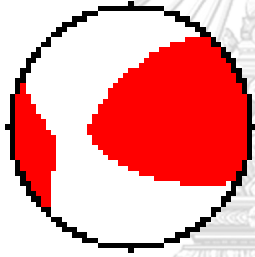
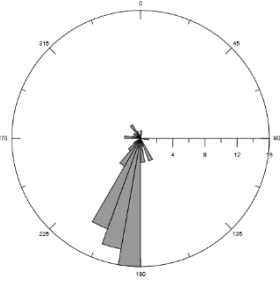
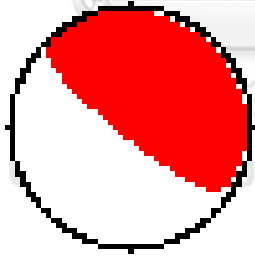
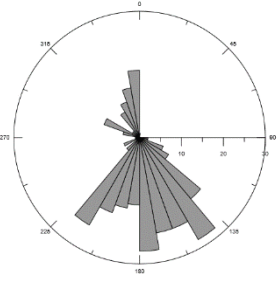
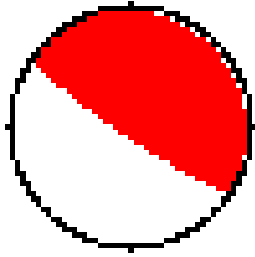
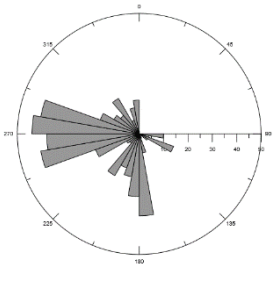
Zone	Event	Focal	Rose Diagram	Parameters
A	$M_w = 7.5$ (2009/8/10) Andaman Islands Lat=14.16 Lon=92.94			n = 110 events average = 218.31 SD = 87.48 Strike 39 Dip 36 Rake - 92 Strike 220 Dip 54 Rake - 89
A	$M_w = 7.5$ (2010/6/12) Nicobar Islands Lat=7.85 Lon=91.65			n = 64 events average = 204.08 SD = 41.27 Strike 220 Dip 63 Rake 31 Strike 115 Dip 63 Rake 149
B	$M_w = 9.0$ (2004/12/26) Off W Coast Of Northern Sumatra Lat=3.09 Lon=94.26			n = 286 events average = 206.02 SD = 72.07 Strike 329 Dip 8 Rake 110 Strike 129 Dip 83 Rake 87
B	$M_w = 8.6$ (2005/3/28) Northern Sumatra Lat=1.67 Lon=97.07			n = 438 events average = 243.26 SD = 62.89 Strike 333 Dip 8 Rake 118 Strike 125 Dip 83 Rake 86

Table 6.1 (Cont.) The case study of the earthquake for 13 seismic source zones (A to M) in the MSEA that represents the distribution of the aftershock occurring after the mainshock and the focal mechanism that indicates the fault types, including the parameters. (Remark: Lat=Latitude, Lon=Longitude)

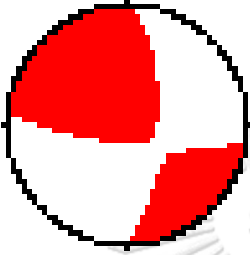
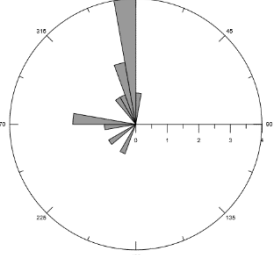
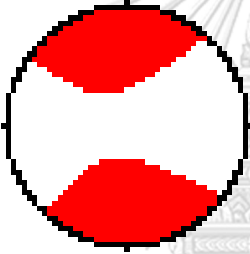
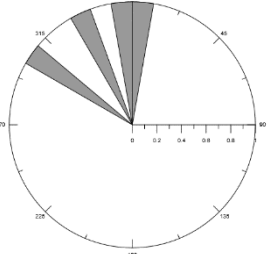
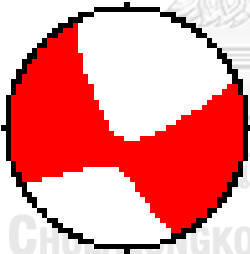
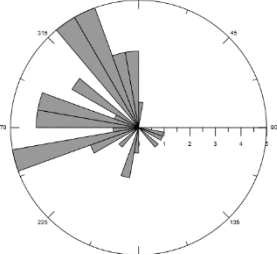
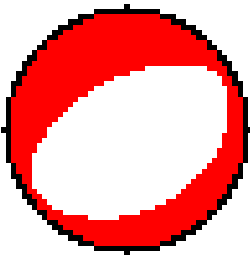
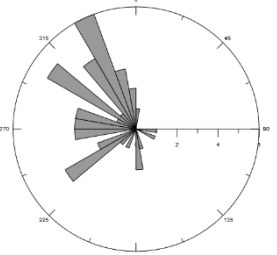
Zone	Event	Focal	Rose Diagram	Parameters
C	$M_w = 6.9$ (1991/1/5) Myanmar Lat=23.61 Lon=96.18			n = 13 events average = 310.29 SD = 53.62 Strike 2 Dip 68 Rake 166 Strike 97 Dip 77 Rake 23
C	$M_w = 5.1$ (2012/7/9) Myanmar Lat=25.29 Lon=96.66			n = 13 events average = 333.03 SD = 26.31 Strike 220 Dip 82 Rake -173 Strike 129 Dip 84 Rake -8
D	$M_w = 6.1$ (2005/1/1) Nicobar Islands Lat= 7.15 Lon= 94.49			n = 43 events average = 280.25 SD = 63.57 Strike 63 Dip 77 Rake -13 Strike 156 Dip 78 Rake -167
D	$M_w = 5.2$ (2006/3/10) Andaman Islands Lat= 15.46 Lon= 96.15			n = 44 events average = 277.62 SD = 63.18 Strike 59 Dip 34 Rake -92 Strike 241 Dip 56 Rake -89

Table 6.1 (Cont.) The case study of the earthquake for 13 seismic source zones (A to M) in the MSEA that represents the distribution of the aftershock occurring after the mainshock and the focal mechanism that indicates the fault types, including the parameters. (Remark: Lat=Latitude, Lon=Longitude)

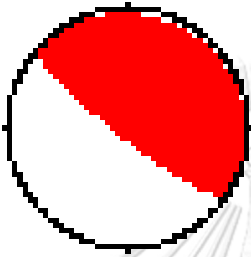
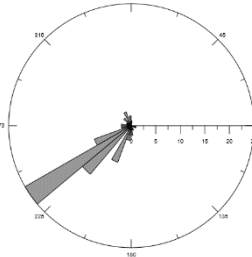
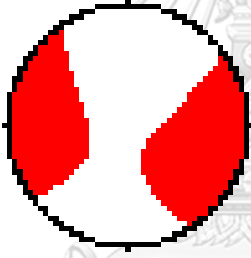
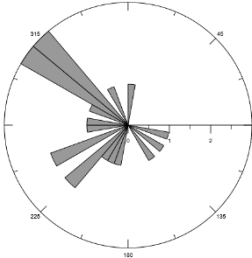
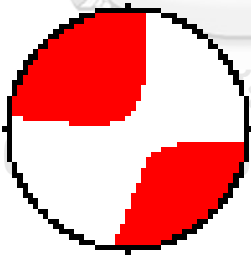
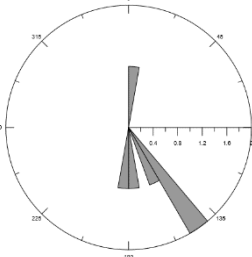
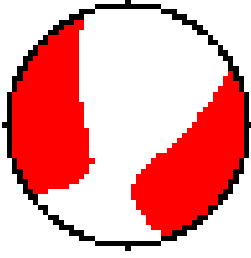
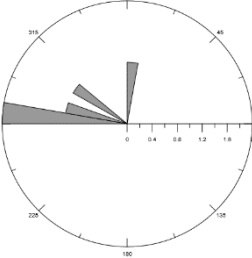
Zone	Event	Focal	Rose Diagram	Parameters
E	$M_W = 7.8$ (2010/4/6) Northern Sumatra Lat= 2.07 Lon= 96.74			n = 82 events average = 235.74 SD = 42.82 Strike 307 Dip 7 Rake 88 Strike 129 Dip 83 Rake 90
E	$M_W = 5.5$ (2015/11/8) Nicobar Islands Lat= 6.98 Lon= 94.68			n = 131 average = 277.91 SD = 38.93 Strike 327 Dip 29 Rake 102 Strike 133 Dip 62 Rake 83
F	$M_W = 6.0$ (2008/8/21) Myanmar- China Border Region Lat= 24.92 Lon= 97.99			n = 5 events average = 159.89 SD = 17.58 Strike 7 Dip 80 Rake 178 Strike 97 Dip 88 Rake 10
F	$M_W = 5.6$ (2001/ 4/12) Yunnan, China Lat= 24.77 Lon= 98.81			n = 4 events average = 286.19 SD = 15.52 Strike 57 Dip 63 Rake -28 Strike 161 Dip 65 Rake -150

Table 6.1 (Cont.) The case study of the earthquake for 13 seismic source zones (A to M) in the MSEA that represents the distribution of the aftershock occurring after the mainshock and the focal mechanism that indicates the fault types, including the parameters. (Remark: Lat=Latitude, Lon=Longitude)

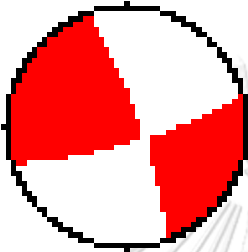
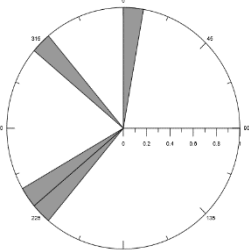
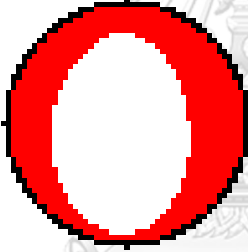
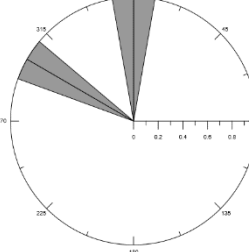
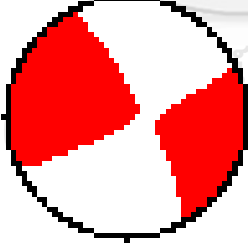
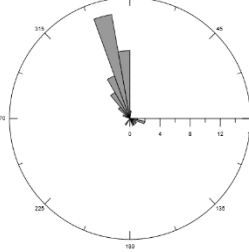
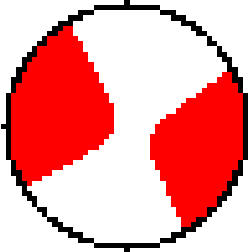
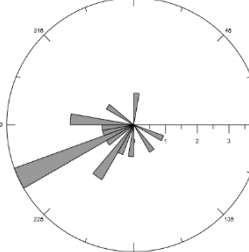
Zone	Event	Focal	Rose Diagram	Parameters
G	$M_W = 5.7$ (1989/3/1) Myanmar Lat= 21.61 Lon= 98.30			n = 4 events average = 256.63 SD = 46.42 Strike 73 Dip 79 Rake 9 Strike 341 Dip 82 Rake 169
H	$M_W = 4.5$ (2006/9/27) Gulf Of Thailand Lat= 11.89 Lon= 100.18			n = 4 events average = 319.15 SD = 28.99 Strike 191 Dip 41 Rake -77 Strike 353 Dip 50 Rake -101
I	$M_W = 7.0$ (1988/11/06) Myanmar- China Border Region Lat= 23.00 Lon= 99.68			n = 43 events average = 306.84 SD = 78.99 Strike 333 Dip 78 Rake 174 Strike 64 Dip 84 Rake 12
I	$M_W = 6.8$ (1995/07/11) Myanmar- China Border Region Lat= 21.89 Lon= 99.22			n = 16 events average = 228.63 SD = 49.99 Strike 330 Dip 89 Rake 175 Strike 60 Dip 85 Rake 1

Table 6.1 (Cont.) The case study of the earthquake for 13 seismic source zones (A to M) in the MSEA that represents the distribution of the aftershock occurring after the mainshock and the focal mechanism that indicates the fault types, including the parameters. (Remark: Lat=Latitude, Lon=Longitude)

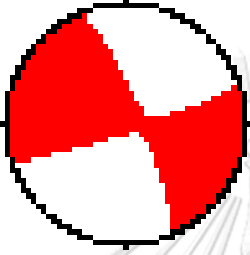
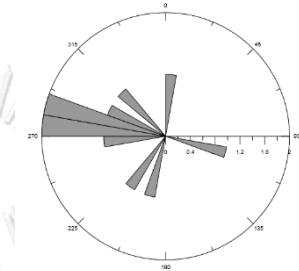
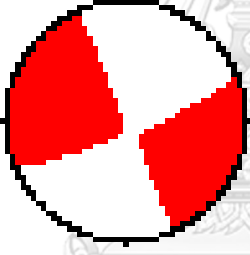
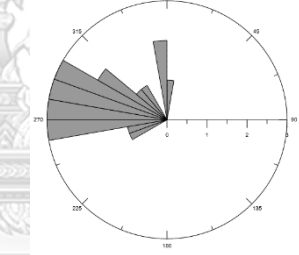
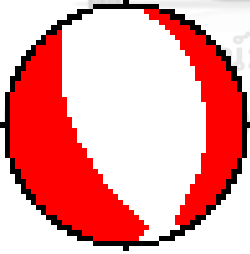
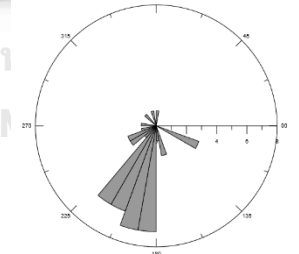
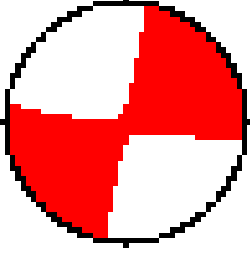
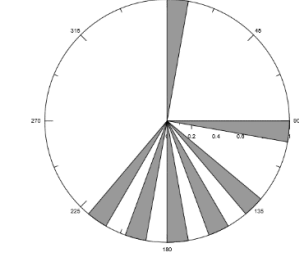
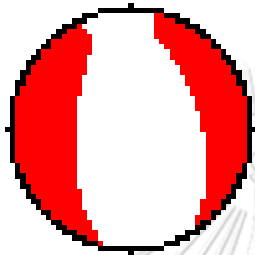
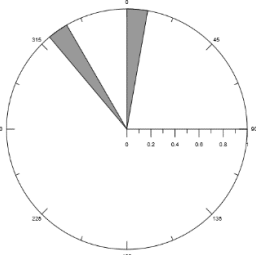
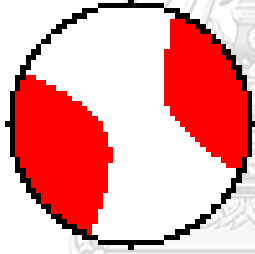
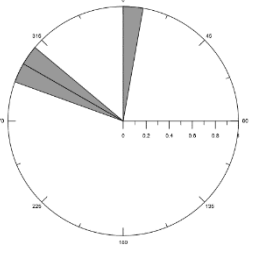
Zone	Event	Focal	Rose Diagram	Parameters
J	$M_w = 6.9$ (2011/3/24) Myanmar Lat= 20.62 Lon= 100.02			n = 10 events average = 251.12 SD = 64.05 Strike 339 Dip 79 Rake 175 Strike 70 Dip 85 Rake 11
J	$M_w = 6.2$ (2014/5/5) Thailand Lat= 19.72 Lon= 99.68			n = 20 events average = 290.50 SD = 30.32 Strike 337 Dip 90 Rake 171 Strike 67 Dip 81 Rake 0
K	N/A			
L	$M_w = 6.6$ (1996/2/3) Yunnan, China Lat= 27.15 Lon= 100.28			n = 41 events average = 204.53 SD = 43.07 Strike 0 Dip 36 Rake -68 Strike 153 Dip 57 Rake -105
L	$M_w = 5.8$ (2008/8/30) Yunnan, China Lat= 26.19 Lon= 102.04			n = 6 events average = 161.16 SD = 43.05 Strike 100 Dip 86 Rake 180 Strike 190 Dip 90 Rake 4

Table 6.1 (Cont.) The case study of the earthquake for 13 seismic source zones (A to M) in the MSEA that represents the distribution of the aftershock occurring after the mainshock and the focal mechanism that indicates the fault types, including the parameters (Remark: Lat=Latitude, Lon=Longitude)

Zone	Event	Focal	Rose Diagram	Parameters
M	$M_w = 5.4$ (2013/3/3) Yunnan, China Lat= 25.94 Lon= 99.84			n = 2 events average = 323.37 SD = - Strike 337 Dip 42 Rake - 113 Strike 187 Dip 52 Rake -71
M	$M_w = 5.0$ (2016/5/17) Yunnan, China Lat= 25.52 Lon= 101.17			n = 3 events average = 299.39 SD = 7.58 Strike 293 Dip 86 Rake 177 Strike 23 Dip 87 Rake 4

Based on the results, it is difficult to compare the information by considering only the images, thus collecting the new information as shown in the Table 6.2, which displays information about the distribution of aftershock that divided into 4 quadrants and the strike, dip and rake, as well as the fault types.

Table 6.2 Collecting the information used to interpret the relationship of the fault type and the aftershocks distribution for 13 seismic source zones (A to M) in the MSEA. (Remark: D_1 =Normal-dip slip, D_2 =Reverse-dip slip, S_1 =Left-lateral strike slip, and S_2 =Right-lateral strike slip)

Zone	Location	Quadrant	Strike1	Strike2	Dip1	Dip2	Rake1	Rake2	Fault type
A	Andaman Islands	2	39	220	36	54	-92	-89	D_1
	Nicobar Islands	3	220	115	63	63	31	149	S_2
		3	29	120	68	89	-2	-158	S_1
	Northern Sumatra	2	92	358	60	82	-171	-31	S_2
	Andaman Islands	3	42	159	52	60	-40	-134	S_2
		2	29	132	56	72	158	36	S_2
	Nicobar Islands	3	112	21	83	86	-176	-8	S_2
	Northern Sumatra	3	300	140	31	60	72	101	D_2
	Nicobar Islands	2	338	162	26	64	86	92	D_2
Andaman Islands	2	359	172	21	69	96	88	D_2	
B	Northern Sumatra	3	329	129	8	83	110	87	D_2
		3	333	125	8	83	118	86	D_2
		3	299	130	11	79	80	92	D_2
		3	297	135	16	75	73	95	D_2
	Myanmar-China Border	2	284	148	45	54	55	120	D_2
	Northern Sumatra	2	306	132	9	81	85	91	D_2
	Nicobar Island	2	351	137	27	67	121	75	D_2

Table 6.2 (Cont.) Collecting the information used to interpret the relationship of the fault type and the aftershocks distribution for 13 seismic source zones (A to M) in the MSEA. (Remark: D1=Normal-dip slip, D2=Reverse-dip slip, S1=Left-lateral strike slip, and S2=Right-lateral strike slip)

Zone	Location	Quadrant	Strike1	Strike2	Dip1	Dip2	Rake1	Rake2	Fault type
C	Myanmar	2	2	97	68	77	166	23	S ₂
		2	0	91	55	88	178	35	S ₂
		3	8	100	71	83	172	20	S ₂
	Myanmar	3	34	124	76	89	179	14	S ₂
		3	122	32	84	85	5	174	S ₂
	South Coast Of Myanmar	2	106	281	25	65	-85	-92	D ₁
		2	95	212	32	74	-31	-118	D ₁
		2	33	251	39	57	-121	-67	D ₁
	Myanmar	2	220	129	82	84	-173	-8	S ₂
2		95	187	77	83	-7	-167	S ₂	
D	Myanmar	2	144	53	78	85	-175	-12	S ₂
		4	154	61	75	80	-170	-15	S ₂
		2	63	156	77	78	-13	-167	S ₂
		2	149	58	78	84	-174	-12	S ₂
		4	166	74	78	81	-171	-12	S ₂
	Andaman Islands	2	59	241	34	56	-92	-89	D ₂
		3	89	232	36	60	-59	-110	D ₂
	Nicobar Island	2	223	333	32	78	-23	-120	S ₂
E	Northern Sumatra	3	307	129	7	83	88	90	D ₂
		4	326	149	22	69	88	91	D ₂
	Nicobar Island	2	144	53	78	85	-175	-12	S ₂
	Northern Sumatra	2	320	133	21	69	97	87	D ₂
		2	327	133	29	62	102	83	D ₂
		2	311	133	22	68	88	91	D ₂
		2	37	132	73	76	-14	-162	S ₂
		2	319	133	25	65	95	88	D ₂
Nicobar Island	2	147	53	72	79	-168	-18	S ₂	

Table 6.2 (Cont.) Collecting the information used to interpret the relationship of the fault type and the aftershocks distribution for 13 seismic source zones (A to M) in the MSEA. (Remark: D1=Normal-dip slip, D2=Reverse-dip slip, S1=Left-lateral strike slip, and S2=Right-lateral strike slip)

Zone	Location	Quadrant	Strike1	Strike2	Dip1	Dip2	Rake1	Rake2	Fault type
F	Myanmar-China Border	4	7	97	80	88	178	10	S ₂
		4	82	351	79	85	5	169	S ₂
		2	57	161	63	65	-28	-150	S ₂
		4	64	333	79	85	5	169	S ₂
		1	271	103	44	46	82	98	S ₂
		4	21	235	42	53	-117	-68	S ₂
		2	342	238	60	67	-154	-33	S ₂
		2	348	79	82	89	179	8	S ₂
G	Burma	3	73	341	79	82	9	169	S ₂
H	Gulf Of Thailand	2	191	353	41	50	-77	-101	D ₁
I	Myanmar-China Border	2	333	64	78	84	174	12	S ₂
		3	60	330	85	89	1	175	S ₂
		4	329	60	81	84	174	9	S ₂
		4	146	247	63	69	156	29	S ₂
		2	64	333	66	88	3	156	S ₂
		4	345	252	68	84	-173	-22	S ₂
		2	61	330	81	82	8	171	S ₂
		4	50	141	82	85	-5	-172	S ₂
		3	76	167	72	89	-1	-162	S ₂
J	Myanmar	2	33	70	79	85	175	11	S ₂
	Laos	4	324	54	81	89	179	9	S ₂
	Thailand	2	67	337	81	90	0	171	S ₂
K		N/A							

Table 6.2 (Cont.) Collecting the information used to interpret the relationship of the fault type and the aftershocks distribution for 13 seismic source zones (A to M) in the MSEA. (Remark: D1=Normal-dip slip, D2=Reverse-dip slip, S1=Left-lateral strike slip, and S2=Right-lateral strike slip)

Zone	Location	Quadrant	Strike1	Strike2	Dip1	Dip2	Rake1	Rake2	Fault type
L	Yunnan, China	3	0	153	36	57	-68	-105	D ₁
	Yunnan, China	4	13	105	75	81	-9	-165	S ₂
		3	200	291	80	84	-6	-170	S ₂
		4	100	190	86	90	180	4	S ₂
		3	204	294	84	87	-3	-174	S ₂
		4	97	284	42	48	-95	-85	D ₁
	Yunnan, China	2	350	236	51	63	35	136	S ₂
		2	360	235	45	60	45	125	S ₂
	Yunnan, China	2	8	98	87	88	-2	-177	S ₂
		2	71	340	81	86	-175	-9	S ₂
M	Yunnan, China	1	330	165	25	66	-104	-84	D ₁
		1	337	187	42	52	-113	-71	D ₁
	Yunnan, China	2	293	23	86	87	177	4	S ₂

Not only display the results as the Table 6.2, it also displays in the graph form, which describes the relationship between the fault type and the aftershock distribution. Referring to Table 6.1 and 6.2 and Figure 6.9, it shows that no matter what the mainshock caused by any fault type, the distribution of the aftershock occurring after the mainshock in the MSEA is spread across all quadrants. Further studies on the coulomb stress transfer concept found that when the mainshock occurred, it will release the stress, which will release in all directions. For example, Yadav et al. (2012) investigated the coulomb stress change of the 2008 earthquake sequence in Baluchistan, Pakistan.

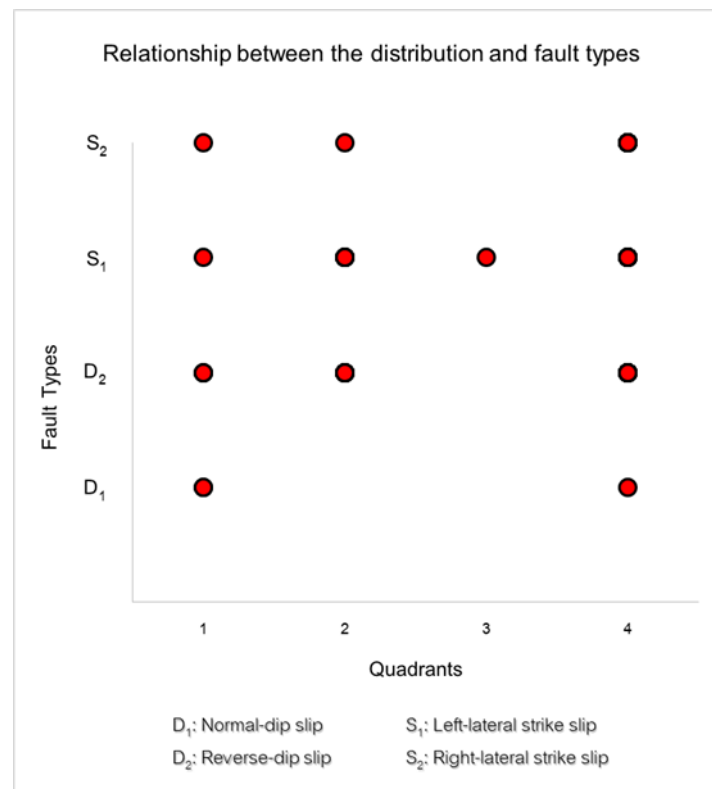


Figure 6.9 The relationships between the distribution of aftershocks that divided into 4 quadrants and the fault type in the MSEA.

It was found that when the M_w -6.4 Baluchistan mainshocks occur, the aftershocks were followed during October 28th, 2008 – December 31st, 2008 which were related with the southeastern direction lobe of the Coulomb stress increasing that located on the fault zone that caused the foreshock and the mainshock, as shown as the yellow circle in Figure 6.10. And also study the relationship of the Coulomb stress increasing zone and locations of the aftershocks occur, it finds that most of the aftershocks occurred in the increased zone, while some aftershocks occurred in the decreased zone.

As mentioned above, this is a good support for the results that the aftershocks generated after the mainshock in the MSEA will be distributed into all areas that conform to the concept of Coulomb stress.

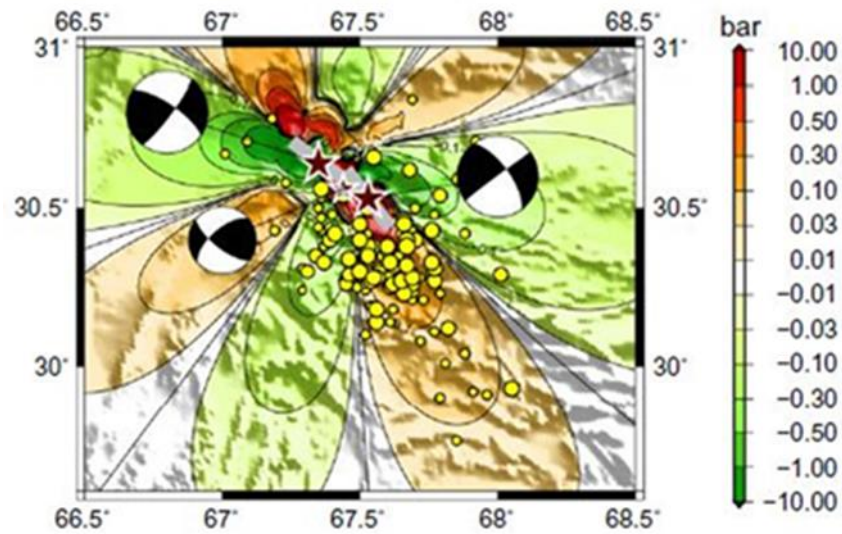


Figure 6.10 Coulomb seismic stress changes due to the M_w -5.3 foreshock, M_w -6.4 mainshock and M_w -6.4 mainshock doublet and the distribution of the aftershocks (yellow circles) (Yadav et al., 2012). Red stars represent the foreshock, mainshock and mainshock doublet while the focal mechanism for foreshock, mainshock and mainshock doublet are shown by beach ball.

CHAPTER 7

CONCLUSION

In this study, focuses on analyzing the characteristics of the aftershock in the MSEA that using the several techniques, including the frequency-magnitude distribution, the modified Omori's law, the Bath's law and the fractal dimension. Based on the all results obtained, the characteristics of the aftershock in the MSEA can be summarized as follows;

i) In this study, the relationship of magnitude of the mainshock and the aftershock in the MSEA will help to determine the maximum magnitude of the aftershock that occurs by using the difference magnitude value of mainshock and aftershock. It is also concluded that in the MSEA, the Western Thailand ($\Delta M_{\max}=0.7$) and Southern Thailand ($\Delta M_{\max}=0.4$) have a lower difference than the other zones, which indicated that these zones should be recognized in particular for aftershock hazard.

ii) According to analyze the modified Omori's law, the decay rate of the aftershock will increase with increasing the magnitude of mainshock. For the whole number of the aftershocks that will occur after the mainshock, it is also interpreted that the larger the mainshock, the more number of the aftershocks. In addition, it reveals that in the interplate zone, there will be more number of aftershocks when the mainshock occurs than in the intraplate zone.

iii) Regarding to the analysis of the G-R relationship, by comparing the b value of the aftershock (in this study) and the mainshock (Pailoplee and Choowong, 2013), it is concluded that the co-seismic stress in the MSEA is no higher than the tectonic stress. Moreover, the temporal variation of aftershock of b value is another support about stress change when the earthquake occurs. It can be concluded that when the aftershock occurs, the co-seismic stress increased suddenly (dropped b value) after

that, the stress decreased with time (high b value). In addition, compared with D_c value, it assures that when the mainshock occurs, the co-seismic stress will be released and gradually decayed with time which spreading over all area, instead of being a trigger for the new earthquake.

iv) Based on the fractal dimension, in the MSEA, the distribution of the aftershocks are randomly distributed into two-dimensional fault plane due to the D_c value of the aftershock are in the range of 2.0-2.5. In addition to the D_c value, the b value varies from 0.8 to 1.8, which is specific in the aftershock. In case of the correlation between D_c and b values of the aftershock in the MSEA, it is a positive relationship.

v) Actually, in this study, it is known that the aftershock sequence in the MSEA is distributed in any direction or quadrant, along with the relationship between the distribution of the aftershock sequence and fault types that caused the mainshock, resulting in the aftershocks by using the spatial distribution. However, the obtained results illustrate that the distribution of the aftershock occurring after the mainshock in the MSEA is generated in all directions or quadrants, regardless of the mainshock caused by any fault type. This is consistent with concept of coulomb stress explained that in each mainshock, the aftershock is generated in 4 quadrants. As mention, the spatial distribution method is not suitable to study the exact distribution of the aftershock sequence, but the coulomb stress transfer method should be used for, which is commonly used in present.

REFERENCES

- Bath, M. (1965). "Lateral inhomogeneities in the upper mantle." Tectonophysics **2**(6): 483-514.
- Bayrak, Y. and E. Bayrak (2011). "An evaluation of earthquake hazard potential for different regions in Western Anatolia using the historical and instrumental earthquake data." Pure and Applied Geophysics **169**: 1859-1873.
- Bayrak, Y. and E. Bayrak (2012). "Regional variations and correlations of Gutenberg-Richter parameters and fractal dimension for the different seismogenic zones in Western Anatolia." Journal of Asian Earth Sciences **58**: 98-107.
- Bayrak, Y. and S. Öztürk (2004). "Spatial and temporal variations of the aftershock sequences of 1999 İzmit and Düzce earthquakes." Earth, Planets and Space **56**: 933-944.
- Bertrand, G. and C. Rangin (2003). "Tectonics of the western margin of the Shan Plateau (central Myanmar): implications for the India-Indochina oblique convergence since the Oligocene." Journal of Asian Earth Sciences **21**: 1139-1157.
- Chan, C. H. and Y. M. Wu (2013). "Maximum magnitudes in aftershock sequences in Taiwan." Journal of Asian Earth Sciences **73**: 409-418.
- Charusiri, P., et al. (2005). Geological and physical effect evaluation in the tsunami damage area for restoration and warning system, Department of Geology, Faculty of Science, Chulalongkorn University, Bangkok, Thailand, Technical report: 412p.

- Charusiri, P., et al. (2004). The study on the investigations of active faults in Changwat Kanchanaburi area, western Thailand, Department of Geology, Faculty of Science, Chulalongkorn University, Bangkok, Thailand, Technical report: 119p.
- Charusiri, P., et al. (2007). Regional tectonic setting and seismicity of Thailand with reference to reservoir construction. GEOTHAI'07 International Conference on Geology of Thailand: Towards Sustainable Development and Self Sufficient Economy. Bangkok: 274-287.
- Chen, C.-C., et al. (2006). "A correlation between the b-value and the fractal dimension from the aftershock sequence of the 1999 Chi-Chi, Taiwan, earthquake." Geophysical Journal International **167**(3): 1215-1219.
- Chingtham, P., et al. (2016). "Statistical analysis of aftershock sequences related with two major Nepal earthquakes: April 25, 2015, M_w 7.8, and May 12, 2015, M_w 7.2." Annals of Geophysics **59**: 16p.
- Cuong, N. Q. and W. A. Zuchiewicz (2001). "Morphotectonic properties of the Lo River Fault near Tam Dao in North Vietnam." Natural Hazards and Earth System Sciences **1**: 15-22.
- Duong, C. C. and K. L. Feigl (1999). "Geodetic measurement of horizontal strain across the Red River fault near Thac Ba, Vietnam." Journal of Geodesy **73**: 298-310.
- Eleftheria, P., et al. (2004). "Earthquake Triggering along the Xianshuihe Fault Zone of Western Sichuan, China." Pure and Applied Geophysics **161**: 1683-1707.

- Felzer, K. R., et al. (2004). "A common origin for aftershocks, foreshocks, and multiplets." Bulletin of the Seismological Society of America **94**: 88-98.
- Fenton, C. H., et al. (2003). "Recent paleoseismic investigations in Northern and Western Thailand." Annals of Geophysics **46**: 957-981.
- Gardner, J. K. and L. Knopoff (1974). "Is the sequence of earthquakes in Southern California, with aftershocks removed, Poissonian?" Bulletin of the Seismological Society of America **64**: 363-367.
- Grassberger, P. and I. Procaccia (1983). "Measuring the strangeness of strange attractors." Physica D: Nonlinear Phenomena **9**: 189-208.
- Gutenberg, B. (1945a). "Amplitudes of Surface Waves and Magnitude of Shallow Earthquakes." Bulletin of the Seismological Society of America **35**: 3-12.
- Gutenberg, B. and C. F. Richter (1944). "Frequency of earthquakes in California." Bulletin of the Seismological Society of America **34**: 185-188.
- Hamdache, M., et al. (2013). "Analysis of aftershock sequences in South and Southeastern Spain." Physics and Chemistry of the Earth **63**: 55-76.
- Kagan, Y. Y. and L. Knopoff (1980). "Spatial distribution of earthquakes: the two-point correlation function." Geophysical Journal of the Royal Astronomical Society **62**: 303-320.
- Kanamori, H. (1977). "The energy release in great earthquake." Journal of Geophysical

Research **82**(20): 2981-2987.

Kanamori, H. (1983). "Magnitude scale and quantification of earthquakes." Tectonophysics **93**: 185-199.

Khana, P. K. and P. P. Chakraborty (2005). "Two-phase opening of Andaman Sea: a new seismotectonic insight." Earth and Planetary Science Letters **229**(3-4): 259-271.

Khatti, K. N. (1995). "Fractal description of seismicity of India and inferences regarding earthquake hazard." Current Science **69**: 361-366.

Lacassin, R., et al. (1998). "Hairpin river loops and strike-slip sense inversion of Southeast Asian strike-slip faults." Geology **26**: 703-706.

Martin, S. (2005). "Intensity distribution from the 2004 M 9.0 Sumatra-Andaman earthquake." Seismological Research Letters **76**: 321-330.

Nuannin, P., et al. (2005). "Spatial and temporal b-value anomalies preceding the devastating off coast of NW Sumatra earthquake of December 26, 2004." Geophysical Research Letters **32**: 4p.

Nuannin, P., et al. (2012). "Spatial and temporal characteristics of aftershocks of the December 26, 2004 and March 28, 2005 earthquakes off NW Sumatra." Journal of Asian Earth Sciences **46**: 150-160.

Nutalaya, P., et al. (1985). Series on seismology-volume II-Thailand. In: Arnold EP (ed) Technical report, Southeast Asia Association of Seismology and Earthquake

Engineering: 402p.

Nuttee, R., et al. (2005). Paleo-earthquakes along the southern segment of the Sri Sawat Fault, Kanchanaburi, Western Thailand: Morphotectonic and TL-dating evidences. Proceedings of the International Conference on Geology, Geotechnology and Mineral Resources of Indochina, Khon Kaen, Thailand: 542-554.

Pailoplee, S. and M. Choowong (2013). "Probabilities of earthquake occurrences in Mainland Southeast Asia." Arabian Journal of Geosciences **6**: 4993-5006.

Pailoplee, S. and M. Choowong (2014). "Earthquake frequency-magnitude distribution and fractal dimension in mainland Southeast Asia." Earth, Planets and Space **66**: 8p.

Pailoplee, S., et al. (2017). "Precursory seismicity rate changes prior to the large and major earthquakes along the Sagaing fault zone, Central Myanmar." Arabian Journal of Geosciences **10p**.

Pailoplee, S., et al. (2009). "Deterministic and probabilistic seismic hazard analyses in Thailand and adjacent areas using active fault data." Earth, Planets and Space **61**: 1313-1325.

Panwoon, N. (2014). Seismicity rate change along the strike-slip fault system, Thailand-Myanmar border. Geology, Chulalongkorn University. **Bachelor of Science**: 44p.

Park, J., et al. (2005). "Performance Review of the Global Seismographic Network for the Sumatra-Andaman Megathrust Earthquake." Seismological Research Letters **76**:

329-341.

Paul, J., et al. (2001). "The motion and active deformation of India." Geophysical Research Letters **28**(4): 647-650.

Petersen, M., et al. (2004). "Probabilistic seismic hazard analysis for Sumatra, Indonesia and across the Southern Malaysian Peninsula." Tectonophysics **390**: 141-158.

Phoung, N. H. (1991). "Probabilistic assessment of earthquake hazard in Vietnam based on seismotectonic regionalization." Tectonophysics **198**: 81-93.

Pipattanajaroenkul, P. (2014). Region-Time-Length Algorithm along the Strike-slip Fault System, Thailand-Myanmar Border. Geology, Chulalongkorn University. **Bachelor of Science**: 42p.

Polachan, S., et al. (1991). "Development of Cenozoic basins in Thailand." Marine and Petroleum Geology **8**: 84-97.

Puangjaktha, P. and S. Pailoplee (2018). "Temporal and spatial distributions of precursory seismicity rate changes in the Thailand-Laos-Myanmar border region: implication for upcoming hazardous earthquakes." Journal of Seismology **22**(1): 303-313.

Rajendran, C. P., et al. (2003). "The 13 September 2002 North Andaman(Diglipur) earthquake: An analysis in the context of regional seismicity." Current Science **84**(7): 919-924.

Reasenber, P. (1985). "Second-order moment of central California seismicity." Journal

of Geophysical Research Atmospheres **90**: 5497-5495.

Rhodes, B., et al. (2015). Tertiary evolution of the Three Pagodas Fault, Western Thailand. Proceedings of the International Conference on Geology, Geotechnology and Mineral Resources of Indochina, Khon Kaen, Thailand: 498–505.

Rhodes, B. P., et al. (2004). "Kinematics and tectonic implications of the Mae Kuang Fault, northern Thailand." Journal of Asian Earth Sciences **24**(1): 79-89.

Scholz, C. H. (1968). "The frequency–magnitude relation of microfracturing in rock and its relation to earthquakes." Bulletin of the Seismological Society of America **58**: 399-415.

Shcherbakov, R. and D. L. Turcotte (2004). "A Modified Form of Bath's Law." Bulletin of the Seismological Society of America **94**(5): 1968-1975.

Sobolev, G. A. and Y. S. Tyupkin (1997). "Low-seismicity precursors of large earthquakes in Kamchatka." Volcanology and Seismology **18**(4): 433-445.

Stiphout, T., et al. (2012). Seismicity declustering, Community Online Resource for Statistical Seismicity Analysis: 25p.

Sukrungsri, S. and S. Pailoplee (2015). "Precursory seismicity changes prior to major earthquakes along the Sumatra-Andaman subduction zone: a region-time-length algorithm approach." Earth, Planets and Space **67**: 10p.

Takemoto, K., et al. (2005). "New paleomagnetic constraints on the extrusion of

Indochina: Late Cretaceous results from the Song Da terrane, northern Vietnam." Earth and Planetary Science Letters **229**(3-4): 273-285.

Traitangwong, P. and S. Pailoplee (2017). "Precursory seismic quiescence along the Sagaing fault zone, Central Myanmar-application of the region-time-length algorithm." Geosciences Journal **21**(4): 543-552.

Udchachon, M., et al. (2005). Paleo-seismic studies along the southeastern portion of the Phrae Basin, Northern Thailand. Proceedings of the International Conference on Geology, Geotechnology and Mineral Resources of Indochina, Khon Kaen, Thailand: 511-519.

Udias, A. (1999). Principles of Seismology. Cambridge University Press, New York. the United States of America: 475p.

Utsu, T. (1961). "Aftershocks and earthquake statistics." Journal of the Faculty of Science, Hokkaido University, Japan **7**: 130-195.

Utsu, T. (1978). "Estimation of parameter values in the formula for the magnitude-frequency relation of earthquake occurrence." Zisin (J. Seism. Soc. Japan) **31**: 367-382.

Utsu, T. (2002a). Statistical features of seismicity. W. H. K. In: Lee, et al. (Eds.), International Handbook of Earthquake and Engineering Seismology Part A. , Academic Press: 719-732.

Utsu, T., et al. (1995). "The centenary of the Omori formula for a decay law of aftershock activity." Journal of Physics of the Earth **43**(1): 1-33.

- Wang, Y., et al. (2014). "Shallow Rupture of the 2011 Tarlay Earthquake (Mw 6.8), Eastern Myanmar." Bulletin of the Seismological Society of America **104**(6): 2904-2914.
- Warren, N. W. and G. V. Latham (1970). "An experiment study of thermal induced microfracturing and its relation to volcanic seismicity." Journal of Geophysical Research **75**: 4455-4464.
- Wiemer, S. (2001). "A software package to analyze seismicity: ZMAP." Seismological Research Letters **72**: 373-382.
- Wiemer, S. and K. Katsumata (1999). "Spatial variability of seismicity parameters in aftershock zones." Journal of Geophysical Research **104**: 13135-13151.
- Wiemer, S. and M. Wyss (1994). "Seismic quiescence before the Landers (M = 7.5) and Big Bear (M= 6.5) 1992 earthquakes." Bulletin of the Seismological Society of America **84**: 900-916.
- Woessner, J. and S. Wiemer (2005). "Assessing the Quality of Earthquake Catalogues: Estimating the Magnitude of Completeness and Its Uncertainty." Bulletin of the Seismological Society of America **95**(2): 684-698.
- Wyss, M. (1973). "Towards a physical understanding of the earthquake frequency distribution." Geophysical Journal of the Royal Astronomical Society **31**: 341-359.
- Yadav, R. B. S., et al. (2012). "Tectonic implications and seismicity triggering during the 2008 Baluchistan, Pakistan earthquake sequence." Journal of Asian Earth

Sciences **45**: 167-178.

Yadav, R. B. S., et al. (2011). "The 2007 Talala, Saurashtra, western India earthquake sequence: Tectonic implications and seismicity triggering." Journal of Asian Earth Sciences **40**(1): 303-314.



VITA

NAME Premwadee Traitangwong

DATE OF BIRTH 13 January 1993

PLACE OF BIRTH Bangkok, Thailand

INSTITUTIONS ATTENDED Bachelor of Science degree in Geology with the seismic hazard from Department of Geology, Faculty of Science, Chulalongkorn University (2005)

HOME ADDRESS 161/44 Residence Park 2 Soi Kubon 27 Ramintra Rd.
Tarang Bangkhen Bangkok 10220

